VELOCITY OSCILLATIONS IN THE SOLAR ATMOSPHERE

K. R. SIVARAMAN

Thesis submitted to the
University of Kerala
for the Degree of
Doctor of Philosophy

Kodaikanal Observatory
Indian Institute of Astrophysics
Kodaikanal

June 1972

Certificate from the Supervisor

I certify that the thesis entitled "Velocity Oscillations in the Solar Atmosphere" by Mr. K.R. Sivaraman is a bona-fide record of research work carried out by him at the Kodaikanal Observatory in full requirement of the Ph.D degree of the University of Kerala. The candidate has worked on this thesis under my supervision. I declare that the thesis has not previously formed the basis for the award to the candidate of any Degree, Diploma, Associateship, Fellowship or other similar title of any other University or Society. The thesis contains an account of the photographic observations made by the candidate with the Kodaikanal solar tower telescope and spectrograph along with the detailed computations of velocity and intensity fields made by him on the basis of these observations. The entire research reported herein is thus a completely independent effort of the candidate to improve our knowledge in a branch of solar physics of considerable topical interest.

M K Vainu Bappu

(M.K. Vainu Bappu)
Director
Kodaikanal Observatory
Indian Institute of Astrophysics
Kodaikanal

ACKNOWLEDGEMENTS

The work reported in this thesis was carried out using the facilities of the Kodaikanal Observatory.

I owe an immense debt of gratitude to Dr. M.K. Vainu Bappu, who initiated me into the study of the spectra of the Wiggly lines. It was his deep interest and direction that have made this investigation possible at all. The inspiration and the emphasis he provided, are behind every aspect of the work connected with this investigation.

Mr. B.N. Bhargava, Director and Mr. D. Radhakrishna Rao of the Indian Institute of Geomagnetism gave me help with FORTRAN programmes for all the analysis. I am extremely grateful to them for this kind help.

I have great pleasure in expressing my sincere thanks to Mr. V. Moorthy who was with me almost from the beginning of this investigation, to assist through the laborious velocity measurements, in processing of the data, in plotting of the results etc.

Mr. K.C.A. Naheem helped me in many aspects of the observing programme. Mr. R.C. Subramanian and Mr. S. Ganeshan also rendered valuable help in the reduction of the data. I am extremely grateful to them.

I am extremely thankful to Dr. J.C. Bhattacharyya for having allowed me to use some of his results for comparison with mine for discussions, before their publication and also to Mr. A. Kubicela of the Belgrade Observatory, Yugoslavia for their many stimulating discussions in the course of my work.

The diagrams were prepared by Mr. A.M. Ghouse and all the photographic work were done by Mr. P. Shahul Hameed and Mr. M. Jan. The typing of the manuscript was done by Mr. A.M. Batcha. I am extremely thankful to these persons for the neat and exemplary job they have done for me. I gratefully acknowledge the valuable help rendered by Mr. C.G. Veeraraghavan and Mr. and Mrs. Krishnamoorthy.

My grateful thanks are due to Mr. D. Mark and Mr. Anthonyraj for their help at the telescope.

Everyone in the observatory, showed interest in the progress of my work and readily gave me assistance whenever I wanted. I gratefully acknowledge all this help.

TABLE OF CONTENTS

TABLE OF CONTENTS

TABLE OF CONTENTS

PREFACE

In this thesis, I have made an attempt to study the temporal and spatial properties of the velocity and intensity fields using the photographic technique.

I have briefly outlined the earlier work in this field in Chapter I. This includes both the theoretical and observational aspects of velocity and intensity fields.

In Chapter II, I have described briefly the three methods in vogue for the study of velocity fields on the solar surface viz. the spectroheliographic, photoelectric and rapid time lapse photography, and discussed their relative merits. Of these, the method of rapid time lapse photography, which enables the simultaneous study of the properties of the velocity and intensity fields at different levels in the solar atmosphere has been used in the present work. The basic material for this study, consists of three time sequences of long duration obtained under exceedingly good seeing conditions. I have given an account of my observing techniques. Following this, I have described the procedure for the velocity measurements with the Doppler comparator constructed for this

purpose, its performance and accuracy of my measurements.

Chapter III deals with the spatial and temporal properties of the quasi-periodic velocity oscillations in detail. The fourteen spectral lines studied from the three sequences have a good coverage of heights in the solar atmosphere. The CI 6587 line, provides information on the very deep photospheric layers around log τ = +0.2. Other weak and medium strong lines studied have mean depths of formation ranging from log τ = -0.6 to log τ = -1.2. The plots of velocities with reference to time for 61 successive points on the sun for all the lines, show an average size of 8000 km for the oscillating cells and a life time of 10-15 minutes for the individual oscillations. The oscillations at the different levels have a high degree of coherence.

The power spectra of velocities have been computed. In this analysis, I have computed spectral estimates, using five different values for the lag in calculating the autocorrelation functions. This method enabled to obtain a high resolution frequency wise for the spectral estimates and thus determine the period of the velocity oscillations

with an accuracy of 5 seconds. The CI 6587 line shows a period of 304 sec. while the high level lines have a period of 295 sec.

In Chapter IV, I have outlined the methods of cross-spectral analysis. These have been applied to compute the coherence and phase spectra between velocity fields of different pairs of lines belonging to the same sequence, to study their spatial properties. The coherence between the velocity fields in the different levels is very high, of the order of 0.98. The oscillations in the high level lines lag behind those in the low level lines. This phase lag varies with frequency. In the resonance range the lag is of the order of 5 sec. between lines having their mean depth of formation, 110 km apart. This suggests a standing mode of oscillation in this range. At high frequencies the phase lags increase fast and have values appropriate for the propagation of sound waves.

Chapter V has been devoted to the spectral analysis of the intensity fluctuations in the continuum, in the line wings and the core of FeI 6358 lines. This Chapter also includes the computation of the cross-spectrum of

velocities with the continuum brightness fluctuations and of the continuum with line wing and line core intensity fluctuations. The continuum and the line wing intensity fluctuations show almost identical power spectra, with marginally detectable power in the oscillation range. The power spectra of the line core shows well the oscillations.

The coherence and phase spectra between velocities and intensities have been computed for four representative lines. The spectra are almost identical and show that the upward velocities in the lines lag behind the brightenings in the continuum by about 30 seconds. There is high coherence between the continuum and line wing intensity fluctuation. The FeI 6358 line wing intensity lags behind the continuum by about 14° while the core intensity leads the continuum by 57°.

I have also computed the coherence and phase spectra of the velocities in FeI 6358 line with its wing brightness and core brightness fluctuations. The velocities lag behind the core brightness by 93°. This is taken as an additional evidence in support of the existence of standing mode of oscillation in the 300-sec. period range.

In conclusion, Chapter VI summarizes the results of the present study and enunciates some of the problems for future investigation in this field. The importance of the study of the velocity and intensity fields cannot be over emphasised. More and more observations in the optical range on similar methods covering high chromospheric lines are most necessary to extend our present knowledge to these levels in the solar atmosphere. This supplemented with observations in the mm and cm range of wavelengths may be very helpful in understanding the physics of these oscillations.

The basic material on which the present investigation is based, consists of three time sequence spectra obtained by me with the 36 metre solar tower telescope and 19 metre Littrow spectrograph of the Kodaikanal Observatory. The computation of the power spectra of the velocity and intensity measurements follow in general, the established methods of power spectrum analysis. In this analysis, the method of using multi-lags for securing a high resolution for the spectral estimates, is original. In the computation of the coherence and phase spectra, I have applied the accepted method of cross-spectral

analysis to my data. The computations were done with a CDC-3600 computer at the Tata Institute of Fundamental Research, Bombay. All the results obtained by these analyses and discussions on these represent my original work in this field.

K.R. Sivaraman

(K.R. Sivaraman)

CHAPTER I

VELOCITY OSCILLATIONS IN THE SOLAR ATMOSPHERE : A SURVEY OF PRESENT KNOWLEDGE

The structure and dynamics of the solar atmosphere can be described in terms of the radiation field as a crude approximation. The energy generated in the core by thermo-nuclear process - the p.p. chain - is assumed to be streaming out by convection in the sub-photospheric layers and by radiation in the outer layers. According to the classical picture, the structure of the solar atmosphere is based on the notion of a gaseous ensemble whose thermodynamic state is specified by the assumption of radiative equilibrium; local thermodynamic equilibrium fixed by the local energy density of the radiation field and negligible velocity fields. In such an analysis of the solar atmosphere, the effect of velocity fields other than thermal is taken into account only as a second order approximation, neglecting their momentum coupling to the thermodynamic state of the atmosphere.

The middle of the present century witnessed a conceptual change in the problem of the coupling between macroscopic and thermal velocity fields. We now believe

that when there is such a coupling between macroscopic velocity field and the thermodynamic state of the gas, then the local kinetic temperature is no longer controlled solely by the radiation field. The importance of the recognition of the inadequacy of the homogeneous models and the necessity to invoke non-thermal phenomena can be seen from the partial success in the attempts to explain a wide variety of phenomena like, scale heights of the chromosphere, chromospheric and coronal heating, shapes of profiles of weak and medium strong lines originating in the photosphere, and also in the field of model atmospheres. This period also witnessed the direct observations of the local fluctuations in intensities in the granulation as well as of intensity variations and velocity shifts in the Fraunhofer lines. The well known "wiggly" structures seen in the Fraunhofer lines under conditions of good seeing, and the spicules seen off the limb, are visible manifestations of the inhomogeneities existing at different levels in the solar atmosphere.

The investigations of the perturbation effects of these velocity fields on the thermodynamic state of the atmosphere come under the class of aerodynamic phenomena in the solar atmosphere. The determination of the velocity fields, other than by direct observations, is by a

comparison of the theoretical line profiles and the ones based on observations. This in turn requires a complete and precise knowledge of the chemical composition and the spectroscopic state of the atmosphere. Very often the approach has been to infer the existence of the aerodynamic phenomenon which modifies the thermodynamic state of the atmosphere over that predicted on classical terms, by looking for features considered anomalous under the classical predictions.

A complete picture of the velocities expressed in terms of the line-of-sight motion can be derived from a measure of the "astronomical turbulence". In such a state, the motion is maintained by some sort of large-scale instability of the velocity field whose energy is transmitted to successively smaller elements having characteristic dimensions, to be ultimately destroyed by viscosity and dissipated into heat through small-scale motions. These measurements of the turbulence will have to be understood in terms of the "scale of turbulence" relevant to any particular situation. Taking L as the characteristic wavelength of the velocity field in the solar atmosphere (L is generally assumed to be of the same order as the scale height of the atmosphere) over which the

kinetic energy of mass motion is transferred to the system, two extreme cases can be distinguished in the interpretation of Fraunhofer line observations:

i) In the case of an optically thin atmosphere, $L\chi << 1$, where χ is the absorption coefficient. In this case, the line of sight passes through many elements giving rise to a fully developed micro-turbulence. Micro-turbulence causes line broadening and consequently an increase in the equivalent width. The flat portion of the curve of growth lies above that predicted for lines broadened by thermal motions alone.

ii) When $L\chi >> 1$, it is a case of macroturbulence. The entire line forming region experiences a uniform motion and thus the spectral line is Doppler shifted. The velocities are determined by measuring the wavelength displacement with reference to the undisturbed position.

In general, in the solar atmosphere, the observed line profiles reflect the effect of both the random and non-random motions, which both displace and broaden the line in a rather complicated manner. Studies on the centre-limb variations of the line profile by Allen, Waddell, Suemoto, Unno, de Jager and Neven, provide information on

the structure of the "astronomical turbulence" and its variation with height in the solar atmosphere. Redman and Suemoto have made a similar study in the chromosphere using eclipse data. Side by side, Böhm, de Jager, Voigt and others aimed at an explanation of the observed shapes of line profiles taking into account the inhomogeneities, and have constructed the two column and three column atmospheric models.

The method most suited to the study of the kinematics of the inhomogeneities of the dimension larger than a second of arc in the solar atmosphere is by measurements of the local Doppler shifts in the spectral line of interest. The Doppler shifts detected and measured in the sunspot spectra by Evershed (1909) is the first evidence of the existence of mass-motions in active regions on the sun. Again the earliest observations of the small scale velocities on the sun are those of Evershed (1922), when he observed the "innumerable small displacements of the lines equivalent to velocities of the order of a few tenths of a kilometre per second when the slit lies across a well defined image of the sun".

The first spectra of spatial resolution sufficient to resolve individual photospheric granules were those

obtained by Richardson at Mount Wilson. From measurements of local Doppler shifts on an excellent spectrum, Richardson and Schwarzchild (1950) obtained a value of 0.37 km/sec. for the velocity (represented by ξ) of the turbulent motions in those wiggly lines and with geometrical dimensions higher than that of the granulation. They also found a weak correlation between the velocity and brightness variations. Later Stuart and Rush (1954) filtering out the large scale fluctuations in the velocity from the data of Richardson and Schwarzchild, found the correlation much higher. At Oxford, Plaskett (1954) independently arrived at the same conclusion. Miss Hart (1956) following Plaskett's work, observed the existence of a large-scale pattern of velocities in the upper levels of the photosphere. But the significance of the velocity pattern became clear only after the appearance of Leighton's work that led to the identification of the supergranular network.

The decade following the work of Richardson and Schwarzchild witnessed a series of measurements of small scale Doppler displacements on many lines from selected spectrograms both at the centre of the disc as well as near the limb. Such studies by the Mc Math solar workers

using their vacuum spectrograph and by Evans and Michard (1962) at Sacramento Peak provide information on the dependence of ζ on the line-strength and position on the disc.

Around 1960, the study of the macroscopic motions and turbulent velocities took a new turn when the time parameter was introduced in the acquisition of the data. The main stimulant for this was the theoretical predictions of the oscillatory motions in the solar atmosphere by Whitney in 1958.

At Mount Wilson, Leighton (Leighton, Noyes and Simon 1962) modified the conventional spectroheliograph to obtain simultaneously two monochromatic pictures of the sun, in the opposite wings of the line profile. From a pair of such simultaneous pictures, he obtained by photographic subtraction singly cancelled 'Doppler plates'. These plates showed vividly that the field of motion on the sun consisted of a large-scale pattern of horizontal velocities within cells, which he termed as "supergranulation". From a series of simultaneous pictures taken in quick succession, Leighton derived "Doubly cancelled or Doppler difference" plates. The Doppler difference plate had the advantage of the time scale in it, as a result of

the finite time taken to obtain a spectroheliogram and Leighton discovered from such plates (in CaI 6103, Ba$^+$ 4554 and NaI 5896 lines) the vertical oscillatory motions in the solar atmosphere. He also observed for the first time similar oscillatory time variation of the intensity field in the core of NaI line with his brightness difference plates. The subsequent work of Noyes and Leighton (1963) on other lines established the existence of velocity oscillations around 300 secs. and its progressive decrease with altitude in the solar atmosphere.

Evans, at Sacramento Peak obtained a number of time sequence spectrograms (with time separation of 20 sec. and 30 sec. between successive exposures) of high resolution, around quiet regions at the centre of the solar surface, with good image quality. These time sequences lasted for nearly half an hour and covered spectral lines formed over a range of heights in the solar atmosphere. The analysis of these time sequence spectra (Evans and Michard 1962, Evans, Michard and Servajean 1963, Jensen and Orrall, 1963; Edmonds, Michard and Servajean 1965) provide the following exploratory information on the properties of the velocity and intensity oscillations:

1) The power spectrum of the velocity field shows a sharp peak in the power in the resonance range around a mean period of 300 seconds.

2) The period progressively decreases with altitude in the solar atmosphere.

3) The amplitude of individual oscillations are of about 0.4 km/sec. in weak lines and 0.8 km/sec. in strong lines.

4) The size of the oscillating elements increases with height from about 1600 km in the Fe I 6102 line to about 3500 km in the Na I line.

5) There is significant power in the low frequency domain; the amount increases with depth and dominates the spectrum for the low lying Ca I 5052 line, which represents a convective component in the velocity field.

6) From a comparison of 40 prominent oscillations Evans and Michard noticed that the high level line lagged behind those in the deeper line by about 8 seconds. This lag decreased from a maximum value at the onset of an oscillation to zero after a few periods. This suggests that an oscillation starts as a progressive wave, rapidly decaying into a standing oscillation.

The coherence and phase analysis of the velocity fields for pairs of lines show some progressive motion in the resonance range, with phase propagation velocities faster than the sonic velocity. Outside the resonance range the phase lag increases with frequency suggestive of ordinary sound waves.

7) The continuum intensity fluctuations show insignificant power in the velocity resonance frequency range. Edmonds, Michard and Servajean (1965) found that there is significant coherence between the velocity field in the line and continuum fluctuations in the resonance range with the velocity lagging behind the continuum intensity.

8) The power spectrum of the brightness fluctuations in the core of the faint CI line mimics the non-periodic continuum fluctuations, but with a phase lag. The fluctuations in a strong line show oscillations in the same period range as the velocity oscillations.

Frazier (1968) studied the velocity and temperature fluctuations in the solar photosphere with a long time sequence of spectra lasting for 55 minutes in the three lines SiII 6371, FeI 6364 and FeI 6355. The power spectrum of the velocities showed a sizeable low frequency or convective component in all the lines, the maximum being for

the SiII line. The oscillatory part for all the three lines showed two components, one with a period of 265 sec. and a weaker one of period 345 seconds. The intensity fluctuations showed primarily the convective component at all levels and a weak oscillatory component.

Howard (1962) using the Mount Wilson magnetograph in the Doppler mode observed these oscillations at discrete points on the solar disc. His extensive observations (1967), on the oscillations, using the lines FeI 5250 and CrI 5247 showed that the oscillatory motions occurred in well defined bursts, each lasting for nearly 30 minutes. His studies on the phase relations by simultaneously observing the oscillations on two lines, showed the same results as of Evans and Michard.

Deubner (1967) made life-time studies of the velocity oscillations and the influence of magnetic fields on the oscillations using the Capri magnetograph.

Tanenbaum et al (1969) used one-dimensional magnetograph scans with varying apertures (from 2.3" to 10" of arc) and studied the 5-minute velocity oscillations and their phase relations with line-wing and line-core brightness using the FeI 5250 and NaI 5896 lines. Their

observations show that the oscillations in the wing brightness lead the velocity oscillations by less than 90° in the photosphere and about 90° in the chromosphere, thus showing the existence of travelling waves in the lower levels and standing waves at higher levels.

Musman and Rust (1970) used the Sacramento Peak Doppler-Zeeman analyser to study the collective phase behaviour of the 5-minute oscillations over large areas (60" x 300" of arc) on the solar disc and their relation to the rather steady component of the line-of-sight velocities associated with the supergranular flow.

Bhattacharyya (1972) using the Kodaikanal Observatory magnetograph in the Doppler mode and with an aperture of 5.6" x 1.4" made a detailed study of the velocity oscillations on a number of spectral lines covering a good range of heights in the solar atmosphere. His study includes velocity observations on H_β. He noticed the average duration of bursts in chromospheric lines to be shorter than those in the photospheric lines. He found that the period of oscillations remain virtually unchanged with height in the photosphere and low chromosphere, but shifts to a lower period around H_β level.

It is now fairly well agreed upon, that the kinetic energy stored in the oscillatory mass-motions observed in the photosphere and the chromosphere by any one of the above observational set-ups, represents an intermediate phase in the energy link between the convection zone and the outermost atmospheric layers. The rapid change in the rate of ionization of hydrogen in the sub-photospheric layers causes the temperature gradient to be higher than the adiabatic gradient leading to convective motion. The photospheric granulation is a direct manifestation of this convective motion. Biermann (1946, 1948) and Schwarzchild (1948) suggested that the acoustic waves generated by the granulation provide the heat input for the upper chromosphere and the corona. Schatzman (1949) showed that the amplitude of these waves steadily increase as the waves propagate upward through regions of decreasing density, ultimately forming a sequence of shock waves. The outer solar atmosphere is heated by the dissipation of the shock waves. In the earlier investigations of Biermann and Schwarzchild, the computed energy brought up by the granules was far in excess of the amount required for maintaining the temperature of the corona. Subsequent work has shown that, only a small part of the turbulent

energy, which is later converted into accoustic energy, escapes dissipation as heat at the source itself.

Whitney (1958) represented the fluctuations of the top of the convection zone resulting from a combination of convective motions and sound waves, by two dimensional equations. The fluctuating top of the convection zone impress motions on the overlying layers, generating waves. His steady state solutions of the wave equations show the existence of a mixture of compressional and gravitational waves of periodicities in the range of 3 to 5 minutes.

Lighthill (1952, 1954) developed a theory of the aerodynamic generation of accoustic noise by isotropic turbulence, in a compressible medium. The turbulent regions act as sources of sound, radiating like a quadrupole. Proudman (1952) derived a numerical expression for the accoustic power so generated. The uppermost layers of the convection zone, confined to a thickness of about 60 km characterised by high Reynold number, are supposed to be the source of flux of accoustic energy. Lighthill's theory has been applied to this turbulent zone by many workers de Jager and Kuperus (1961), Osterbrock (1961), Moore and Spiegel(1964), Kuperus (1965), to derive an order of

magnitude for the acoustic flux, which approximately balances the energy necessary for the coronal heating.

Under the combined influence of gravitational forces and a magnetic field, three modes of wave propagation are possible in a compressible medium:

1) Ordinary sound waves controlled by compressibility, can propagate in all directions.

2) Internal gravity waves, also play a vital role in the transport of mechanical energy in the photosphere and chromosphere. Lighthill (1967) has shown that these waves are generated in the stable layers above the convection zone, by 'tongues of turbulence' penetrating into the stable layers. Whitaker (1963) has worked out the propagation and dissipation of these waves.

3) The Alfvén's waves, which propagate along the magnetic lines of force.

Osterbrock (1961) and Lighthill (1967) following Alfvén considered the propagation in the presence of a magnetic field, consisting of the fast-mode, slow-mode and Alfvén mode magnetohydrodynamic waves. The fast-mode

disturbances which are sound waves to a good approximation generated in the hydrogen convection zone travel through the photosphere and their dissipation is the main source of chromospheric heating, while the corona is heated by Alfvén waves. In plage areas, the wave generation in the convection zone is larger leading to more heating.

The present state of theory broadly explains the wave propagation characteristics of the solar atmosphere. However, there are numerous details of observation that have been dramatically uncovered in recent years of observational effort that cannot yet be interpreted with the aid of our present theoretical concepts. Progress here will depend much on the availability of a consistent set of observational information that specifies the mechanisms operative and sets limits to the parameters characteristic of them. It is the aim of the present study to effect a contribution towards such a goal.

—

CHAPTER II

THE OBSERVATIONAL TECHNIQUES

2.1. General

Since the question of the origin of the velocity field is rather insecure, its solution has to be regarded more as a desired result rather than as a physical parameter available to start the investigation. This assigns a great importance to the observations on velocity fields, since a comprehensive picture of the physical processes taking place can provide a secure basis for inference on the question of origin. Table II-1 classifies the details of observations of the temporal and spatial properties of the inhomogeneities made so far by the three different techniques in vogue. Also included in the list are the measures reported in this thesis.

2.2. Relative merits of the different techniques

Leighton's Doppler spectroheliogram is a two-dimensional map of the velocity field at one wavelength position in one line. The two-dimensional aspect gives a good qualitative insight into the nature of these velocity fields and the size distribution of the cellular structures. At the same time it has the disadvantage that most

Table II-1

A summary of measures

Author	Year	Mode of Observation	Spectral line studied	Nature of analysis.
1.	2.	3.	4.	5.
Leighton, Noyes and Simon Noyes and Leighton	1961 1963	Doppler spectroheliograms	FeI 6102 CaI 6103 NaI 5896 BaII 4554	Period of velocity oscillations derived from estimation from a number of Doppler difference plates. Intensity oscillations for NaI 5896 line core determined from "Brightness difference" plates.
Howard	1962	Magnetograph in the Doppler mode	FeI 5250	Continuous records of velocity field obtained, each lasting for about five hours.
	1967	Aperture varying from 2.5" to 10" of arc.	FeI 5250 CrI 5247	Period of velocity oscillation determined for these 2 lines; also distribution of amplitudes and characteristics of bursts of oscillations.

Table II-1 continued

1.	2.	3.	4.		5.
Deubner	1967	Magnetograph in the Doppler mode. Aperture 3"x3" of arc	FeI	5250	Data consists of repeated scans over the same straight line on the sun's disc. The mean life time of oscillation in the quiet regions and in the neighbourhood of spot groups and distance of oscillating regions have been studied.
	1971	Magnetograph in the Doppler mode. Aperture 3"x3" of arc	CI FeI NaI MgI	5380 5124 5896 5172	Oscillatory motions detected in the deep photosphere with CI 5380 line. Horizontal motions studied in all the lines.
Tanenbaum et-al	1969	Magnetograph in the Doppler mode. Varying aperture 2.3" to 10" of arc	FeI NaI	5250 5896	Velocity fluctuations in the lines; intensity fluctuations in the wings, line core and continuum. Phase relation studies.
Bhattacharyya	1972	Magnetograph in the Doppler mode. Aperture 1.4" x 5.6" of arc.	NiI FeI TiI BaII NaI MgI H_β	5094 5072 5210 4554 5890 5172 4861	Data consists of continuous records for each line of duration ranging from 2 to 4 hours. Temporal properties and period of velocity oscillations studied by power spectra analysis, studies on characteristics of individual bursts.

Table II-1 continued

1.	2.	3.	4.	5.
Evans and Michard	1962	Time sequence spectra	TiI 5173 MgI 5172 FeI 5171	Periods of oscillation in individual lines and phase lag between high level and low level lines derived from prominent oscillations.
Evans, Michard and Servajean	1963	Time sequence spectra	TiI 5173 MgI 5172 FeI 5171	Power spectra studies of velocities; Brightness in the continuum and brightness in the cores of 5172 MgI and 5171 FeI lines.
			FeI 8514 CaII 8498 CaII 8542	Power spectra of velocities.
Jensen and Orrall Orrall	1963 1966	Time sequence spectra	FeI 3931 FeI 3937 CaII K line	Power spectra of velocities.

Table II-1 continued

1.	2.	3.	4.	5.
Edmonds Michard and Servajean	1965	Time sequence spectra	CI 5052 CrI 5051 FeI 5049	a) Power spectra of velocities b) Coherence and phase spectra of velocity fields between pairs of lines, velocity fields of CrI 5051 against continuum intensity. Central intensity of CI 5052 against continuum intensity c) Cross correlation of velocity fields with continuum.
Frazier	1968	Time sequence spectra	SiII 6371 FeI 6364 FeI 6355	Power spectra of velocities; power spectra of intensities in the lines and the continuum; coherence and phase spectra of 1) velocities in pairs of lines 2) continuum intensity against velocities 3) continuum intensity against central depths.
Elliott	1969	Time sequence spectra	H_α 6563	Power spectra of velocities.
Blondel	1970	Time sequence spectra	CaI 4227 FeI 5049 CrI 5051 CI 5052	Power spectra of velocities in the lines and phase relation between two of the lines. Comparison studies of the nature of velocity in facular and quiet regions on the sun.

Table II-1 continued

1.	2.	3.	4.	5.
Sivaraman	1972	Time sequence spectra	FeI 6330 FeI 6335 FeI 6336 FeI 6338 NiI 6339 FeI 6344 SiII 6347 FeI 6358	Power spectra of velocities; power spectra of intensities in the continuum, and in the line wing and core of FeI 6358. Coherence and phase spectra of 1) Velocities in pairs of lines 2) Continuum intensity against velocities 3) Continuum intensity against line wing and core brightness 4) Core brightness and line wing brightness of 6358Å with its velocity.
			CaI 6572 NiI 6586 CI 6587 FeI 6593	Power spectra of velocities and coherence and phase spectra of velocities of CI 6587 against the remaining 3 spectrallines.
			CH 4281 CaI 4283	Power spectra of velocities.

of the information about the line profile is lost. Also simultaneous information characteristics derivable from other lines are not easily available. Moreover, the time resolution obtainable is rather poor, due to the inherent slow scanning speed in a spectroheliograph.

The photoelectric technique, which utilizes the magnetograph in the Doppler mode, also suffers from the same disadvantage as Leighton's method, since the light from the two wings of a spectral line is viewed to derive the velocity field and hence cannot provide any information beyond those positions in the profile of the particular line. The spatial resolution is limited by the use of large size apertures which are necessary for obtaining a reasonable level of signal above the noise. Thus the properties studied represent an average behaviour of a certain area on the sun, as specified by the entrance aperture of the magnetograph. The advantage exists of the possibility of obtaining a continuous record of the velocities over long periods. The temporal properties of the oscillations can thus best be studied with a reasonable high time resolution, which is limited only by the photomultiplier noise and atmospheric seeing. It is also possible to aim at good instrumental sensitivity for the velocity measurements.

The rapid time lapse photography aims at obtaining spectrograms in a rapid sequence covering simultaneously many lines. The spectrograph slit samples a long, narrow strip of the sun's surface. The sequence thus provides detailed information on the physical state and the time-development of a long, narrow strip of the solar atmosphere. High resolution solar spectrographs usually combine extremely high spectral resolution with a spatial resolution as good as one second of arc. In such cases the spatial resolution is limited only by the seeing conditions. The spatial properties of the velocity fields are studied best by this technique, as one can derive the line-of-sight velocity fields at different levels by merely obtaining the Doppler shifts in the different lines. The drawbacks are that the data obtained are not continuous, but limited by the time separation between successive exposures. But, such a limitation is more than off-set by the supreme advantage this technique has to offer in the study of spatial and temporal properties simultaneously of the velocity and intensity fields with an unparalleled accuracy in resolution.

Table II-1 shows that most of the earlier studies have concentrated on the temporal properties of the inhomogeneities, as the analyses have been confined to only 2 or 3 spectral lines at one time. Also, no observational evidences are available on the behaviour of the inhomogeneities in the temperature minimum region in the solar atmosphere. Information on the temporal behaviour and other characteristics of the waves like the amplitude of oscillation in the temperature trough are desirable for a better understanding of the nature of the velocity fields.

Any fresh investigation should, therefore, concentrate on the study of the spatial behaviour of the inhomogeneities depth-wise by taking into account as many spectral lines as possible obtained simultaneously.

2.3. Observations

The observations were obtained with the 36 metre horizontal solar telescope and the 18-metre spectrograph at the Kodaikanal Observatory. A two mirror coelostat of fused quartz and of 61cm aperture mounted on top of a 11-metre tower feeds a 38cm two element achromat of 36 metres focal length via a third mirror which converts the vertical beam from the coelostat into a horizontal beam.

The f/90 beam forms a 34cm diameter solar image in the plane of the slit with an image scale of 5.5"/mm. The first mirror is driven by a synchronous motor which in turn is run by a frequency stabilised oscillator. The frequency of the oscillator can be varied over a small range, at the will of the observer by operating a control, to compensate for the day to day minor variations in R.A. and Dec. in the sun's position. The solar image can be guided on the slit in Right Ascension and Declination by the controls for the second mirror of the coelostat and can conveniently be operated from the slit end. The Littrow spectrograph has a 20cm two element achromat of 18.3 metres focal length and a Babcock grating of ruled area 135 x 200 mm with 600 lines/mm and blazed in the fifth order green. In the blazed region, the grating has a resolving power of 600,000.

A number of time sequences were obtained around chosen spectral regions with the slit of the spectrograph located at the centre of the solar disc. On these occasions it was ensured that the regions in and around the centre of the sun was very quiet. The effective length of the slit was 19mm and a width of 100 μ was maintained in all the sequences. A hair stretched across the spectrograph

slit during the observations served as a fiducial line along the dispersion. The overlapping orders of the grating were eliminated by the use of glass filters mounted in front of the entrance slit. The solar rotation was compensated by a line shifter placed in front of the slit. The solar image was moved relative to the slit by proper amounts with the aid of the line shifter in order to ensure that the same part of the sun lay over the slit, throughout the period of observation. In the early hours after sunrise, the value of sec z falls quite rapidly and its contribution to the increase in brightness of the solar image is very significant. The exposure time was, therefore, continually decreased to compensate for the increase in brightness of the sun's image. 35mm films in spools of 100 feet were used in a camera with mechanical film transport. The films were tank-developed for 10 minutes in D-19 maintained at 68°F.

Of the many time sequences, three sequences obtained under exceedingly good seeing conditions have been chosen for the present study. The details pertaining to the spectra are set out in Table II-2.

Table II-2

Some details of the spectrum exposure sequences used in this study

Sequence Designation	Date	Spectral region	Grating order	Dispersion	Emulsion	Filter for cutting off overlapping orders	Time of Exposure (Mean)	Time between successive exposures	Duration of the sequence
A1082	April 16 1969	6340Å	IV	6.677 mm/Å	Kodak IV-E	RG2 Schott filter	3^s	20 seconds	40 minutes $01^h\ 49^m\ 00^s$ to 02 29 00 U.T
A1100	January 11, 1970	6587Å	IV	7.096 mm/Å	Kodak IV-E	RG2 Schott filter	3^s	20 seconds	22 minutes 02 12 00 to 02 34 00 U.T
A1133	March 12, 1971	4280Å	VI	10.306 mm/Å	Ansco Hypan-X Type 5100	7-59 corning filter	$2\frac{1}{2}^s$	15 seconds	40 minutes 02 03 00 to 02 43 00 U.T

The seeing conditions at Kodaikanal in the mornings are by and large above average during the winter months (December to February) and also in March and April. As is typically characteristic of mountain observatories, these periods are confined to about two to three hours after sunrise. The definition falls off rapidly when the solar hour angle is less than three hours. But, during the months of March and April, the mornings following a day of heavy thundershowers can offer exceedingly fine conditions of seeing. We have used such spells of good seeing for obtaining the sequences. The high image quality shown by the high contrast in the continuum streaks and the line wiggles are maintained throughout the lengths of the sequences without significant change. A measure of the resolution attained is given by the autocorrelation curve of the granulation intensity field. This can be seen in Figure II-1. Four frames have been chosen for such study, three of which were very typical of the good seeing and the fourth one chosen at random from amongst the later frames of the sequence when the seeing quality had deteriorated. The full width at half maximum (FWHM) of the A.C. curve, which provides an objective measures of the cell dimensions based on measurements on these four frames is seen to be

FIGURE II-1

Spatial auto-correlation functions of continuum intensity for four frames. The abscissa is in units of 630 km. The mean value of the full width at half maximum (FWHM) is 1100 km.

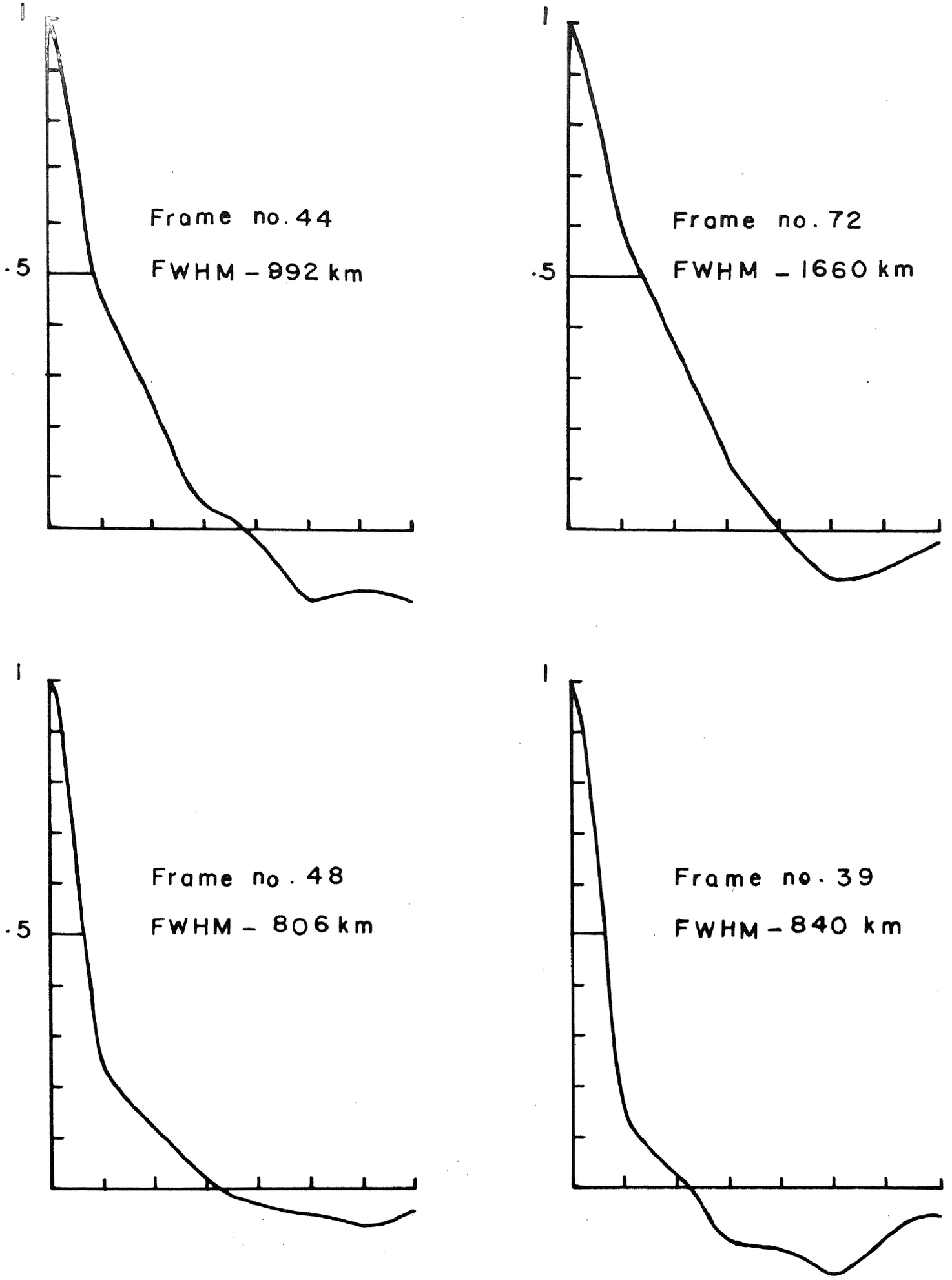
I
.5
Frame no. 44
FWHM – 992 km
I
.5
Frame no. 72
FWHM – 1660 km
I
.5
Frame no. 48
FWHM – 806 km
I
Frame no. 39
FWHM – 840 km

Fig. II –1

1100 km and may be considered an average value. The best of these frames gives a value of FWHM close to 1.1 seconds of arc. The average value of our sequence is identical with that of the time sequence obtained under excellent seeing conditions by Evans at Sacramento Peak and studied by Edmonds, Michard and Servajean (1965). The guiding excursions could not have exceeded ± 0.5" of arc; this accuracy being ensured by the photoelectric guiding unit employed in my observations.

A way of quantitative assessment of the quality of guiding is provided by the correlation coefficient of the granulation intensity field of successive frames which are separated by an interval far less than the life time of the structures. This coefficient has a value of 0.99 from the beginning to the end of the sequence.

2.4. Measurements of the Spectra

The Doppler displacements in the spectral lines of the three sequences were measured, to derive the velocity fields. The measurements were done with a Doppler comparator constructed for this purpose. In this device, an image of the line, magnified 18 times by a Zeiss spectrum projector, is projected on the plane of a system of two

identical slits, with their centres located at $\pm \Delta\lambda$ on the line profile. The widths of the slits lie in the direction of dispersion and are kept as small as possible to avoid considerable depth averaging in the solar atmosphere. The lengths of the slits which lie along the length of the line is chosen to conform to the needs demanded by the spatial resolution desired by the observer. The light from the wings after passing through the slits, is reflected on to two light dependent resistors (Philips LDR) having identical responses to light. The LDR's are connected with the help of other precision resistors to form a Wheatstone network. When the line is centred accurately over the slits, the unbalanced voltage output from the LDRs is zero. The null measuring instrument is a Dumont cathode ray oscilloscope operated as a D.C. Voltmeter in the finest range. When the line is decentred by a Doppler shift of the line, the resulting unbalanced voltage shows up as a displacement of the spot on the oscilloscope screen. The image of the line is centred by displacing the slit system which is mounted on a Hilger micrometer screw. The displacement is read on the micrometer scale which has a least count of 10 μ and this corresponds to a Doppler shift of 3.5 metres/sec in the fourth order red region. The

spectral line is scanned along its length and the Doppler displacements are obtained at successive points spaced according to the resolution desired by the observer. This instrument is admirably suited for the present measurements because of the ease with which measurements can be done and of its linear response. The accuracy of the measures is limited only by the properties of the line profile studied and the emulsion used to record the spectra and not by the comparator.

2.5. Evaluation of accuracy of measurement with the comparator

Extensive test measurements were carried out with the comparator to assess the reproducibility of the Doppler shift measures. Doppler shifts for six Fraunhofer lines of Rowland intensity ranging from -1 to 8 were measured. The measurement procedure was as follows. Doppler shifts in each line of the above set of six were measured under identical conditions of spatial resolution and light signal level, as to be used in the subsequent measurements of the time sequence spectra. The measures for the six lines made thus on one occasion constituted one measurement series. This was repeated six times for

all the six lines, one measurement series following another after a lapse of a day or two. The six measurements series plotted for the six lines showed remarkable consistency. The probable error ranged from 5 meters/sec for the strong lines to 10 meters/sec for the very weak lines. The deliberate lapse of a day or two introduced between the successive measurement series was to test the stability of the instrument, particularly of the electrical system.

When measurements on lines of different Rowland intensities are required, it is desirable to adjust the level of light of the projector lamp, so as to keep the light level reaching the LDRs same, irrespective of the strength of the line to be measured. This will ensure that the operating points on the response curve of the LDRs are same for all the measurements. Although this was possible in the present set up, the light level was deliberately kept different for two of the measurement series. The consistency of these measures with those of the remaining measurement series ensured the linearity of the system.

To test the reliability of the comparator, the Doppler shifts were determined independently by the

procedure of Evans and Michard. Two microdensitometer traces were made parallel to the length of the line, each on either wing of the line profile in the same location as the two slits of the Doppler comparator. The local Doppler shifts were then evaluated from the microdensitometer records by the Evans and Michard method (1962). The results obtained from the comparator and by the above method showed very good agreement.

2.6. Sources of noise in the measurements

Two of the sequences were recorded on the Kodak emulsion IVE, which has a fine granularity. The noise resulting from the photographic grain in the case of the Ansco Hypan X film, estimated from measurements on a frame of the time sequence is found to be 40 metres/sec.

Another source of noise is the turbulence inside the spectrograph. The observed Doppler shifts in spectral lines are the actual Doppler shifts in the lines modified by turbulence. Both the time sequences in the red region cover telluric lines. Measurements of velocities were done on one telluric line from each sequence for all the exposures. This yields the pattern of turbulence along a

vertical column and a comparison of the pattern from frame to frame, a picture of the temporal variation of turbulence prevailing inside the spectrograph. The r.m.s value of the turbulence estimated along the length of slit is 59 metres/sec.

These errors being so small, will have no significant effect on the results to be discussed in the next chapter.

—

CHAPTER III

THE SPATIAL AND TEMPORAL PROPERTIES OF THE QUASI-PERIODIC OSCILLATIONS

3.1. General

The temporal characteristics of the velocity fields are studied well with a time sequence lasting for as much duration as can be obtained in practice. Their spatial characteristics depthwise are best studied with spectra covering as many lines as possible. It is very desirable to include lines of different intensities and excitation potentials, so as to obtain a good representation of the vertical cross-section of the solar atmosphere. But it has not been possible to fully satisfy the latter condition in practice. Weak Fraunhofer lines with high excitation potentials provide data on the deeper photospheric layers. An exposure aimed at obtaining weak lines of the correct density, for measurement of velocity and intensity, will result in under-exposure of strong lines on the same frame. Therefore, it becomes necessary to seek a compromise in choosing a wavelength region containing as many lines as possible and which will

reasonably represent a major part of the photosphere and chromosphere. Information of this kind from two or three sequences can help to build up a composite picture of the spatial characteristics of the velocity fields.

Table III-1 contains detailed information on the absorption lines used in the present study from the three time-sequence spectra.

In sequence A 1082, I measured the Doppler shifts for 9 solar lines. This sequence includes a SiII line of high excitation potential and FeI lines of varying intensities and excitation potentials. In sequence A 1100, I measured the radial velocities for 4 solar lines. This sequence includes 6587.622Å of atomic carbon formed in the very deep photospheric layers. The high contrast and the very low granularity of the Kodak IV-E emulsion on which these two sequences were obtained, enabled the measurement of small Doppler shifts even in the broad, hazy deep-lying lines like CI and SiII lines. The noise level is, however, not negligible, as in the other lines investigated. The two sequences A1082 and A1100 have telluric lines in the wavelength region studied.

Table III-1

Details of the spectral lines included in this study

Sequence Designation	Line λ	Element	Rowland Intensity	Excitation potential Lower level (e.v)	$\pm \Delta\lambda$ (Å)	w (Å)	ζ Km/sec.
A1082	6330.859	FeI	2	4.73	0.0464	0.0329	0.31
	6335.345	FeI	6	2.188	0.0659	0.0419	0.34
	6336.837	FeI	7	3.67	0.0659	0.0419	0.35
	6338.588	FeI	2	4.79	0.0464	0.0329	0.32
	6339.125	NiI	2	4.136	0.0464	0.0329	0.31
	6344.162	FeI	4	2.422	0.0584	0.0329	0.34
	6347.104	SiII	2	8.085	0.0479	0.0928	-
	6358.695	FeI	6	0.855	0.0659	0.0419	0.39
	6342.389	Telluric		-	0.0374	0.0329	-
A1100	6572.795	CaI	1	0.000	0.0437	0.0310	0.30
	6586.319	NiI	1	1.942	0.0437	0.0395	0.30
	6587.622	CI	-1	8.53	0.0613	0.0592	0.34 *
	6593.884	FeI	4	2.43	0.0437	0.0395	0.30
	6586.511	Telluric		-	0.0352	0.0310	-
A1133	4281.974	CH	2	-	0.0427	0.0272	0.34
	4283.016	CaI	4	1.878	0.0427	0.0272	0.35

$\zeta = \sqrt{2}$ x root mean square velocity

* Velocity records are noisy and hence a high value of ζ.

$\pm \Delta\lambda$ (Å) Location of the Doppler comparator slits on the line profile in Å

w (Å) Width of the Doppler comparator slit used in measuring radial velocities.

The main interest in sequence A1133 comes about from the fact that it contains the line 4281.974Å of the CH molecule. I have made measurements of velocities on this molecular line and also on the neighbouring CaI line 4283, the latter to serve as a comparison.

The fourteen solar lines chosen for study, have their mean depths of formation well distributed in height in the solar atmosphere, ranging almost from the granulation layers through the photosphere up to the low chromosphere. This is shown by their contribution curves to be discussed in detail later.

3.2. Measurements with the Doppler comparator.

The microphotometer scans along the direction of dispersion of one frame from each of the three sequences gave the shapes of the line profiles of all the spectral lines. From these traces, it was possible to decide the widths of the slits to be used for each line, for measurements on the Doppler comparator that would satisfy the condition that the slits be located on the steep part of the profile, so as to offer high sensitivity in the measurements. In doing so one must keep slit widths within a maximum value, so as to keep the depth averaging

in the solar atmosphere within reasonable limits. The location of the slits on the corresponding profiles are given in Table III-1 under the column $\pm\Delta\lambda(\mathring{A})$ and the width of the slit under the column $w(\mathring{A})$ for the lines measured. The length of the slits was maintained uniform throughout the measurements, corresponding to 1080 km on the sun, as this was considered a sufficient value for the spatial resolution. This length for the comparator slits gave measurements of velocities at 61 points, regularly spaced 1080 km apart for each spectral line along the slit of the spectrograph.

Measurements at the comparator of each spectral line yielded a $A(x_i)$ curve of velocity, as a function of position along the slit. Such A (x) data consist of a series of 61 numbers that are the Doppler comparator readings. These numbers are against an arbitrary zero point, which changes from line to line and frame to frame for the same line.

The A1082 sequence has 120 frames exposed successively. Hence for each spectral line the data consists of a two dimensional array represented by $A(x_i, t_j)$ with 'i' running from 1 to 61 corresponding to the 61 points along

the slit and 'j' running from 1 to 120 corresponding to the 120 frames. The array for each line thus consists of 120 columns and 61 rows.

Sequence A1100, with 62 exposures, has for each line 62 columns and 61 rows forming the array. For A1082 and A1100, successive values of t_j are 20 seconds apart and x_i 1080 km apart on the sun.

A1133 has 160 exposures and the array for each line has 160 columns and 61 rows. Successive values of t_j are separated by 15 seconds, x_j remaining the same.

The output of the Doppler comparator for all the solar lines consisted of more than 10^5 readings, which were then punched on cards for further processing.

3.3. Numerical analysis - Practical procedure

The A (x) curves were plotted for one line in each sequence to detect the possibility of any declination drift which manifests itself as a drift along the spectrograph slit during the observations. The fiducial line along the direction of dispersion was provided by the shadow of the hair line across the spectrograph slit. The 61 points along the length of the spectral line at

which velocity measurements have been made are located with reference to this fiducial line. The A (x) curves of successive frames plotted on semi-transparent paper, when superposed, matched very well every-where and did not show any sign of drift along the slit within detectable limits. This is also confirmed by the high correlation coefficient of the granulation field between consecutive frames referred to in Chapter II. A similar correlation coefficient worked out between successive frames for velocities range from 0.65 to 0.85. This is probably due to changes in velocity at individual points during the 20 second interval.

The velocity shifts in the two telluric lines, one in A1082 and the other in A1100 were measured in the same way as for the solar lines. Their A (x) curves represent the turbulence in the earth's atmosphere and inside the spectrograph. These A (x) curves were averaged to form one final $\bar{A}$ (x) curve. This was the average of 120 curves for A1082 and of 62 curves for A1100. This average $\bar{A}$ (x) curve provided the reference curve, deviations from which yielded velocities. In the case of velocities, the shape of this reference curve results only from the curvature of the spectral lines, produced by a plane grating on

account of the change of the effective groove separation for oblique rays. For the sequence A1133, in the absence of a telluric line in the spectral region, the reference curve was derived by averaging the 160 velocity curves of one of the solar lines. This reference curve was fitted to each A (x) curve at its mean value and the difference $A(x_i, t_j) - \bar{A}(x) = V(x_i, t_j)$ read at the 61 points. The $V(x_i, t_j)$ values form the fluctuating component of the velocity measured with reference to the mean of each frame. These values were then converted to vertical velocities in km/sec using the Doppler relation valid for a stationary atmosphere. This was done with a CDC-3600 computer for all the 14 solar lines. The output of the computer gave the data points to form the array $V(x_i, t_j)$ for all the lines. By reading horizontally, one gets a V (t) curve. For any one line there are 61 such V (t) curves. Sample plots of these velocities as functions of position along the slit and time for 6 spectral lines are shown in Figures III-1 to III-4.

These velocity measures are not absolute. They were measured, as mentioned earlier, with respect to the mean taken over each frame. This procedure has automatically

filtered out all modes of large horizontal wave lengths particularly, those of the supergranulation cells which have a horizontal wavelength of about 30,000 km. Also, in the measurement procedure, the 61 points on the slit are 1080 km apart. This would have filtered out the small wavelengths in the velocity measures to some extent. But this is not serious, as the size of the oscillating cells, is much larger, as will be shown shortly.

3.4. General properties of the oscillations

The Figures (III-1 to III-4) of the velocity plots show the temporal properties of the oscillations over the entire length of the slit, corresponding to 75250 km on the sun. At any one instant, the velocity plots for lines in the same sequence show the simultaneous behaviour of the velocity fields at different levels in the solar atmosphere. The oscillations occupy a substantial part of the solar surface with measurable amplitudes and stand out prominently. The amplitude and period of the oscillations change irregularly. The velocity plots of the CI 6587 line are noisy, although the oscillations are recognisable. In the case of the lines formed at higher levels, the regions oscillating in coherence can very

FIGURES III-1 to III-4

Sample plot of velocity vs time and position. The curves represent the velocity at consecutive points, separated by 1080 km on the sun. The high amplitude feature at 'A' can be seen in 6330 and 6338 lines in Figure III-1.

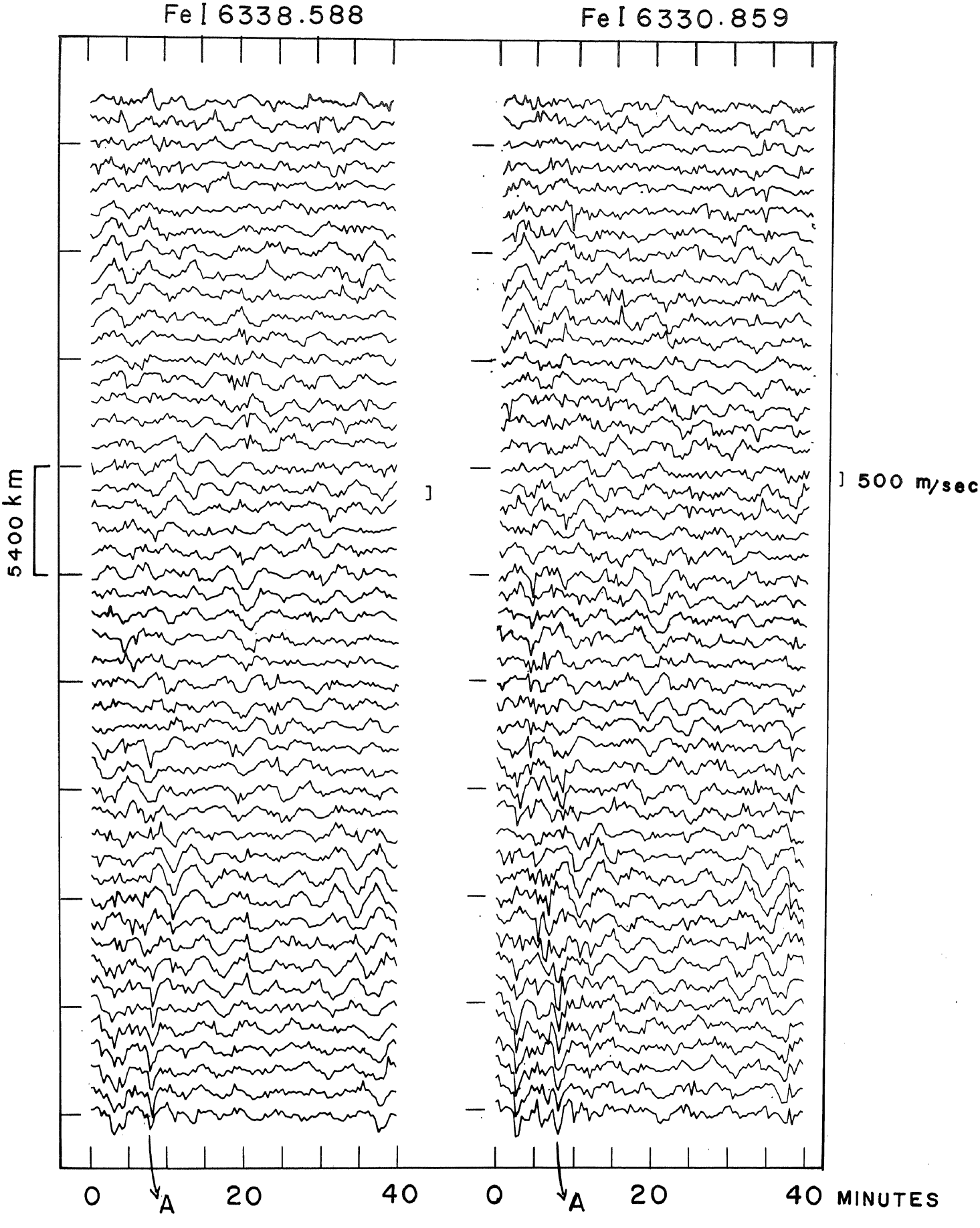
Fe I 6338.588
Fe I 6330.859
5400 km
500 m/sec
0
A
20
40
0
A
20
40
MINUTES

Fig . III - 1

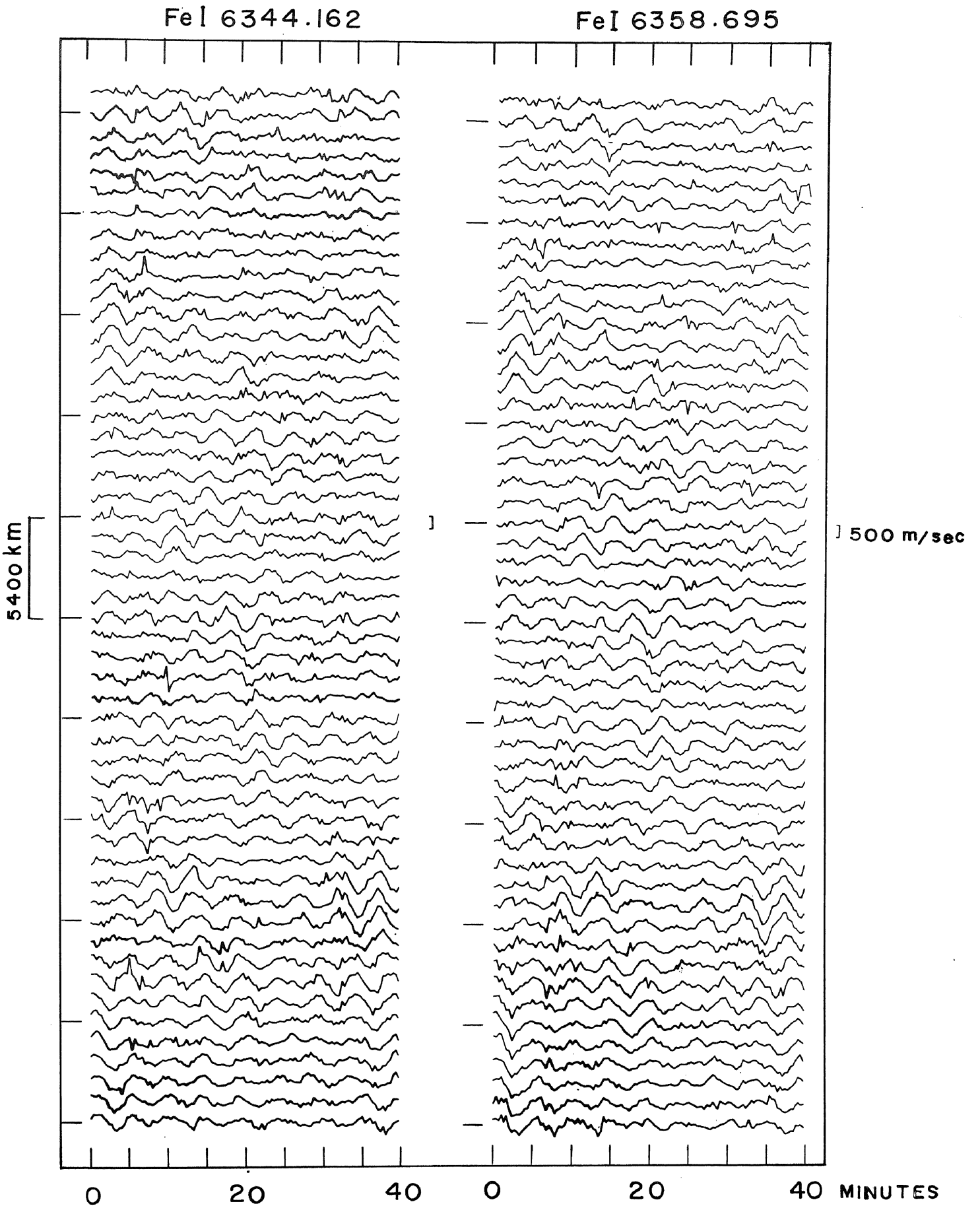
FeI 6344.162
FeI 6358.695
5400 km
500 m/sec
0
20
40
0
20
40
MINUTES

Fig . III - 2

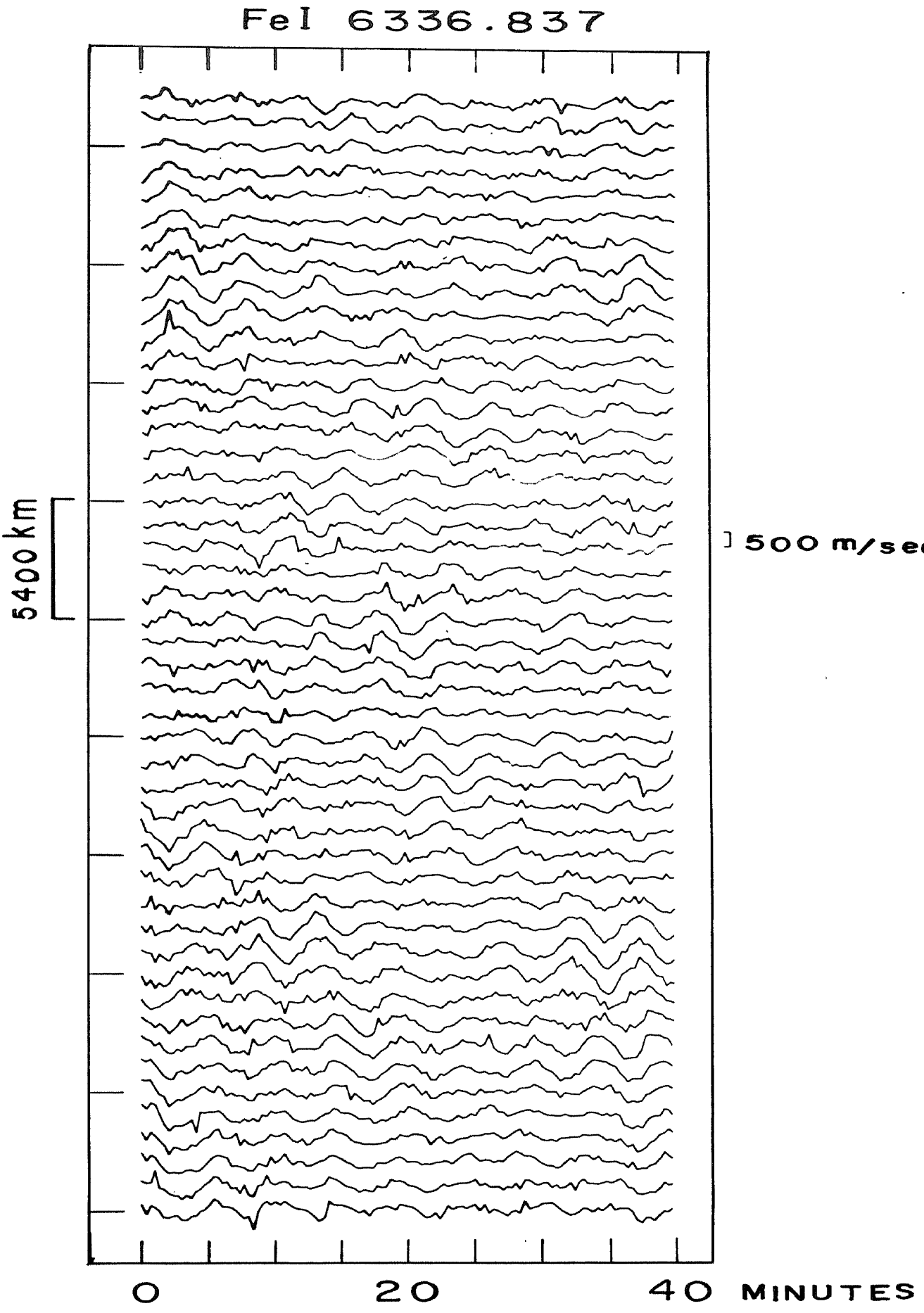

Fig . III - 3

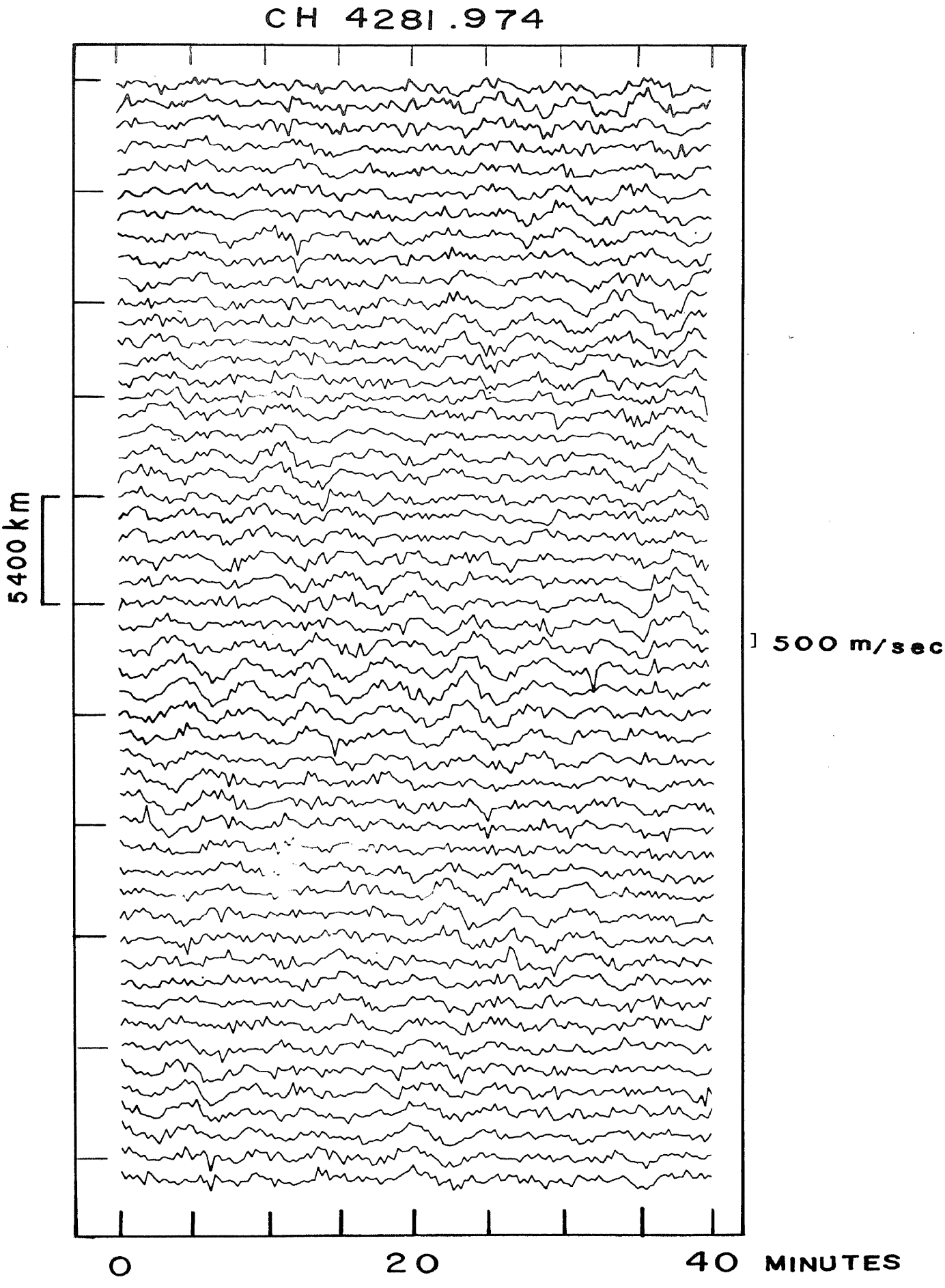

Fig. III - 4

easily be identified. In most of the cases, the boundaries of areas oscillating coherently, both with reference to space and time are not well defined, which shows that the onset and dying down of these oscillations are not clear cut. In between these areas oscillating with large amplitudes are those with very irregular oscillations of amplitudes much less than 100 metres/sec. These represent regions where oscillations have died down.

By placing a straight edge vertically on any of the Figures (III-1 to III-4) to represent the slit, it is possible to count the number of consecutive waves that oscillate in phase and also the number, where the oscillations are very weak or not discernible. Such a measurement done for several positions of the straight edge, shows that at any instant, the regions oscillating in phase occupy dimensions along the slit of about 10 to 12 seconds of arc, corresponding to an average dimension of 8,000 km on the sun. In between these regions are those with very weak oscillations of almost the same dimension. Considering this to be a typical size for the diameter of an oscillating cell, it is seen that at any time about 50% of the sun's surface around the centre is oscillating with vertical velocities of amplitudes above 150 metres/sec.

The root mean square of the amplitude determined from the prominent oscillations for the lines are given in Table III-2. The values of the amplitudes do not show a definite increase with height, although there is a suggestion of this. Also, the height difference between the lines is not large enough for a substantial decrease in density of the solar material to cause a significant increase in amplitude. In the CI 6587 line, the amplitude has been magnified by the noise in the records.

It is possible to follow the individual bursts of oscillations occurring at many points on the sun. The oscillations with amplitudes of 200 metres/sec and above last in general for 10 to 15 minutes. This can be considered to be a measure of their life time at these levels in the atmosphere. The amplitudes then fall off rapidly to negligible values. After a lapse of about 12-15 minutes, the oscillations build up again in the same region. There are many exceptions to this possibility, where one finds that the oscillations remain at insignificant amplitude levels for much longer periods of time, without any significant change.

Table III-2

r.m.s. amplitudes of oscillations in the spectral lines

Line	r.m.s. amplitude km/sec.
FeI 6358.695	.28
FeI 6344.162	.26
FeI 6335.345	.28
FeI 6593.884	.23
CaI 6572.795	.24
FeI 6336.837	.23
NiI 6586.319	.23
NiI 6339.125	.22
CH 4281.794	.23
CaI 4283.016	.25
FeI 6338.588	.22
FeI 6330.859	.22
CI 6587.622	.41 *

* Value high as the records are noisy.

The occurrence of oscillations, in bursts, have prompted many workers to favour the model, where the granules act as individual pistons giving rise to oscillatory motions, observed at these levels. This appears to be a simplification of the real situation. Such individual impulses generated in a random manner over space by the granular pistons, cannot obviously supply energy for the oscillations to occur coherently over a scale many times the size of the granules themselves.

The plot of velocity with reference to time, shows the solar surface to be covered with oscillations, but a careful scrutiny will reveal these oscillations to be quite complex in nature. When examined in detail, the oscillations in neighbouring regions do not seem to have a one to one correspondence, but only some gross characteristics in common. The behaviour of these quasi-periodic oscillations can best be described only in statistical terms. The dimensions of the oscillating regions, the life time of the bursts etc. estimated above should be considered only to represent some of their general characteristics and not as rigid quantitative estimates.

The oscillations in the weak lines (e.g. 6330.859Å and 6338.588Å) show noise, seen as fluctuations superposed on the oscillations. The high level lines are free from these. Prominent oscillations can be easily traced at all the levels; thus there is a high degree of coherence in the wave pattern spatially. One high amplitude oscillation extending for about 8500 km in the region indicated by 'A' (Figure III-1) in the plot of 6330.859Å line is also seen in the 6338.588Å line. But this feature is not seen so markedly in the high level lines. This may be due to the filtering effects in the solar atmosphere.

The line 6330.859Å has a Rowland intensity 2, an excitation potential of 4.73 e.v. and a gf value of 0.19. For the line 6338.588Å, the corresponding values are 2, 4.79, e.v. and 0.42 respectively. The velocity plots for the two lines show only as much similarity between themselves, as they have with any other line. There is a gross resemblance in the waveforms, but the similarity does not extend upto the smallest features. It looks as though, two lines having identical strengths and excitation characteristics may not show identical velocity patterns.

The oscillations having amplitudes more than 200 metres/sec. have been picked out and the periods have been determined from such waves. The results are plotted in the form of histogram in Figure III-5 for all the lines. The histograms show that the predominant period of oscillation in the levels under study, lie in the range of 280 to 310 seconds. Precise determination of the period of these oscillations requires detailed statistical analysis which are discussed in the following paragraphs.

3.5. Power spectrum analysis

For a reliable and precise determination of the predominant periods, I have done power spectrum analysis of the velocity data for all the lines. The auto-correlation functions were first calculated and then the Fourier transformation of these functions yielded the power spectra in the frequency domain. The theory and application of the techniques of power spectra analysis have been discussed in detail by Blackman and Tukey (1958). The present analysis closely follows the methods of Blackman and Tukey and is briefly described below.

A continuous record of velocity at any point on the solar surface, lasting for a finite length of time T,

FIGURE III-5

The distribution of periods of oscillation in 10 lines

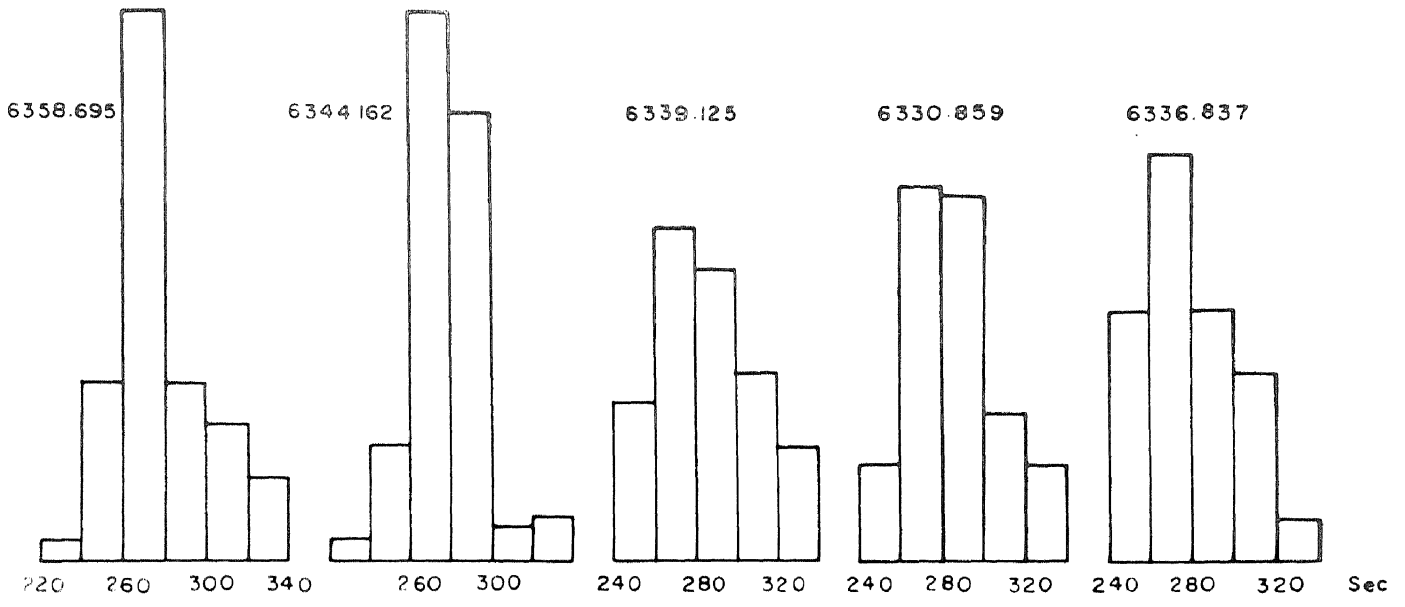
6358.695
6344.162
6339.125
6330.859
6336.837
220 260 300 340
260 300
240 280 320
240 280 320
240 280 320 Sec

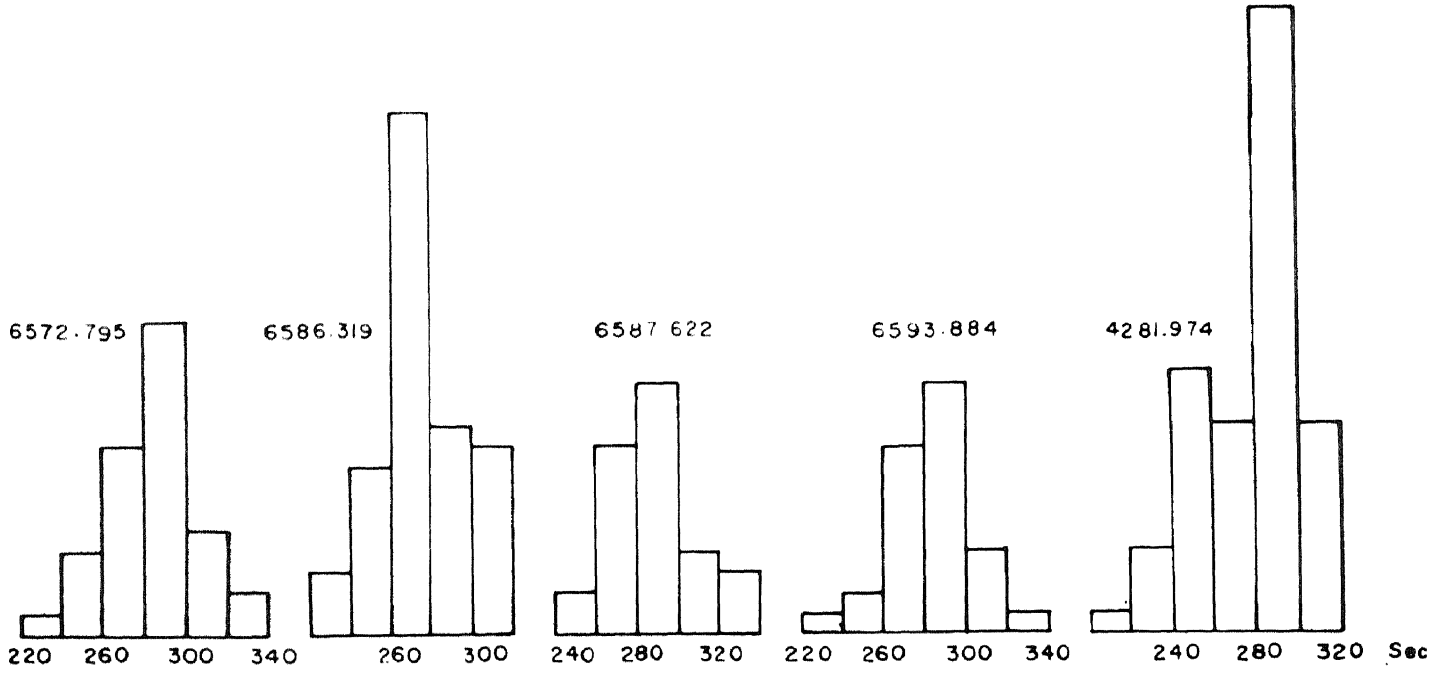
6572.795
6586.319
6587.622
6593.884
4281.974
220 260 300 340
260 300
240 280 320
220 260 300 340
240 280 320 Sec

Fig. III-5

represented by V (t), can be considered to form a stationary time series.

The auto-covariance function for such a series for a lag τ is given by

$$C(\tau) = \lim_{T \to \infty} \frac{1}{T} \int_{-T/2}^{+T/2} V(t) \cdot V(t+\tau) \cdot dt \qquad (3.1)$$

The power spectrum of the above function at frequency 'ν' expressed as a two sided cosine transform is given by

$$P(\nu) = \int_{-\infty}^{+\infty} C(\tau)\, e^{-i 2\pi \nu \tau}\, d\tau \qquad (3.2)$$

The relation between C (τ) and P (ν) may be more simply expressed as a one sided cosine transform viz.

$$P(\nu) = 2 \int_{0}^{\infty} C(\tau) \cos 2\pi \nu \tau \cdot d\tau \qquad (3.3)$$

Usually, as in the present case, the data consists of velocities in digitised form spaced at as close intervals as permitted by observational procedures.

instead of continuous records. Thus if V_1, V_2, V_3 ... V_n are the values of the velocities at equispaced intervals of time, then the general term for the auto-covariance function C_r is given by

$$C_r = \frac{1}{n-r} \sum_{1}^{n-r} V_t \cdot V_{t+r} - \left(\frac{1}{n} \sum_{1}^{n} V_t \right)^2 \qquad (3.4)$$

This is the mean lagged product with adjustment for the mean, for a total of 'n' data points. A series of auto-covariance functions C_1, C_2 ... C_m are calculated with values for $r = 0, 1, 2 \ldots m$. In practice, it is necessary to keep the maximum value of r at a small fraction of n, to preserve a reasonable stability for the estimates. Next, using these values, the finite cosine series transforms are calculated and the general term is given by,

$$P_r(\omega) = \Delta\tau \left[C_0 + 2 \sum_{l=1}^{m-1} C_l \cos\left(\frac{l r \pi}{m}\right) + C_m \cos r\pi \right] \qquad (3.5)$$

where $\Delta\tau$ is the interval between two consecutive data points. This represents the unsmoothed power estimate for a frequency of $(r/2m\,\Delta\tau)$ cycles per second. The spectral estimates are smoothed by using a suitable

smoothing or 'window' factor. I have used a 'hanning window' in this analysis. This modifies the spectral estimates by the following weighting functions.

$$U_0 = 0.5\,V_0 + 0.5\,V_1$$

$$U_r = 0.25\,V_{r-1} + 0.5\,V_r + 0.25\,V_{r+1} \qquad (3.6)$$

and $$U_m = 0.5\,V_{m-1} + 0.5\,V_m \qquad 1 \leq r \leq m-1$$

The time sequences have been obtained at intervals of 20 seconds and 15 seconds. The velocities obtained at this interval has meant some loss of information. This does not, however, affect the results, as the information is lost only for frequencies above the nyquist frequency which is $\nu_n = \frac{1}{2\Delta\tau} = 25 \times 10^{-3}$ Hz. Besides, 20 sec. is an interval too small compared to the period of oscillation. Also, with a spacing of 20 sec. or 15 sec. there is no problem due to aliasing of frequencies.

3.6. Power spectrum analysis of "High Resolution"

It is the usual practice to obtain the power spectrum with one value for the maximum lag, for calculating the auto-correlation functions. This value of the lag is so chosen as to yield estimates in the neighbourhood of

frequencies, where the suspected periodicities lie. But, with limited length of data the power spectrum obtained thus has usually a poor frequency resolution for the spectral estimates. In the present analysis, I have varied the lag and computed spectral estimates of velocities for all the lines, for five different lags. The five values chosen are close to one another and are around 30% of the total length of the data. Each lag gives power estimates at the frequencies appropriate to it. With the estimates for the different lags put together, the frequency resolution can be considerably increased. This was done the following way. The total number of velocity values or data points in any one row of the array is 120 for sequence A1082. The power spectrum with say 29 lags, gave the estimates at 286.6 sec. 290 sec. and 232 sec., with 30 lags, the estimates were at 400 sec., 300 sec., and 240 sec., besides at other periods far away from the period range of present interest. Similarly, with 31, 37 and 38 lags, the estimates at periods 310 sec., 296 sec., and 304 sec., respectively were obtained, besides the estimates of power at periods above and below these values. The power spectral density derived from all the five lags for the periods 290 sec., 296., 300., 304., and 310 sec., were then

collected together for comparison. A correction is required before these results can be directly compared. The band width corresponding to each estimate may be taken as $1/T_m$, where T_m is the maximum value of the lag used. Therefore, when the lag is increased, the frequency bandwidth over which the estimates are obtained, decreases and consequently the power falls. This fall in power, due to the change in bandwidth can be compensated for, by multiplying by a factor equal to the ratio of the bandwidths, i.e. the estimates obtained with lag 38 can be compared with that of lag 31 after multiplying the former by the factor (38/31) in the period range of our interest. Thus the estimates with different lags were brought to a common scale and then compared. It became possible by this method to determine uniquely the predominant period of the oscillations for the different lines, within 5 seconds. It is necessary, that the lags chosen, lie close together; otherwise for lags far apart the stability may significantly change and make such a comparison impossible.

3.7. Contribution curves for the solar lines

Contribution curves for eight of the solar lines utilized in this study were computed by the method of

weighting functions. This method first developed by Unsöld and Minnaert for weak lines was extended to strong lines by Pecker, by the introduction of the saturation function ψ .

The model atmosphere, I have used for these computations is the one proposed by Elste (1967). This model is a modification of the Bilderberg continuum atmosphere. The numerical values of the parameters of the model viz. the temperature T, electron pressure P_e and the continuous absorption coefficient $K_o P_e$ are given as a function of log τ for the wavelength 5000Å in Table III-3. The log τ values range from -3.2 to + 1.0 in steps of 0.2.

Following Pecker (1953) the line depth r, defined as

$$r = \frac{\bar{I}_{\lambda_0}(0,\mu) - \bar{I}_{\Delta\lambda}(0,\mu)}{\bar{I}_{\lambda_0}(0,\mu)} \qquad (3.7)$$

may be written in the form

$$r = \int_0^\infty G(\tau')\,\psi\left(\frac{k_{\Delta\lambda}}{k_{\lambda_0}}\right)\frac{d\tau'}{\mu} \qquad (3.8)$$

Table III-3

Model Atmosphere - Slate Model

Log τ_{5000}	T °K	P_e dynes/Cm^{-2}	K_o in 10^{-26} per hydrogen atom.
-3.2	4594	.1858	2.1446
-3.0	4586	.2296	2.6312
-2.8	4574	.2818	3.2351
-2.6	4574	.3491	3.9623
-2.4	4574	.4315	4.8630
-2.2	4586	.5383	5.9428
-2.0	4615	.6823	7.2938
-1.8	4684	.8995	8.9770
-1.6	4773	1.205	11.0619
-1.4	4874	1.633	13.6682
-1.2	4995	2.265	17.1007
-1.0	5132	3.206	21.6405
-0.8	5294	4.732	28.2027
-0.6	5490	7.516	38.9329
-0.4	5734	13.27	58.2553
-0.2	6043	27.04	97.8848
0.0	6428	62.52	180.6828
+0.2	6876	151.71	348.9100
+0.4	7347	349.12	649.3260
+0.6	7802	717.80	1126.9460
+0.8	8182	1242.02	1738.8000
+1.0	8470	1845.01	2416.9500

where G (τ') is the weighting function and is given by

$$G_1(\tau') = \frac{\int_{\tau'}^{\infty} B(\tau)\, e^{-\tau/\mu} \frac{d\tau}{\mu} - B(\tau')\, e^{-\tau'/\mu}}{\int_0^{\infty} B(\tau)\, e^{-\tau'/\mu} \frac{d\tau'}{\mu}} \qquad (3.9)$$

The saturation function introduced by Pecker can be written as,

$$\psi = e^{-\int_0^{\tau'} \left(\frac{k_{\Delta\lambda}}{k_{\lambda_0}}\right) \frac{d\tau}{\mu}} \qquad (3.10)$$

The source function which has been set equal to the Plank function can be expanded in the form

$$B(\tau) = a + b\tau + c\, E_2(\tau) \qquad (3.11)$$

where E_2 (τ) is the exponential integral. Substituting the expansion of B (τ) from 3.11 in equation (3.9) and integrating the expression, the weighting function can be written as

$$G_1(\tau) = \frac{\mu e^{-\tau/\mu}\left[b - c\,E_1(\tau) + c\,E_1\left(\frac{\tau}{\mu}+\tau\right)\right]}{a + b\mu + c\left[1 - \mu \ln\left(1+\frac{1}{\mu}\right)\right]} \qquad (3.12)$$

I computed the weighting functions for three wavelengths viz. 6600Å, 6350Å and 4300Å which correspond to the region of the three time sequences. The values of $E_1(\tau)$ for the corresponding values of τ of the model atmosphere were picked out from the tables prepared by Katterbach and Krause (1949). The values of the constants, a, b and c at these wavelength regions were obtained by interpolation from the limb darkening observations of Pierce and Waddell (1961). Since my observations are at the centre of the solar disc μ can be set equal to 1.

Table III-4 gives the values of the weighting functions thus computed. It is convenient to integrate equation 3.8 over a log scale as done by Slate (1955). Equation 3.8 then becomes,

$$r = \int_{-\infty}^{+\infty} \frac{G\, k_{\Delta\lambda}\, \tau\, \psi}{\mu\, k_{\lambda 0}\, \mathrm{Mod}}\, d(\log \tau) \qquad (3.13)$$

where Mod = 0.4343

and $$\psi = e^{-\int_{\alpha}^{\log \tau'} \frac{k_{\Delta\lambda}\, \tau}{k_{\lambda 0}\, \mu\, \mathrm{Mod}}\, d(\log \tau)} \qquad (3.14)$$

Table III-4

Weighting functions for Elste Model

Log τ_{5000}	λ = 4300Å	λ = 6350Å	λ = 6600Å
-3.2	.891668	.722417	.704965
-3.0	.898392	.733376	.716034
-2.8	.896806	.731547	.714212
-2.6	.896806	.731547	.714212
-2.4	.894352	.728994	.711693
-2.2	.890675	.725194	.707914
-2.0	.887928	.722121	.704866
-1.8	.879823	.713907	.696742
-1.6	.869483	.703346	.686302
-1.4	.851278	.684649	.667771
-1.2	.826113	.659436	.642836
-1.0	.785575	.618190	.602018
-0.8	.729787	.565048	.549642
-0.6	.645245	.482086	.467681
-0.4	.535883	.381786	.368999
-0.2	.405545	.271314	.260867
0.0	.266284	.164562	.157104
+0.2	.141992	.081299	.077040
+0.4	.054678	.029706	.027995
+0.6	.012469	.006647	.006252
+0.8	.001212	.000644	.000605
+1.0	.000030	.000016	.000015

The selective absorption coefficient $k_{\Delta\lambda}$, per hydrogen atom can be expressed as

$$k_{\Delta\lambda} = \frac{\sqrt{\pi}\, e^2 \lambda_0^2}{m c^2} \cdot A \cdot f \cdot \frac{Nia}{Na} \frac{1}{\Delta\lambda_D} e^{-\left(\frac{\Delta\lambda}{\Delta\lambda_D}\right)^2} \qquad (3.15)$$

where, A is the abundance of the element, f is the oscillator strength for the transition concerned, N_{ia} is the number of atoms of the element at the energy level corresponding to the transition giving rise to the line, Na is the total number of atoms of that element, and $\Delta\lambda_D$ is the Doppler width given by

$$\Delta\lambda_D = \frac{\lambda}{c}\left(\frac{2KT}{M} + \xi_t^2\right)^{1/2}$$

where K is the Boltzman's constant, T the effective temperature, M - is the mass of the atom and ξ_t is the micro-turbulent velocity component. ξ_t has been neglected in the computations.

Equation (3.13) can now be written as

$$r = C \int_{-\alpha}^{+\alpha} \frac{G \tau \psi\ Nia}{\mu K_{\lambda_0}\ Na\ \Delta\lambda_D} e^{-\left(\frac{\Delta\lambda}{\Delta\lambda_D}\right)^2} d(\log\tau) \qquad (3.16)$$

where $C = \dfrac{\sqrt{\pi}\, e^2 \lambda_0^2}{m c^2} A \cdot f \cdot \dfrac{1}{Mod}$

and the saturation function,

$$\psi = e^{-C \int_{-\infty}^{\log \tau'} \frac{\tau \, N_{ia}}{\mu K_{\lambda_0} N_a \Delta\lambda_D} e^{-\left(\frac{\Delta\lambda}{\Delta\lambda_D}\right)^2} d(\log \tau)} \qquad (3.17)$$

The saturation functions were computed for each value of ($\log \tau$) of the model atmosphere for all the lines, except for CI 6587. This line has a Rowland intensity of -1 and the ψ values calculated had no significant effect on the contribution functions.

An expression for N_{ia}/N_a from the combined Saha and Boltzmann equations, can be written as

$$\frac{N_{ia}}{N_a} = \frac{P_e g_{ia} e^{-\chi/kT}}{\left[U_0(T) P_e + 2U_1(T) e^{-I/kT} \phi T^{5/2}\right]} \qquad (3.18)$$

where P_e - is the electron pressure

g_{ia} - is the statistical weight of the level

U_0 (T) and U_1 (T) are the partition functions of the neutral and ionized atoms respectively and

$$\phi = (2\pi m)^{3/2} h^{-3} K^{5/2}$$

χ - the excitation potential

and I - is the ionization potential

For each line, the values of $\frac{N_{ia}}{N_a}$ were computed for the 22 temperature and electron pressure values corresponding to the 22 levels of the model atmosphere. The partition functions were picked out from a graphical interpolation of the values of Claas (1950). The oscillator strengths are those by Corliss and Warner (1964) or from N.B.S. Tables.

The contribution function which is the integrand of equation (3.16) given by

$$\Delta r(\tau) = C \psi \left[\frac{G \tau N_{ia}}{\mu K_{\lambda_0} N_a \Delta\lambda_D} e^{-\left(\frac{\Delta\lambda}{\Delta\lambda_D}\right)^2} \right] \qquad (3.19)$$

was computed for the 8 lines at a value of $\Delta\lambda$, where the Doppler displacements were measured. The curve for CH 4281.794 line was borrowed from the computations of Nirupama (1965). The contribution curves for these lines are plotted in Figures III-6 to III-10. The maximum of the curve corresponds on the log τ scale to the mean depth of formation of the absorption line. Table III-5 contains the values of the mean depth of formation of these lines.

FIGURES III-6 to III-10

Contribution curves of 8 solar lines as a function of optical depth τ . These are computed for the $\Delta\lambda$ at which the Doppler shifts were measured.

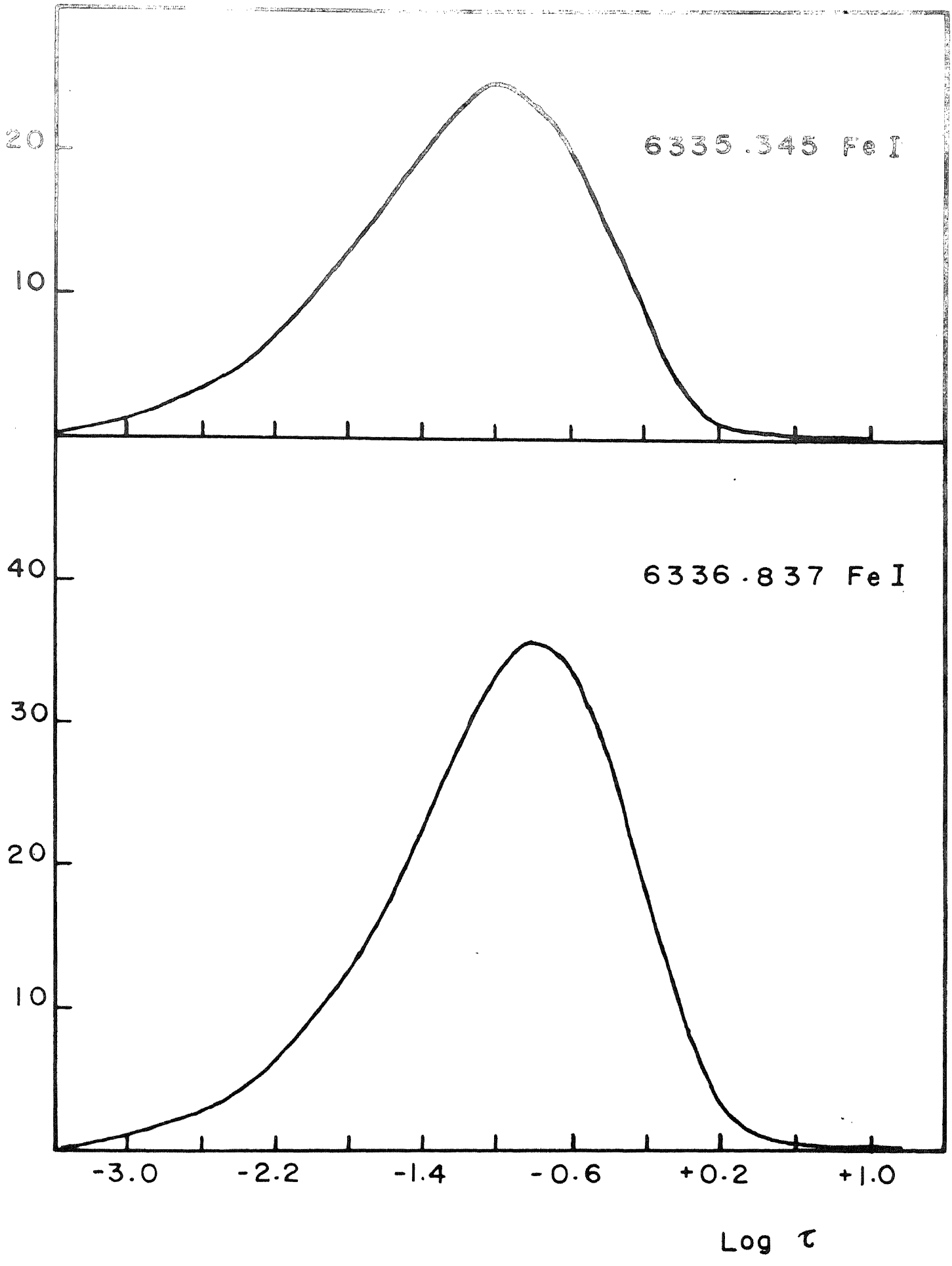

Fig. III-6

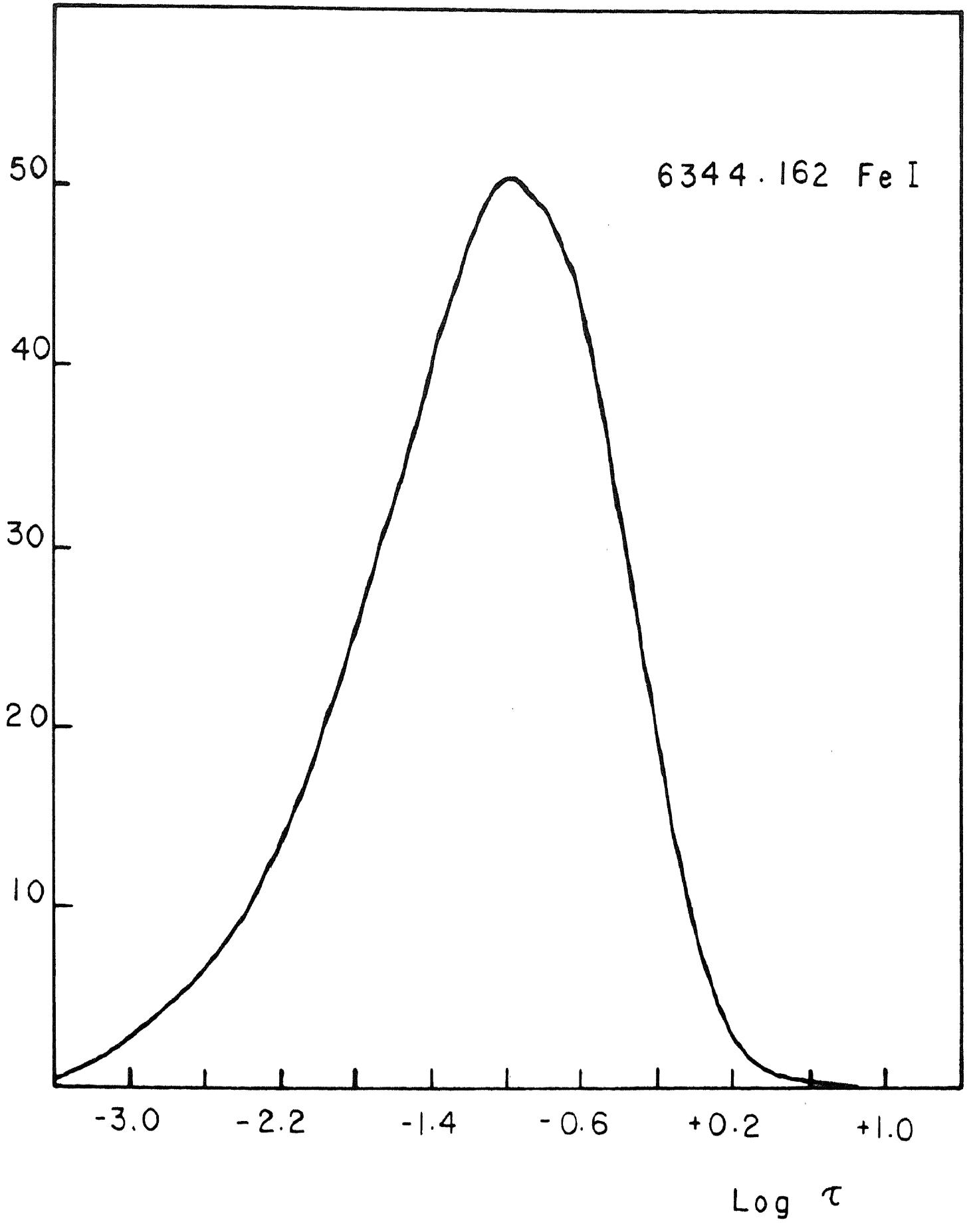

Fig. III-7

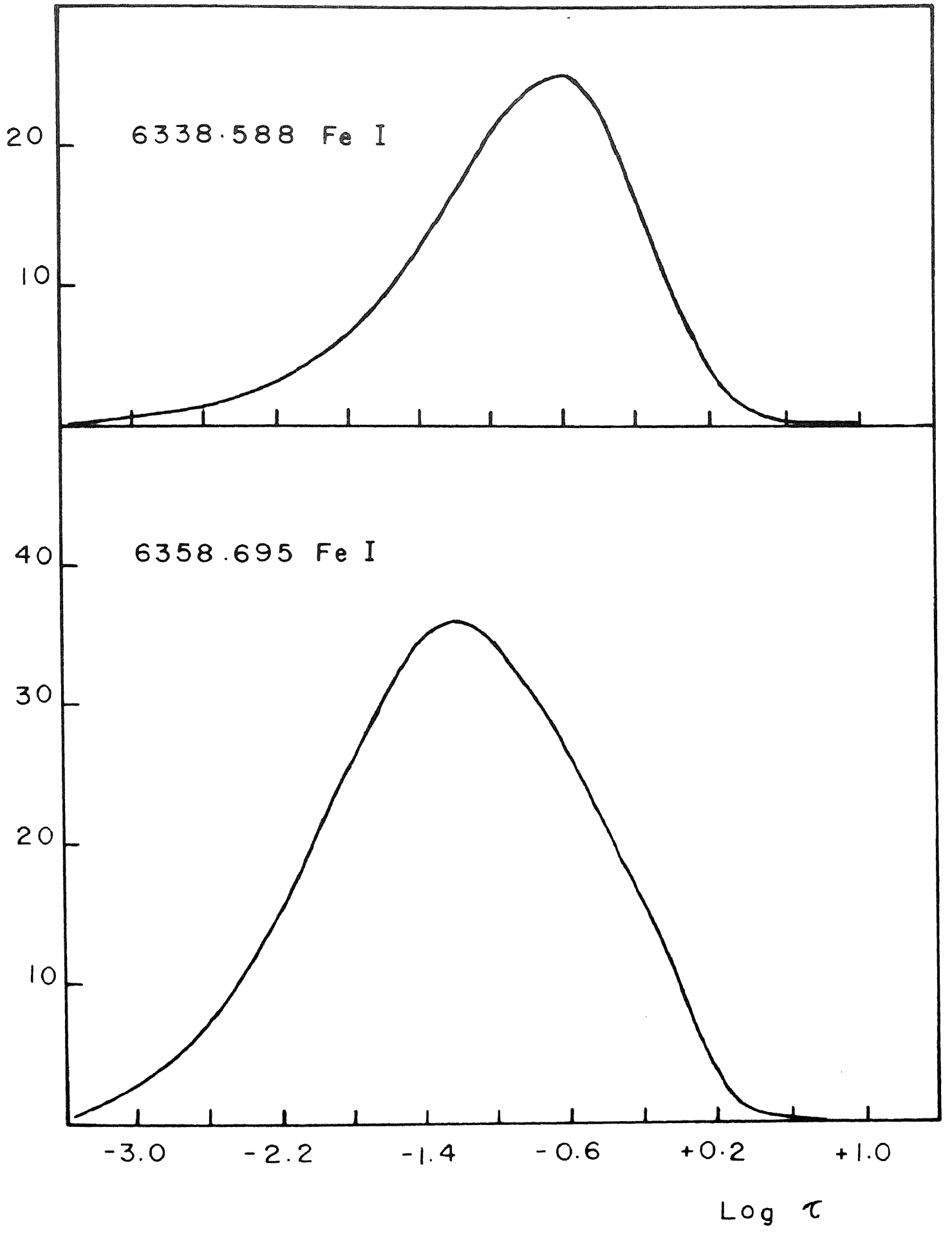

Fig . III - 8

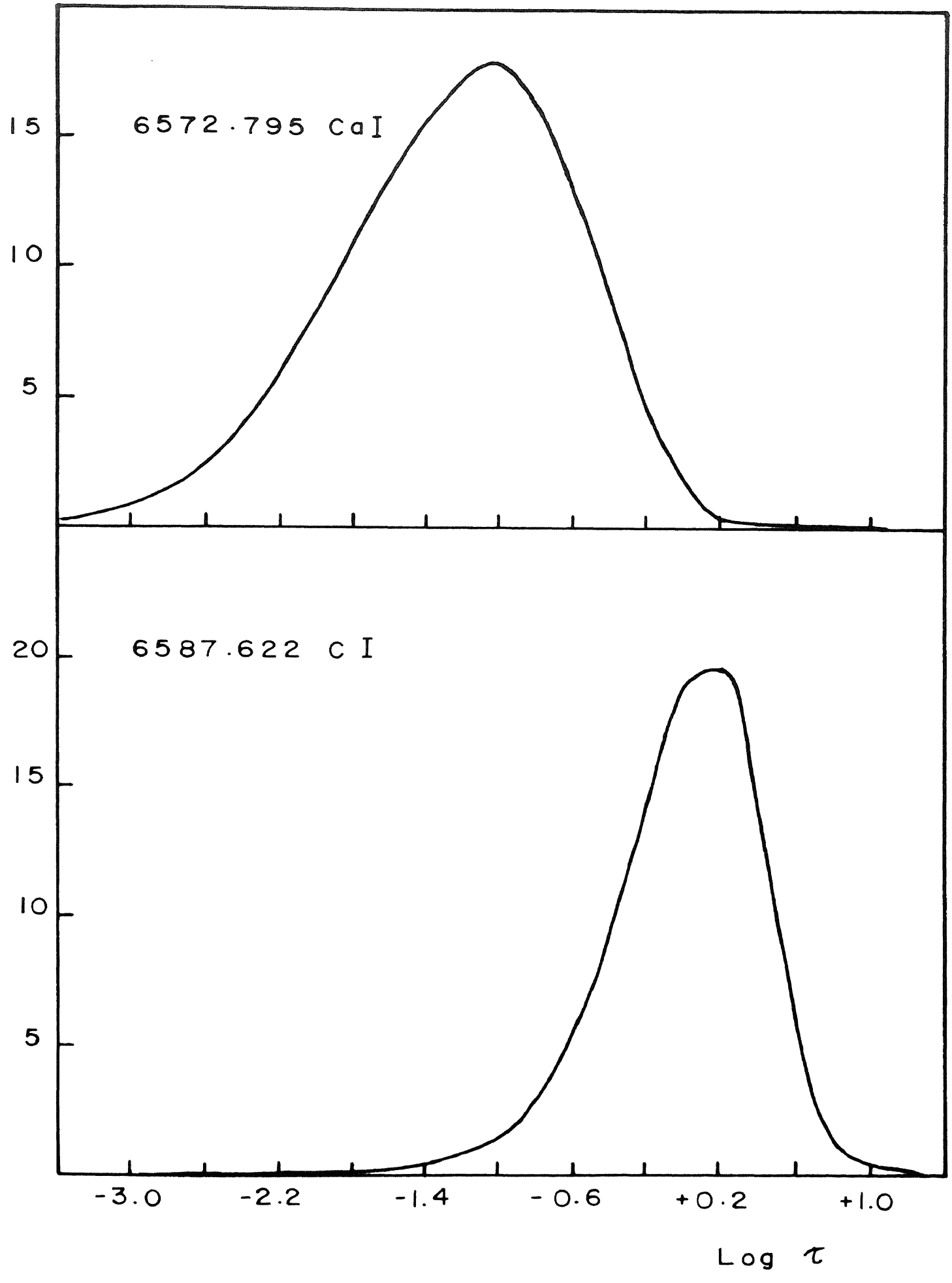

Fig . III - 9

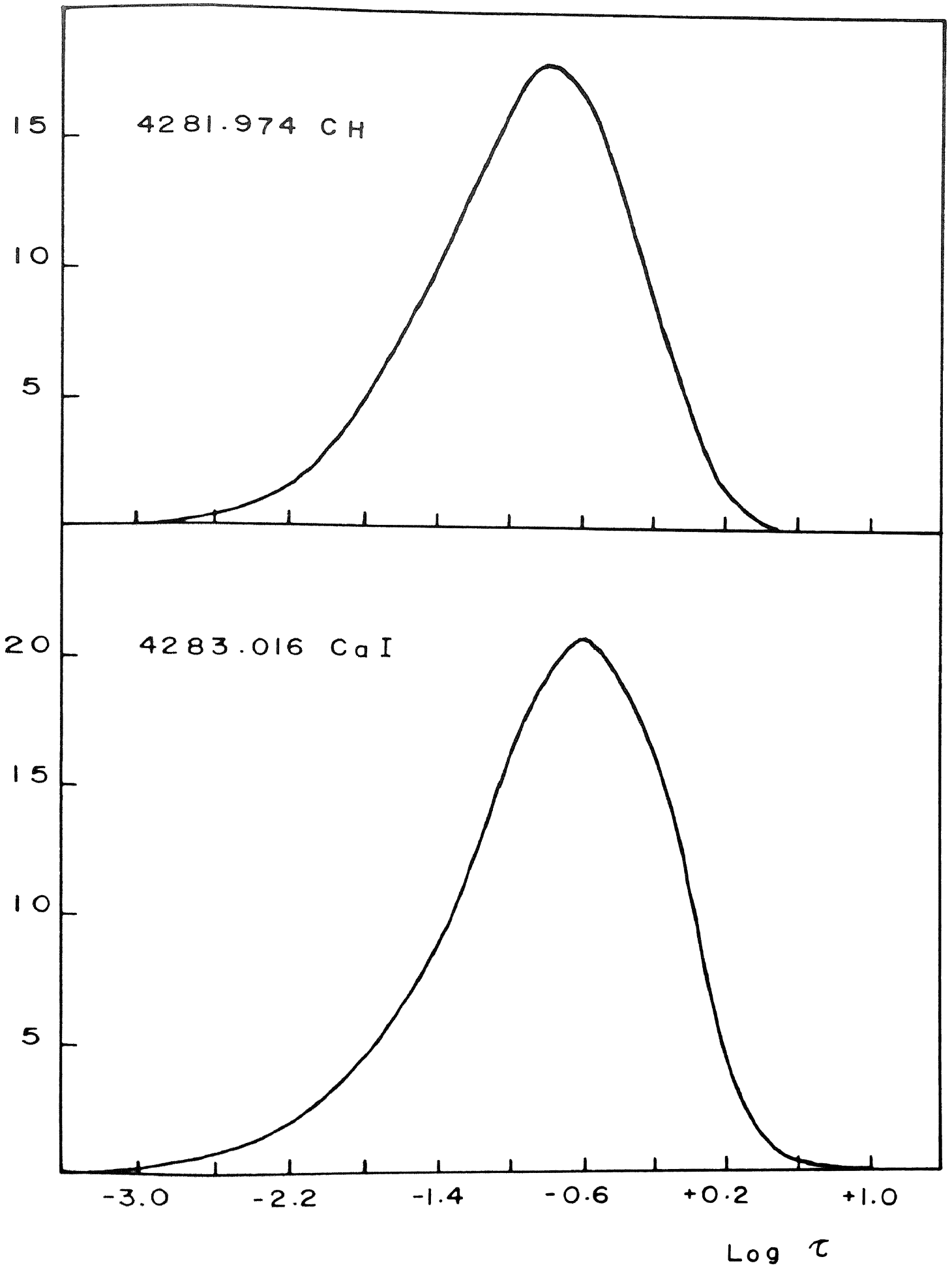

Fig . III-10

Table III-5

Mean depth of formation of lines

Line	λ	$\log \tau_{5000}$
FeI	6358.695	-1.2
FeI	6344.162	-1.0
FeI	6335.345	-1.0
CaI	6572.795	-1.0
FeI	6336.837	-0.8
CH	4281.794	-0.8
CaI	4283.016	-0.6
FeI	6338.588	-0.6
CI	6587.622	+0.2

3.8. Discussion of the velocity power spectra

For any one line the velocity data consists of 61 rows. The power spectrum for each row was calculated. The power spectrum for two of the lines FeI 6338 and FeI 6358 are shown in Figures III-11 and III-12 for 50 consecutive rows. The behaviour of individual points on the sun, 1080 km apart shown by these curves can be summarized thus:

1) The regions where, coherent oscillations prevail can be picked out much easier by their high power. The dimension of the oscillating cell can be seen to be about 8000 km, by counting successive curves looking alike.

2) The frequency (or period) shift in the curves can be noticed. Occasionally there are curves with two peaks, one at 337 seconds and another at 236 seconds. These show that a unique value cannot be assigned for the period for any line. This is to be expected since a line is formed over a range of depths in the solar atmosphere, within which, the physical properties cannot be uniform and the levitation effects are significant. The resonant frequency of such an atmosphere is bound to have a range of values, rather than a unique value.

FIGURE III-11

Power spectra of velocities in FeI 6338.588 line at 51 consecutive points 1080 km apart on the solar surface. The distribution of periods of oscillation can be seen from the shifts of the peak in the power curve. Areas oflarge amplitude oscillations and areas of no oscillations can also be seen.

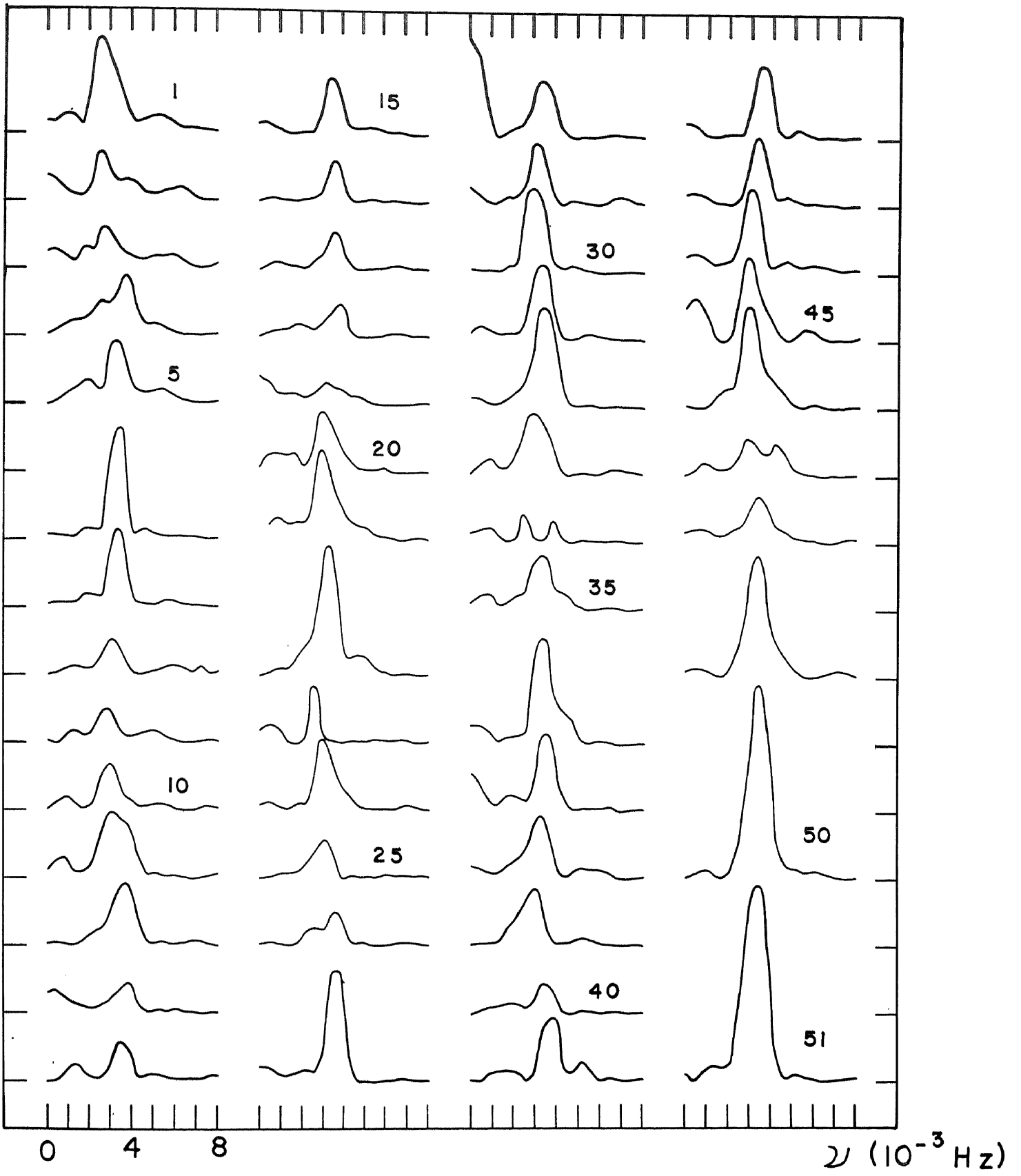

Fig. III - 11

FIGURE III-12

Power spectra of velocities in FeI 6358.695 line at 49 consecutive points, 1080 km apart on the solar surface.

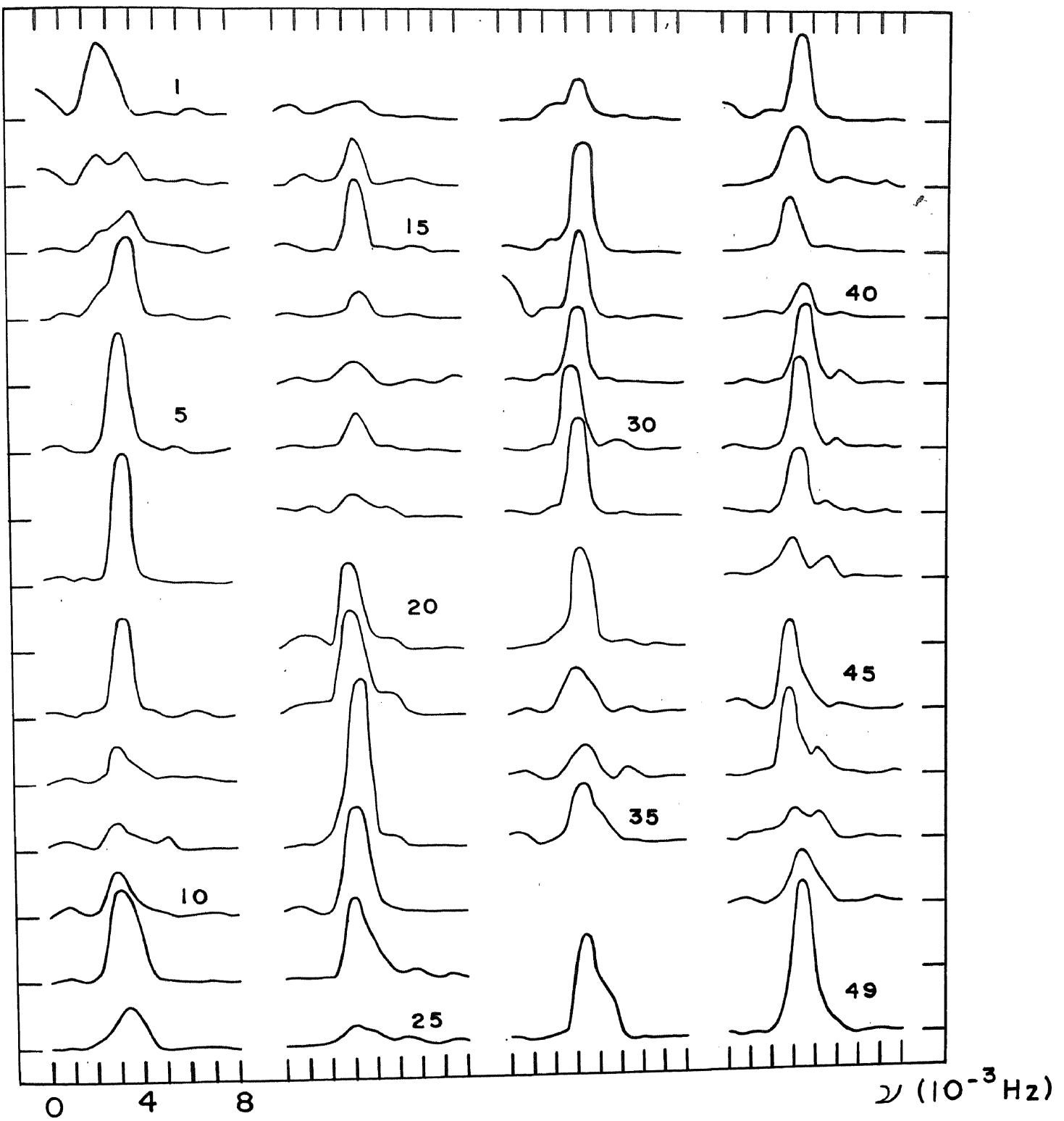

Fig. III-12

3) There is a high degree of resemblance in the power spectra at the two levels both in the vigorously and weakly oscillating regions.

The 61 power spectrum curves were then averaged frequency-wise to yield the final average power spectrum curve for each line. This process of averaging will enhance the statistical weight of the power spectrum. The average time power spectra of velocities for the lines are shown in Figures III-13 to III-19. The abscissa is in units of frequency for convenience in plotting. All the curves show pronounced peak power around the period 300 seconds ($\nu = 3.33 \times 10^{-3}$ Hz) which represents the resonance range of the oscillations on the solar surface. The tall peak in the power suggests that the noise in the measurements is quite small. The power in the resonance range obtained for the five lags were compared after applying the correction factor, described earlier. This gave me the period of oscillations for the different levels in the solar atmosphere. Although, I am aware that no unique value for the period can be assigned, my aim was to determine a value for the most probable period of these oscillations characterising each line, accurately at a high resolution in the frequency domain.

FIGURES III-13 to III-19

Power spectra of the velocity fluctuations in all the 14 lines under study. The sharpness of the resonance peak increases with height in the solar atmosphere

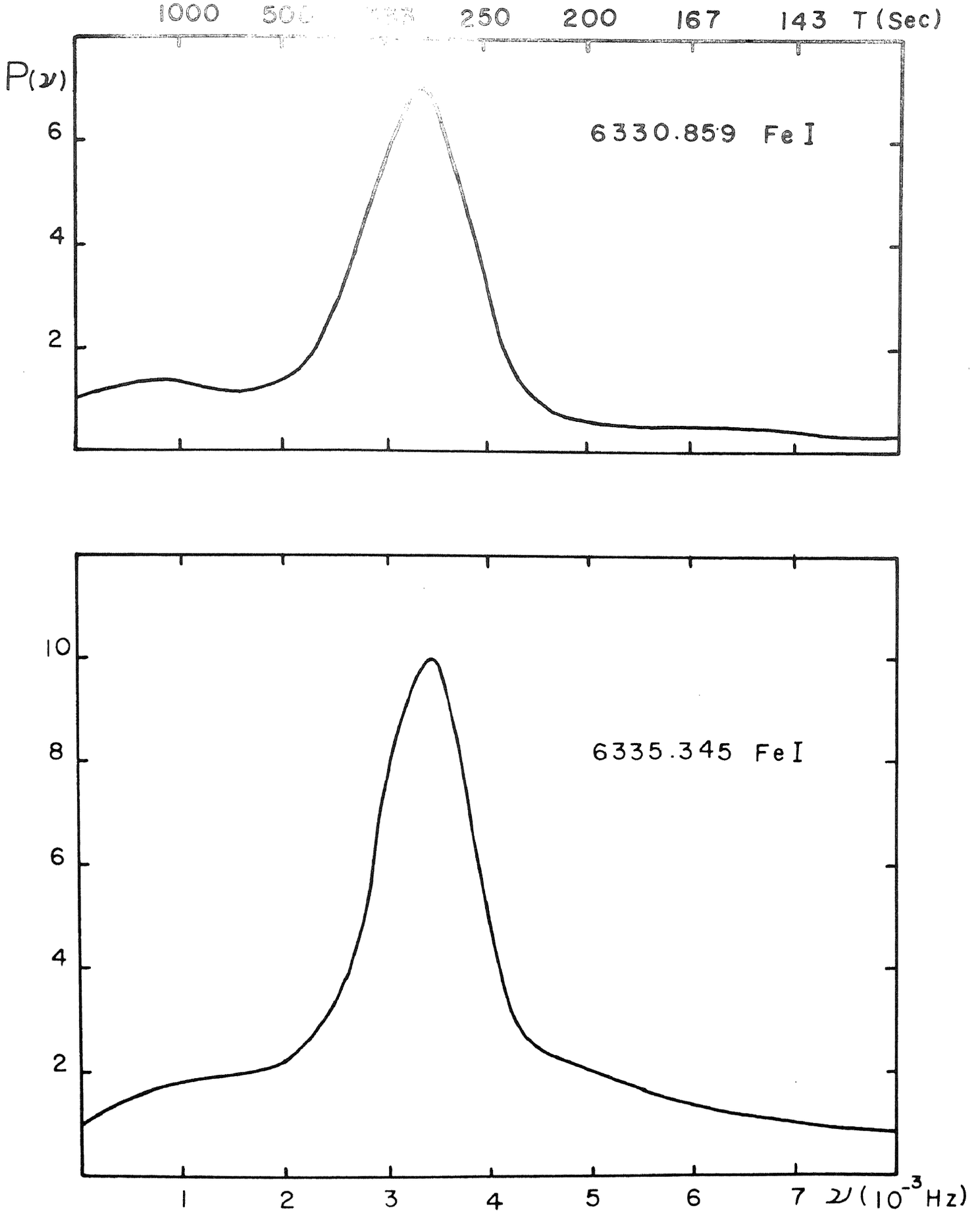
1000
250
200
167
143
T (Sec)
P(ν)
6
4
2
6330.859 Fe I
10
8
6
4
2
6335.345 Fe I
1
2
3
4
5
6
7
ν (10⁻³ Hz)

Fig. III-13

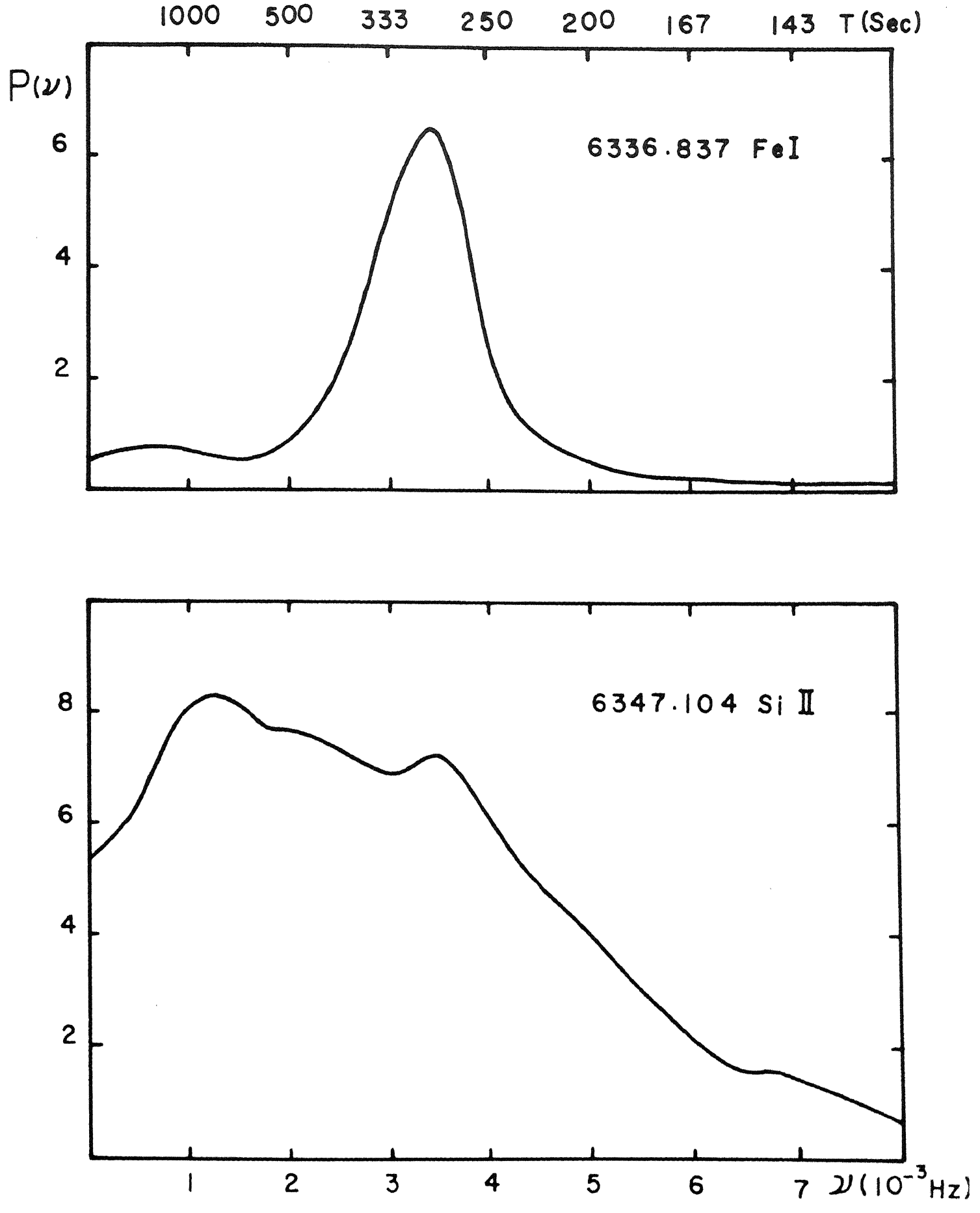
1000 500 333 250 200 167 143 T(Sec)
P(ν)
6
4
2
6336.837 FeI
8
6
4
2
6347.104 Si II
1 2 3 4 5 6 7 ν(10⁻³Hz)

Fig. III-14

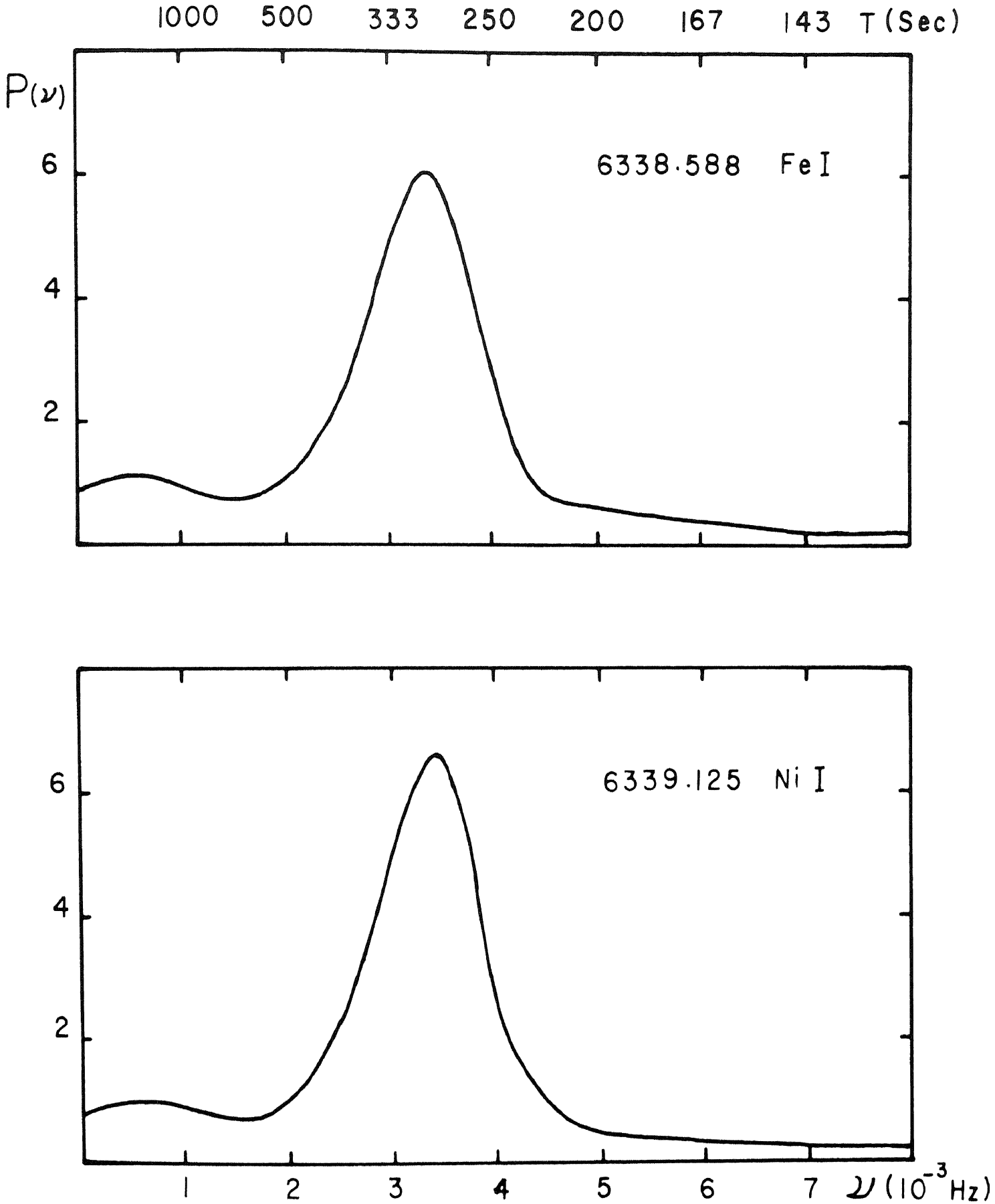
1000 500 333 250 200 167 143 T (Sec)
P(ν)
6
4
2
6338.588 Fe I
6339.125 Ni I
1 2 3 4 5 6 7 ν (10⁻³ Hz)

Fig . III - 15

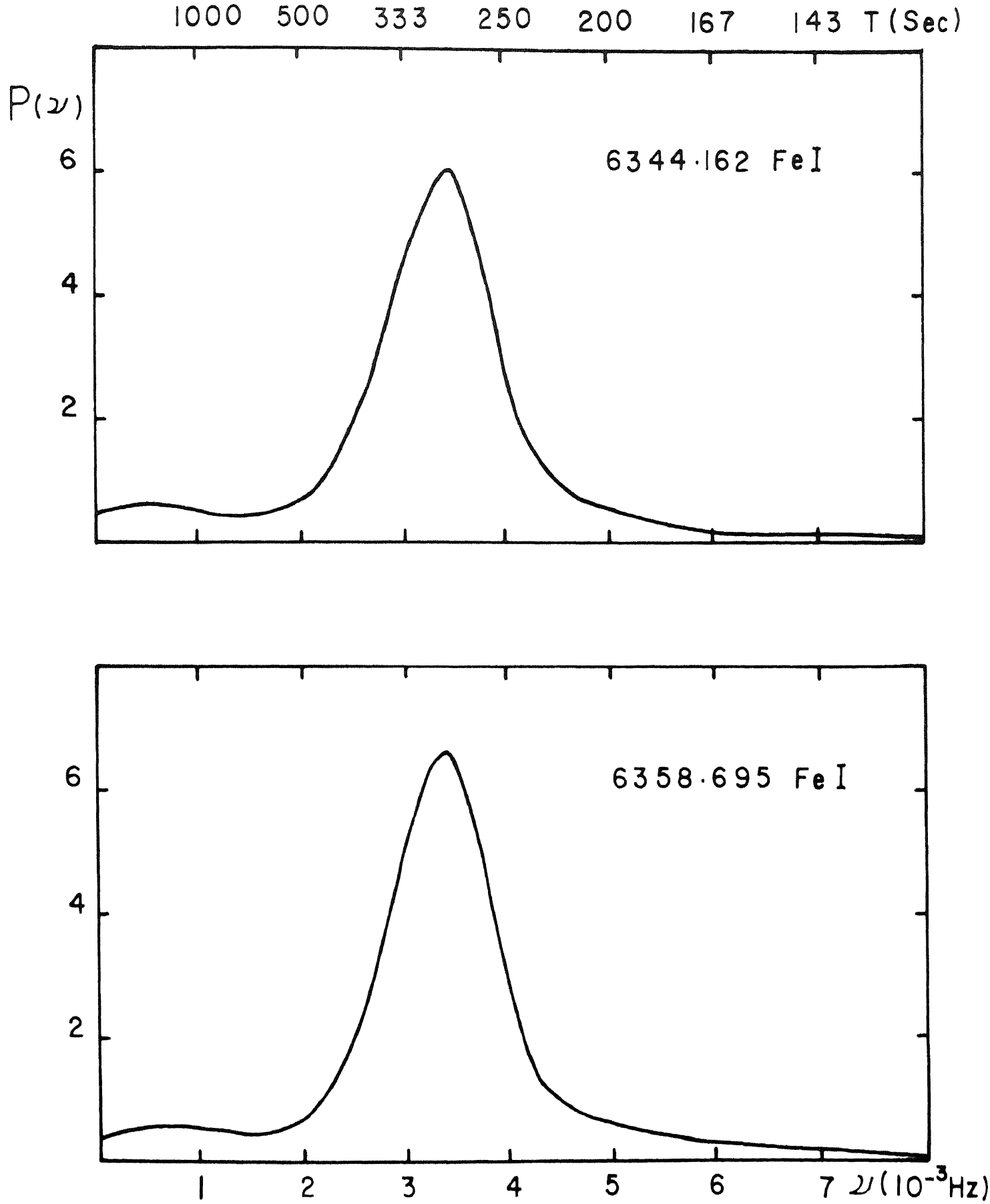
1000 500 333 250 200 167 143 T(Sec)
P(ν)
6
4
2
6344·162 FeI
6358·695 FeI
1 2 3 4 5 6 7 ν(10⁻³Hz)

Fig . III-16

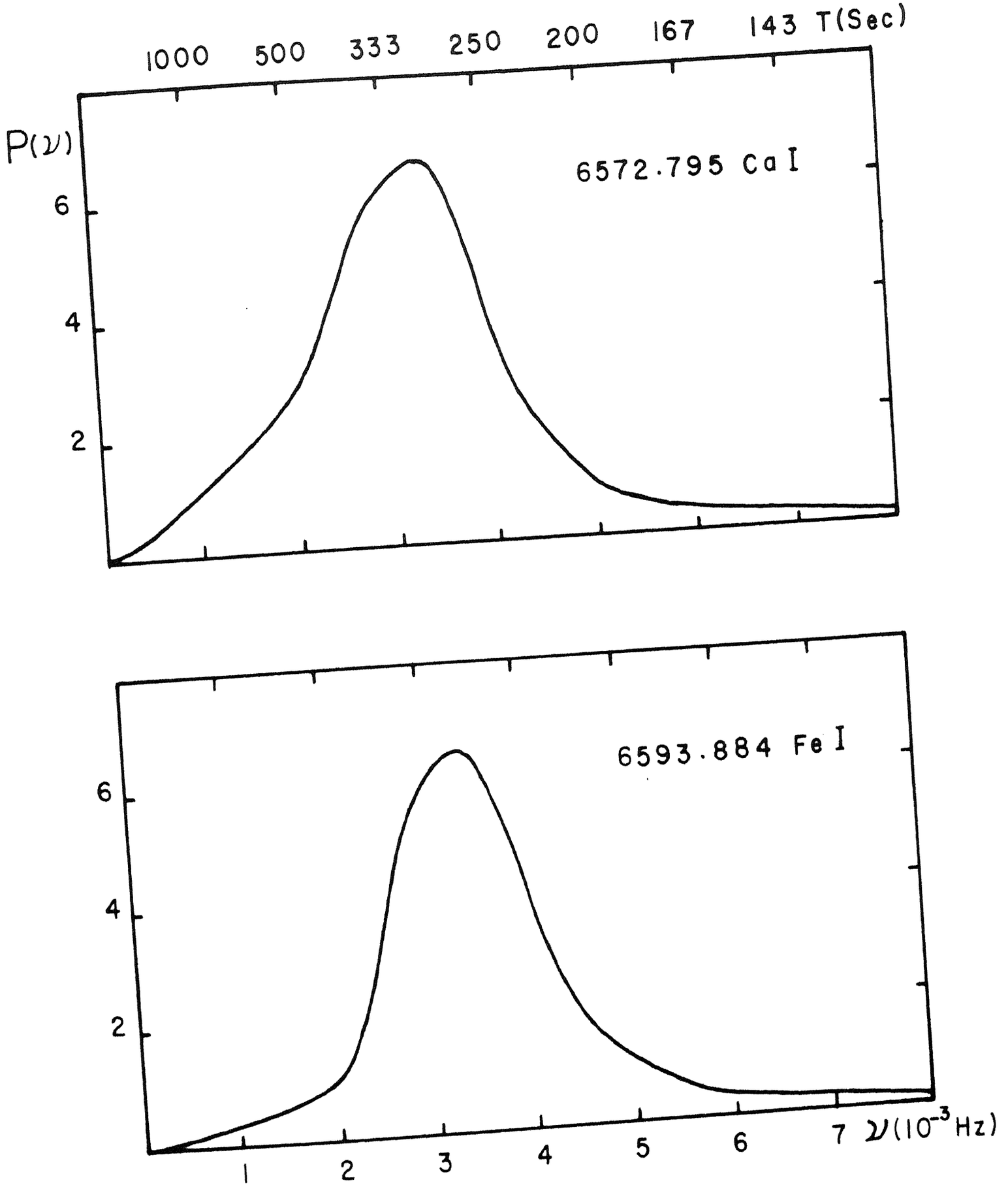
1000 500 333 250 200 167 143 T(Sec)
P(ν)
6572.795 Ca I
6
4
2
6593.884 Fe I
6
4
2
1 2 3 4 5 6 7 ν(10⁻³ Hz)

Fig. III - 17

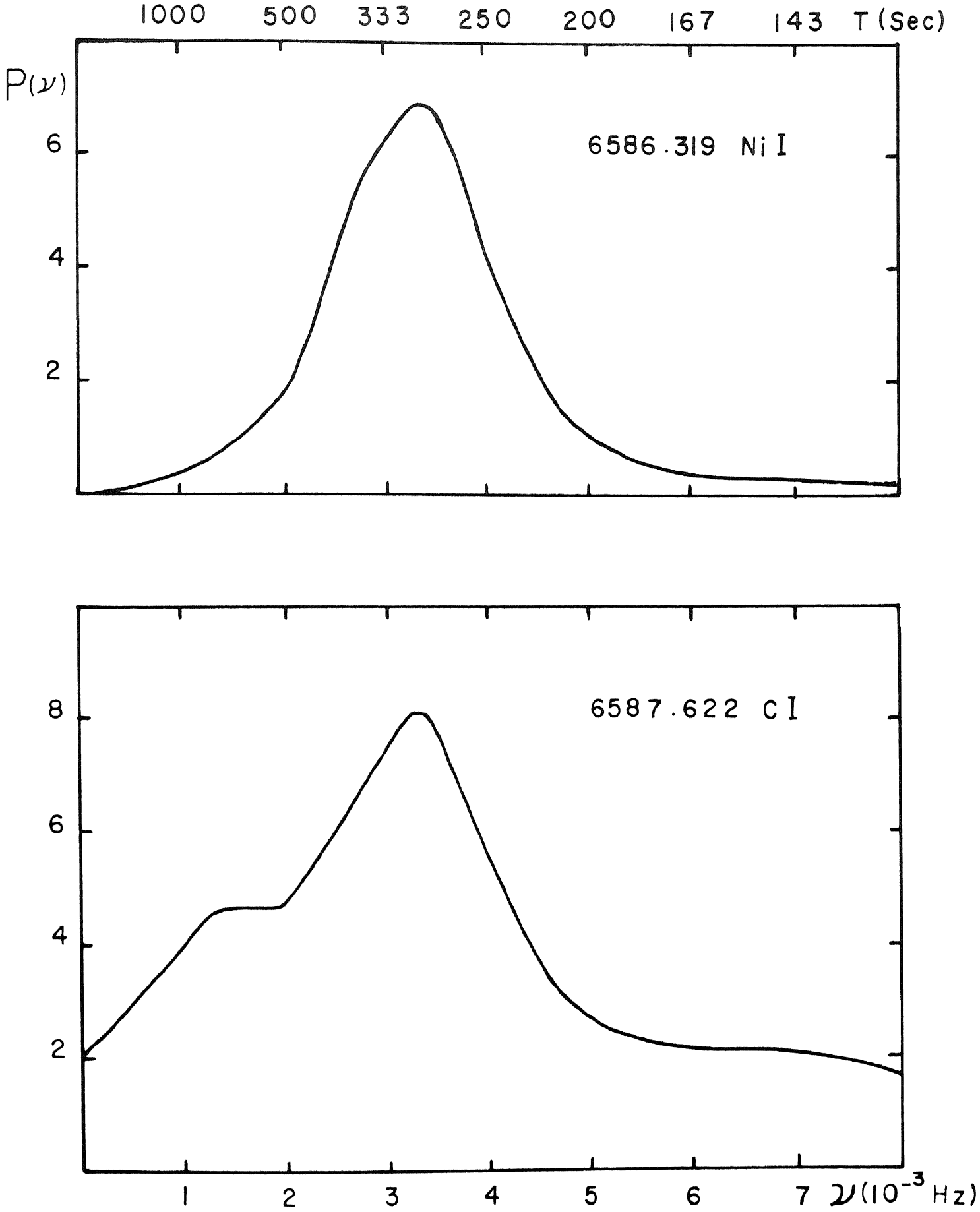
1000
500
333
250
200
167
143
T (Sec)
P(ν)
6
4
2
6586.319 Ni I
8
6
4
2
6587.622 C I
1
2
3
4
5
6
7
ν(10⁻³ Hz)

Fig . III - 18

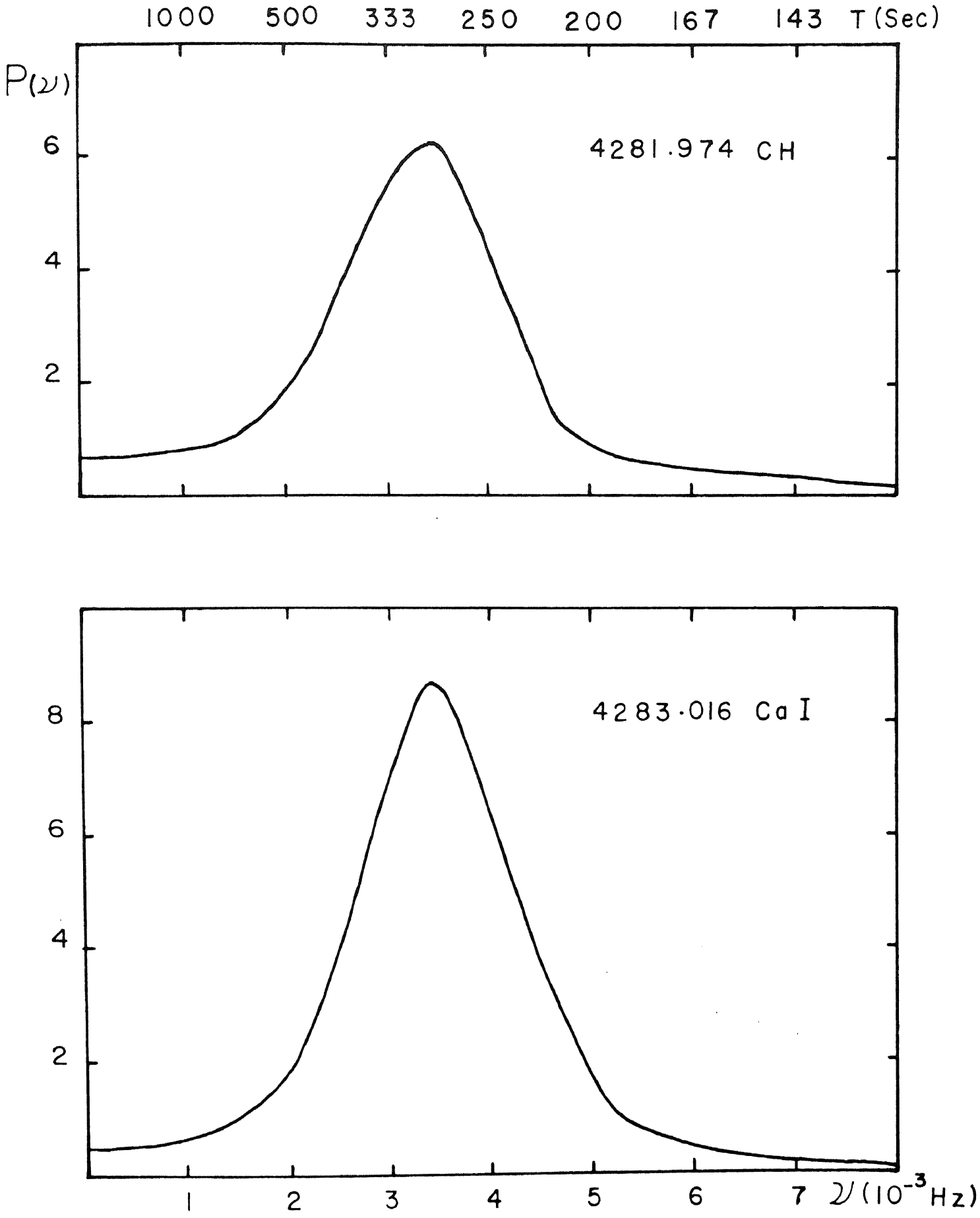
1000 500 333 250 200 167 143 T(Sec)
P(ν)
6
4
2
4281.974 CH
8
6
4
2
4283.016 Ca I
1 2 3 4 5 6 7 ν(10⁻³Hz)

Fig. III-19

The values of the periods are set out in Table III-6, where the lines are arranged the way they occur in height in the solar atmosphere, with the CI 6587 line at the bottom and the FeI 6358 line at the top. The mean depth of formation of these lines have also been included in the table, in terms of log τ_{5000} derived from the contribution curves for these lines. Figure III-20 shows a plot of the periods against the mean depth of formation of the lines.

Table III-6

Period of oscillation in the spectral lines.

Line	λ	Period Secs.	Log τ
FeI	6358.695	295	-1.2
FeI	6344.162	295	-1.0
FeI	6335.345	295	-1.0
FeI	6593.884	295	-
CaI	6572.795	295	-1.0
FeI	6336.837	295	-0.8
NiI	6586.319	295	-
NiI	6339.125	295	-
CH	4281.794	295	-0.8
CaI	4283.016	295-300	-0.6
FeI	6338.588	295-300	-0.6
FeI	6330.859	295-300	-
CI	6587.622	304	+0.2

FIGURE III-20

A plot of the period of oscillation observed in the lines against their mean depth of formation in terms of log τ.

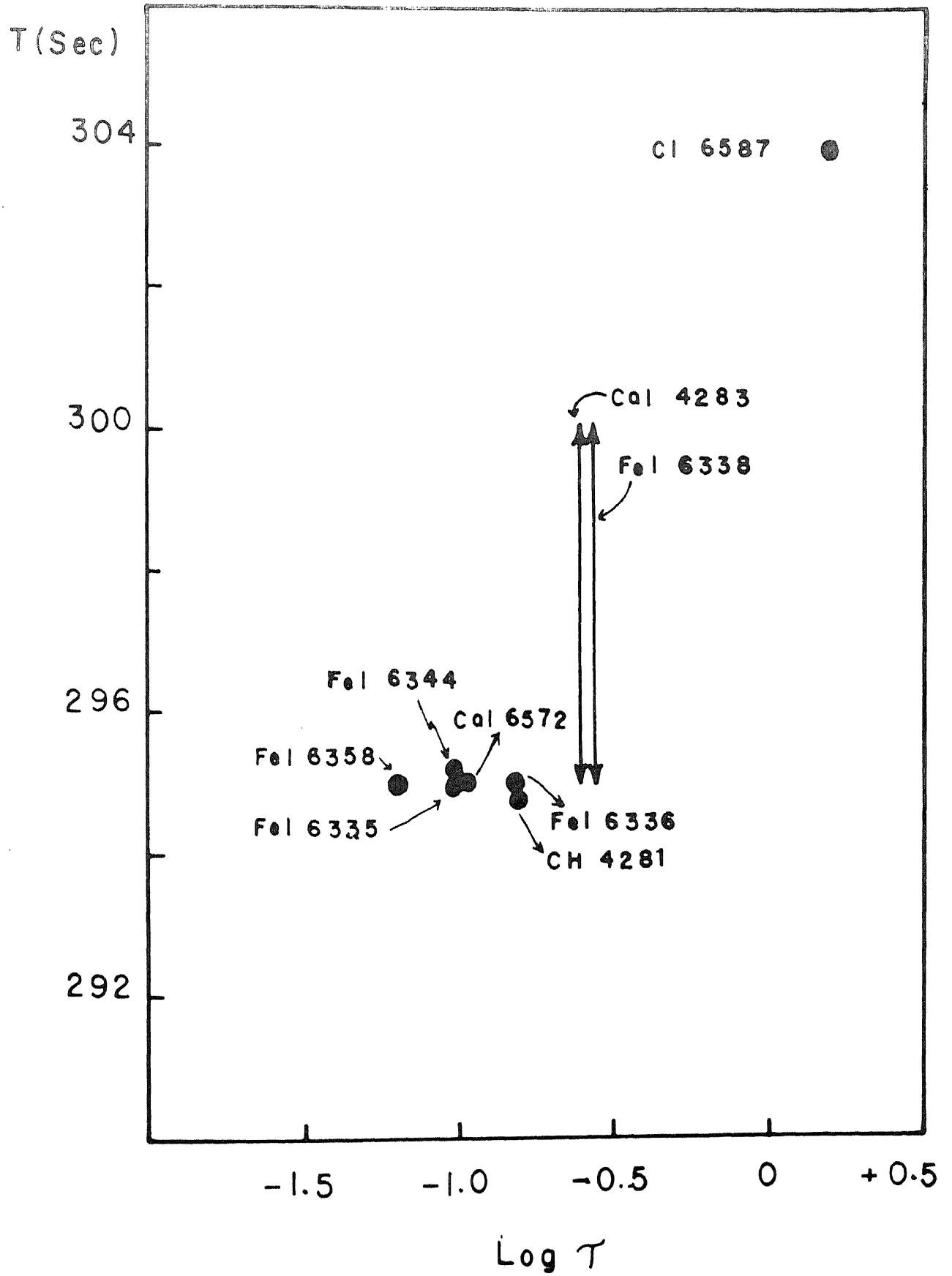
T(Sec)
304
300
296
292
CI 6587
CaI 4283
FeI 6338
FeI 6344
CaI 6572
FeI 6358
FeI 6335
FeI 6336
CH 4281
-1.5
-1.0
-0.5
0
+0.5
Log τ

Fig. III – 20

The period decreases with increase in height. The low level CI 6587 line shows a period of oscillation of 304 sec. and the high level FeI 6358 line, a period of 295 seconds. The decrease in period with height, is in agreement with the observations of Evans and Michard (1962) and of Noyes and Leighton (1963) on other spectral lines. The periods determined from individual wave trains or bursts by Bhattacharyya (1972) with the magnetograph with aperture 1".4 x 5".6 do not show a height dependence. The periods given in Table III-6 represent the most probable value with a high statistical weight, being the average of 61 points on the sun. It is this mean period that shows a height dependence. It is possible that either the period variations from burst to burst are too large so as to drown the variations with reference to height or that the spectral analysis carried out did not have enough frequency resolution to show up this property.

It is known that an isothermal atmosphere is a dispersive medium and for a given direction of propagation there exists two critical frequencies ω_1 and ω_2 given by

$$\omega_1 = \frac{\gamma g}{2c} \quad \text{and} \quad \omega_2 = \frac{(\gamma-1)^{1/2} g}{c}$$

where γ , g, and c are the ratio of specific heats, the acceleration due to gravity and the adiabatic sonic velocity respectively.

For frequencies $\omega > \omega_1$ they are sound waves propagating in the vertical direction, and for frequencies $\omega < \omega_2$ they are gravity waves. For frequencies within ω_1 and ω_2, no propagation is possible. According to Moore and Spiegel (1964) the observed oscillations in the solar atmosphere correspond to the forced oscillations due to the action of the non-propagating frequencies in the interval $\omega_1 - \omega_2$. If this is accepted, then, at any height only frequencies $> \omega_1$ can propagate upwards without attenuation. The other alternative of frequencies $< \omega_2$ in the form of gravity waves is ruled out, since gravity waves cannot exist at these levels due to low radiative cooling time of the solar atmosphere. Thus, the solar atmosphere acts as a high-pass filter, filtering all frequencies $< \omega_1$, the value of ω_1 itself increasing monotonically with height due to the change in physical conditions with height. Thus, the frequency spectrum will be different at different heights. This is reflected in the power spectral curves; the dominant frequency or the frequency possessing maximum power shifts towards high frequencies

with increase in height. Since the trapped frequencies at any level will not contribute to the power at higher levels, the period of oscillation from the power spectra can be expected to show a decrease with height.

In Figure III-14, the lower curve is the power spectrum of SiII 6347.104 of the sequence A1082. This line is formed in the very deep layers in the solar atmosphere. The spectrograms of A1082 obtained at a high dispersion showed this line to be a very close doublet on a visual examination. The Utrecht Atlas shows this line to have undoubtedly clean wings. Despite the appearance of the line as a double, the microphotometer trace of the spectrum along the direction of dispersion did not show any evidence of the doublet structure. I felt, the power spectra of such a combination will be of general interest and included this in my measurement programme. During these measurements, the lines being so close to each other, one slit of the Doppler comparator was located on the violet wing of one line and the other slit was in the red wing of the other. The two lines are almost of the same strength. It is interesting to note that although the power spectra resembles in general that due to random noise, the peaks at the low frequency (around $\nu = 1.25 \times 10^{-3}$ Hz) as well as the peak in the oscillatory range

(around $\nu = 3.33 \times 10^{-3}$ Hz) are distinguishable, showing the typical characteristics of a low level line. The power spectrum of velocities can thus reveal the doublet structure of lines, not visible in the microdensitometer tracings of the line profile.

The power spectra curves cover a range from $\nu = 0$ to 8×10^{-3} Hz. To examine the relative content of power at the different frequencies and their behaviour with height, I classified the frequency range into three domains - the low frequency region, $\nu = 0$ to 1.5×10^{-3} Hz, the oscillatory or resonance range $\nu = 2.75$ to 4.25×10^{-3} Hz, and the high frequency range $\nu = 5.5$ to 8×10^{-3} Hz. I have then obtained the power in these ranges by measuring the areas enclosed by the power spectra curves in the three frequency domains defined above, as well as the total power which is the total area enclosed by the curve from $\nu = 0$ to 8×10^{-3} Hz. These are given in Table III-7. The power in the frequency ranges are expressed as percentage of the total power, whereas the total power for each line is directly the area in square units. The lines are arranged according to their mean depth of formation. The value of this mean depth is also given in the last Column of Table III-7.

Table III-7

Distribution of power in the ν - domain

Line λ	Total power	% power contained in: Oscillatory range ν = 2.75 - 4.25 x 10^{-3} Hz.	% power contained in: Low frequency range ν = 0 to 1.5 x 10^{-3} Hz.	% power contained in: High frequency range ν = 5.5 to 8.0 x 10^{-3} Hz.	Log τ
6358.695	2125	66.1	5.1	3.7	-1.2
6344.162	2033	65.9	5.8	3.6	-1.0
6335.345	4606	61.0	10.3	12.1	-1.0
6533.884	2392	65.3	5.9	5.6	-
6572.795	3111	51.1	7.4	4.8	-1.0
6336.837	2136	63.9	9.1	3.6	-0.8
6586.319	2920	58.1	6.2	4.7	-
6339.125	2320	60.4	8.7	6.3	-
4281.794	2792	51.7	8.0	6.6	-0.8
4283.016	3869	55.8	5.0	3.8	-0.6
6338.588	2260	57.9	12.1	6.0	-0.6
6330.859	2749	55.3	11.9	7.7	-
6587.622	6461	35.1	15.9	15.5	+0.2

The following characteristics are evident from the table:

1) The oscillatory range gains strength as one goes up in height in the solar atmosphere, starting from the deep lying CI line and passing through lines originating in the photosphere to those in the low chromosphere.

2) In addition to the peak in the resonance frequencies, the low level lines show significant power in the low frequency range ($\nu = 1.5 \times 10^{-3}$ Hz). In the CI 6587 line, a minor peak is also seen around $\nu = 1.25 \times 10^{-3}$ Hz. This low frequency power decreases fast with height. This is in agreement with the findings of Edmonds et-al (1965) on the CI 5052 line. This power appears to be due to the convective component in the macroscopic velocity field in the low photosphere. This is in conformity with the prediction of the "convective overshoot" into the stable regions of the photosphere caused by the convective motions prevailing in the unstable layers below. Also the observations of Bray and Loughead (1967) show that the granules are visible up to an optical depth of $\tau = 0.1$. The other possibility is the existence of gravity waves from period considerations

alone; but gravity waves cannot be sustained at these levels. However, the low frequency tail which becomes important in CaII 8542 and CaII 3933 lines (Noyes 1967) could possibly be due to gravity waves. Gravity waves can propagate at these levels due to the very high radiative relaxation time (Souffrin 1966). But more definite observations are required to confirm this conjecture.

3) The high frequency tail remains substantially constant in the range of heights studied above.

4) The CI line alone shows large power in the high frequency range. Also, the CI line possesses the maximum total power amongst the lines, with FeI 6335 excluded. This is obviously due to the proximity of this line to the source of mechanical flux and which is bound to have a very broad frequency spectrum for the energy at the place of generation.

The high frequency component seen in all the lines possibly represent the sound waves which travel up and finally provide the energy for the heating of the upper chromosphere and the corona.

It is, however, difficult to argue in favour or otherwise on the existence of gravity or sound waves from considerations of periods and shapes of individual power

spectrum of velocities alone. Additional information like the phase difference between the oscillations in the different levels observed simultaneously and also the phase relation between the velocity fields and temperatures oscillations may help to provide a better basis for interpretation.

CHAPTER IV

COHERENCE AND PHASE PROPERTIES OF THE VELOCITY FIELDS

4.1. General

In this chapter, I investigate the depthwise spatial correlation of the quasi-periodic oscillations by cross-correlating these oscillations that occur simultaneously at two levels. The sequences A1082 and A1100 containing many spectral lines permit such an investigation.

The existence of oscillations in the solar atmosphere raises the interesting question as to the nature of the waves and their modes of propagation. The phase difference between the oscillations occurring at different levels will be of considerable importance in determining the nature of these waves. This is best done by cross-spectral analysis of the velocity data, of one spectral line with another.

4.2. Cross-spectral analysis

This analysis gives a measure of the cross-correlation and the phase difference, commonly termed as the coherence and phase spectra respectively between the

frequency components of two groups of data. The method of analysis follows that of Edmonds et-al (1965) and is briefly described below.

Designating the fluctuating velocities measured in two lines observed simultaneously, by a(t) and b(t), the cross-correlation between the two sets $C_{ab}(\tau)$ can be worked out. The Fourier transform of the cross-correlation function $C_{ab}(\tau)$ gives the cross-spectrum,

$$P_{ab}(\nu) = \int_{-\infty}^{+\infty} C_{ab}(\tau)\, e^{2\pi i \nu \tau}\, d\tau \qquad (4.1)$$

The function $P_{ab}(\nu)$ is in general, a complex quantity and can be expressed as

$$P_{ab}(\nu) = R_{ab}(\nu) + i\, S_{ab}(\nu) \qquad (4.2)$$

Goodman (1957), has worked out the methods of cross-spectral analysis and has shown that

$$R_{ab}(\nu) = 2 \int_{-\infty}^{+\infty} C^{+}_{ab}(\tau) \cos 2\pi \nu \tau . d\tau \qquad (4.3)$$

and

$$S_{ab}(\nu) = 2 \int_{-\infty}^{+\infty} C^{-}_{ab}(\tau) \sin 2\pi \nu \tau . d\tau \qquad (4.4)$$

where $C^{+}_{ab}(\tau)$ and $C^{-}_{ab}(\tau)$ are the even and odd parts respectively of the function $C_{ab}(\tau)$.

$R_{ab}(\nu)$, the real part of the cross-spectrum is called the co-spectrum and $S_{ab}(\nu)$, the imaginary part is called the quadrature spectrum. The quantity defined by the expression

$$G_{ab}(\nu) = \left[\frac{R^2_{ab}(\nu) + S^2_{ab}(\nu)}{P_a(\nu)\ P_b(\nu)}\right]^{1/2} \qquad (4.5)$$

gives the coherence, and

$$\theta(\nu) = \arctan\left[\frac{S_{ab}(\nu)}{R_{ab}(\nu)}\right] \qquad (4.6)$$

describes the relative phase of the Fourier components of Set (a) and Set (b). Here, Pa (ν) and Pb (ν) are the power spectra or the cosine Fourier transform of the auto correlation functions described in Chapter III.

For a cross-spectral analysis, it is necessary that the two groups of data (a) and (b) contain the same number of data points. In the sequence A1082 there are 61 rows of velocity data each having 120 columns. In the

sequence A1100, there are 61 rows and 62 columns. The analysis for the lines in the two sequences were done as follows.

Consider the velocity data of any two lines belonging to the same sequence whose coherence and phase are to be computed. The first row of one spectral line was cross-correlated with the first row of the second spectral line with a chosen value for the lag. The co-spectrum and the quadrature spectrum were now computed and from these the coherence and phase were derived. This was repeated row by row for the entire data. Finally, the coherence and phases were averaged over the entire array, frequency wise, to give the mean coherence and phase between the velocity data of the two lines.

4.3. Properties of the velocity fields

I have computed the coherence and phase spectra as a function of frequency ν, for 10 pairs of lines. These are shown in Figures IV-1 to IV-10. Of these Figures IV-1 to IV-3 show the coherence and phase spectra between the velocity fields of

CI 6587.622 and FeI 6593.884
NiI 6586.319
CaI 6572.795

FIGURES IV-1 to IV-3

Coherence and phase spectra of the velocity fields in the four lines of the time sequence A1100.

CI 6587.622 with FeI 6593.884
NiI 6586.319
CaI 6572.795

The velocity in the solar line listed first, leads the velocity in the second line for a positive value of the phase. For a negative value of the phase, the first line lags the second line. The oscillations in all the 3 lines lag behind those in the CI 6587.622 line by about 5° in the resonance range and by 29° in the high frequency range. 'V' after the wavelength of the spectral line stands for velocity in the line.

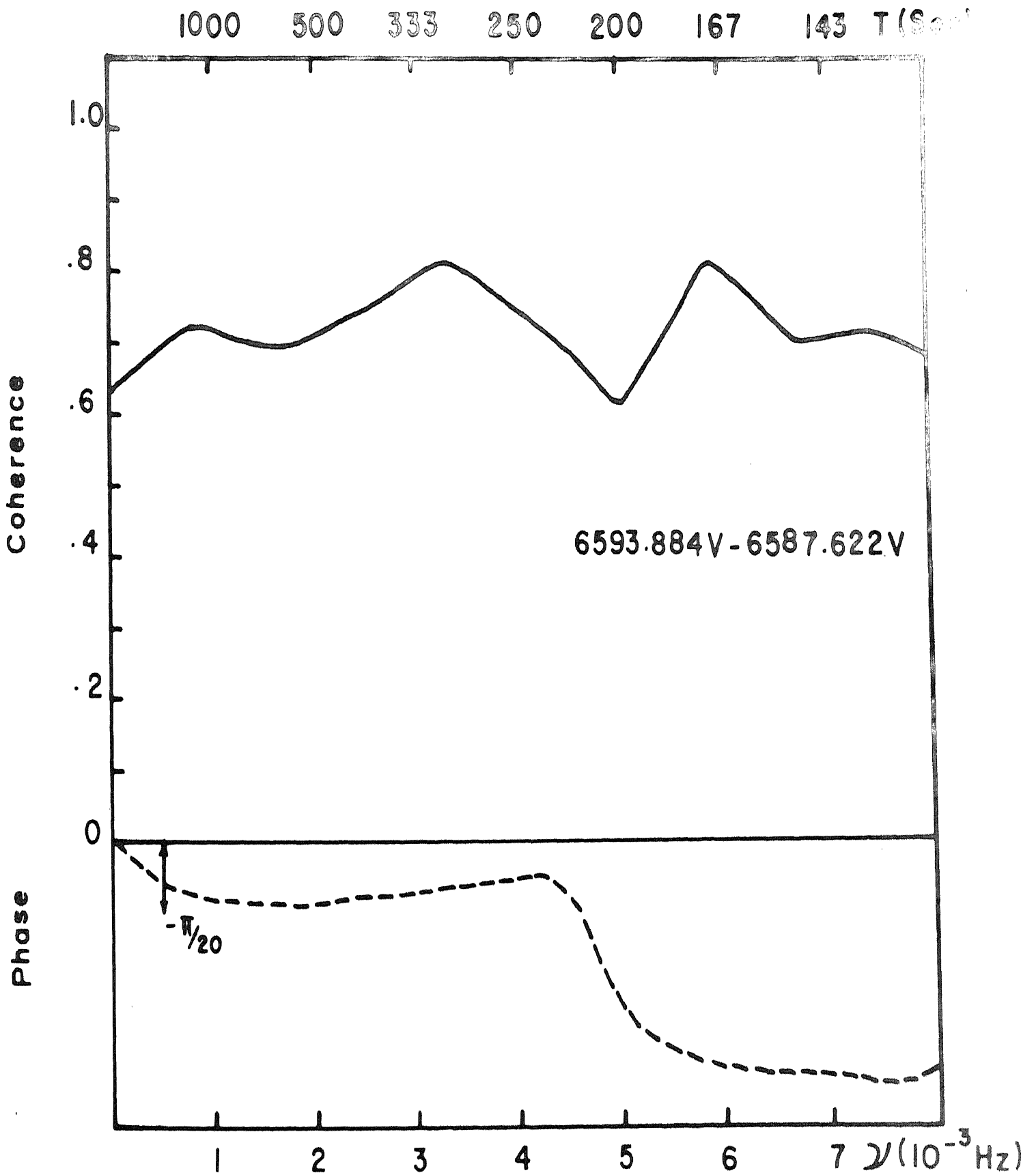
1000
500
333
250
200
167
143
T(Sec)
1.0
.8
.6
.4
.2
0
Coherence
6593.884V-6587.622V
Phase
-π/20
1
2
3
4
5
6
7
ν(10⁻³Hz)

Fig . IV-1

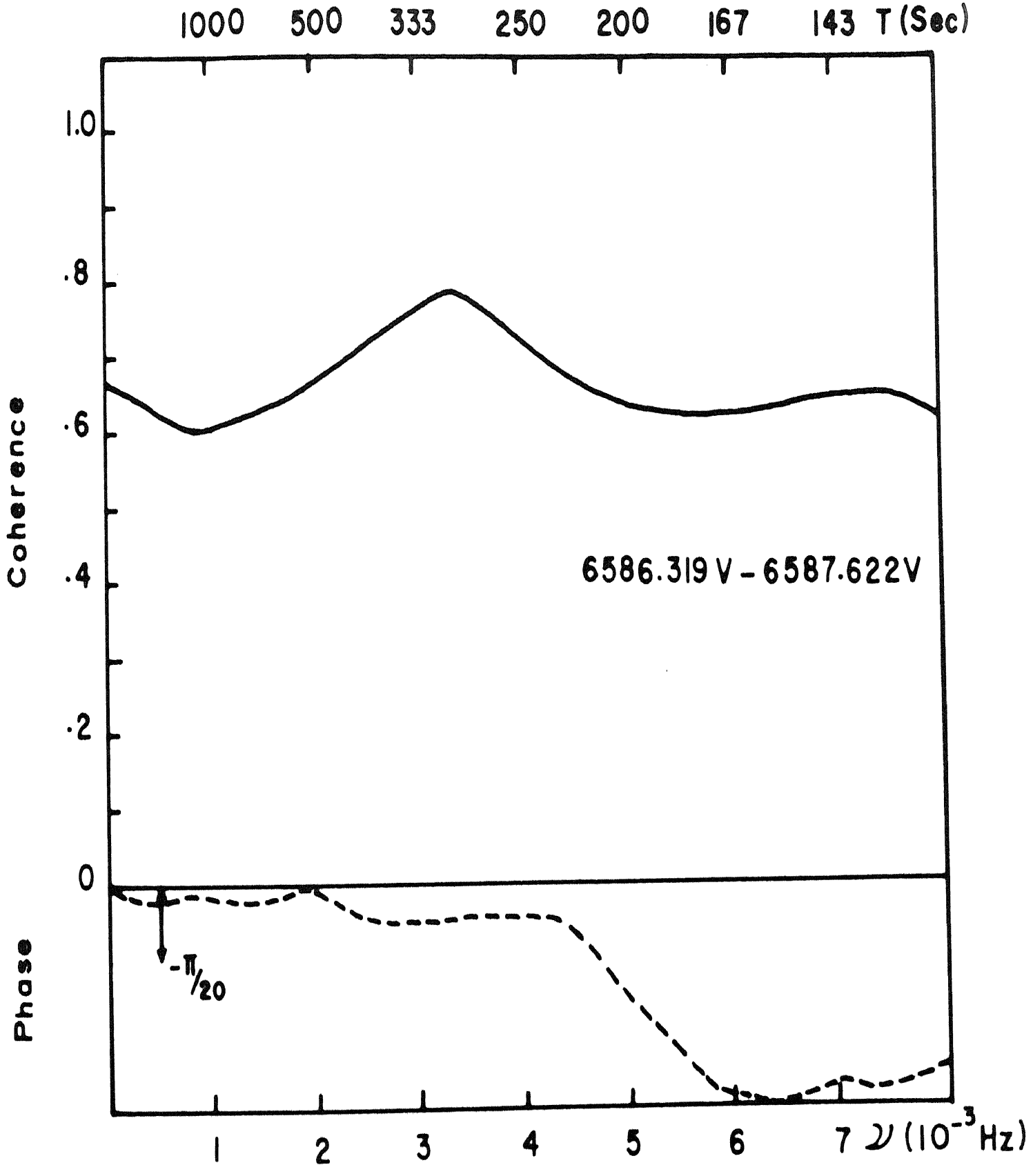
1000 500 333 250 200 167 143 T (Sec)
1.0
.8
.6
.4
.2
0
Coherence
6586.319 V - 6587.622V
Phase
-π/20
1 2 3 4 5 6 7 ν (10⁻³ Hz)

Fig. IV - 2

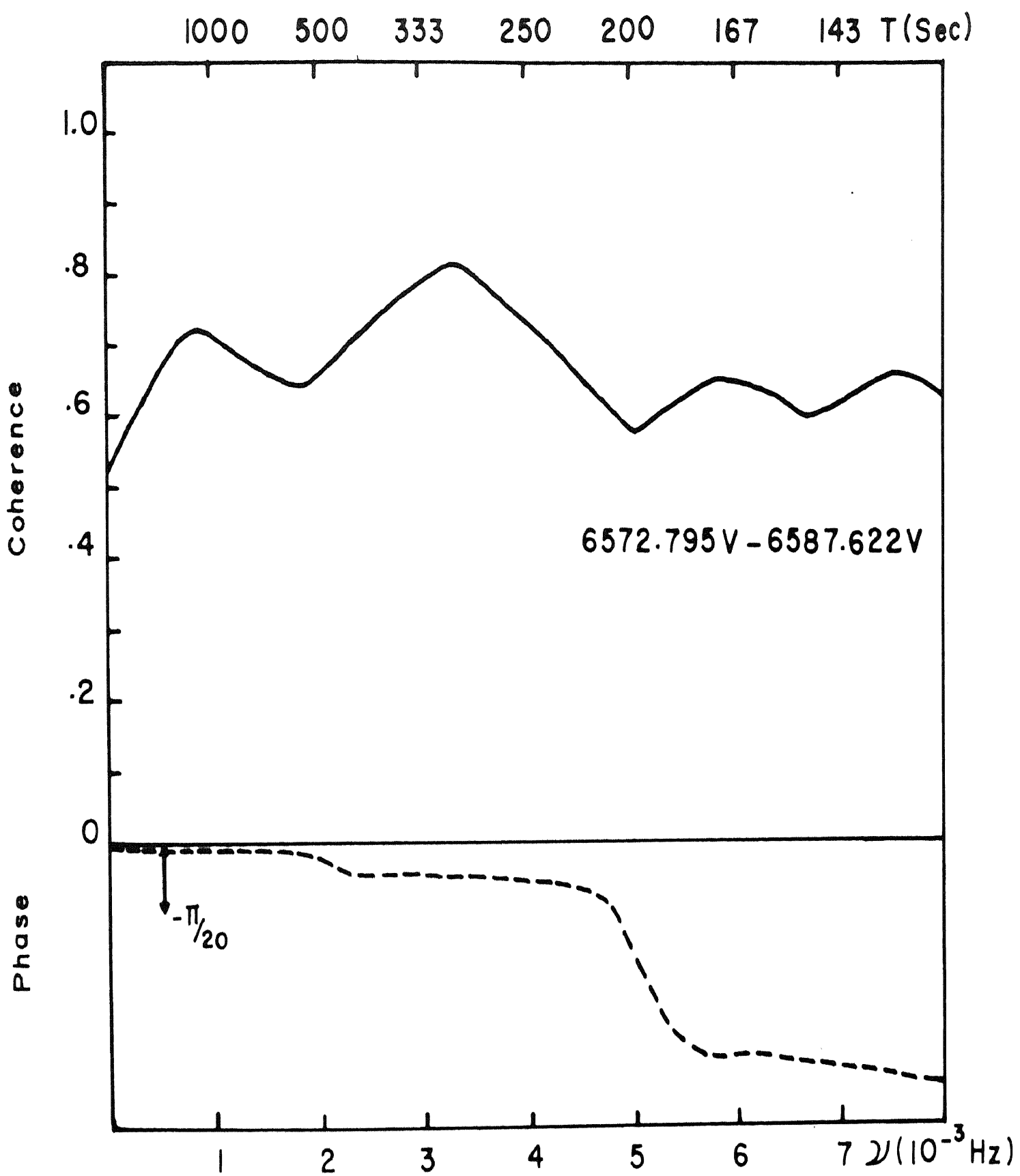
1000 500 333 250 200 167 143 T(Sec)
1.0
.8
.6
.4
.2
0
Coherence
6572.795V - 6587.622V
Phase
-π/20
1 2 3 4 5 6 7 ν(10⁻³ Hz)

Fig. IV-3

In the resonance range, the coherence between the velocity fields in the different pairs of lines has an uniform value of 0.8. This value of the coherence while high by itself, could have been higher, were it not for the noise present in the measures of the CI line spectra. The coherence outside the resonance range on either side falls off to 0.6. A similar drop is seen in the coherence plot between CI 5052.16 and FeI 5049.83 lines of Edmonds et al (1965). The three upper photospheric lines lag behind the deep CI line and this phase lag remains uniform over the entire range of frequencies (ν = 2.5 to 4.5 x 10^{-3} Hz). The amounts by which the lines lag are:

θ; (6593.884Å - 6587.622Å) = -6°.3 or 5.2 Sec.
θ; (6586.319Å - 6587.622Å) = -3°.9 or 3.2 Sec.
and θ; (6572.795Å - 6587.622Å) = -4°.2 or 3.5 Sec.

For frequencies, ν = 2.0 x 10^{-3}, the phase lag is almost the same as in the resonance range for (6572.795Å - 6587.622Å), but the amount of such phase lags are higher in the case of the other two pairs of lines. For frequencies above ν = 5.0 x 10^{-3} the lag increases rapidly. At frequency ν = 6.0 x 10^{-3} the lag is 29° or 14 sec. The phase difference of about 4° to 6° observed in the

resonance range, corresponds to an average difference in time of 5 sec or even less. The three photospheric lines are formed at a mean level of log τ = -1.0 and the CT line at a mean level of log τ = +0.2. This difference in log τ would correspond to a height difference of about 110 km in the solar atmosphere. The time delay of 5 sec. would result in a value for the phase velocity very much higher than the sonic velocity. In the high frequency range the time difference observed is of the order of 14 sec. This leads to a value for the speed which agrees very well with that of sound waves in the medium. The significance of the phase lag observed in the low frequency is not clear, since convective motion can be seen at these levels as shown by the individual velocity power spectra discussed in Chapter III.

Coming to the coherence and phase spectra between the pairs of lines of the sequence A1082 (Figures IV-4 to IV-10), the coherence is seen to be very high, reaching a value of 0.98 in all the cases, in the resonance range. This is obviously due to the close similarity of the lines in terms of depth of formation. In these pairs too, the high level lines always lag behind the low level lines. In some of the cases the phase difference in the resonance

FIGURES IV-4 to IV-10

Coherence and phase spectra of the velocity fields between different pairs of lines of the time sequence A1082.

The velocity in the solar line listed first leads the velocity in the second line for a positive value of the phase. For a negative value of the phase, the first line lags the second line. 'V' after the wavelength of the spectral line stands for velocity in the line.

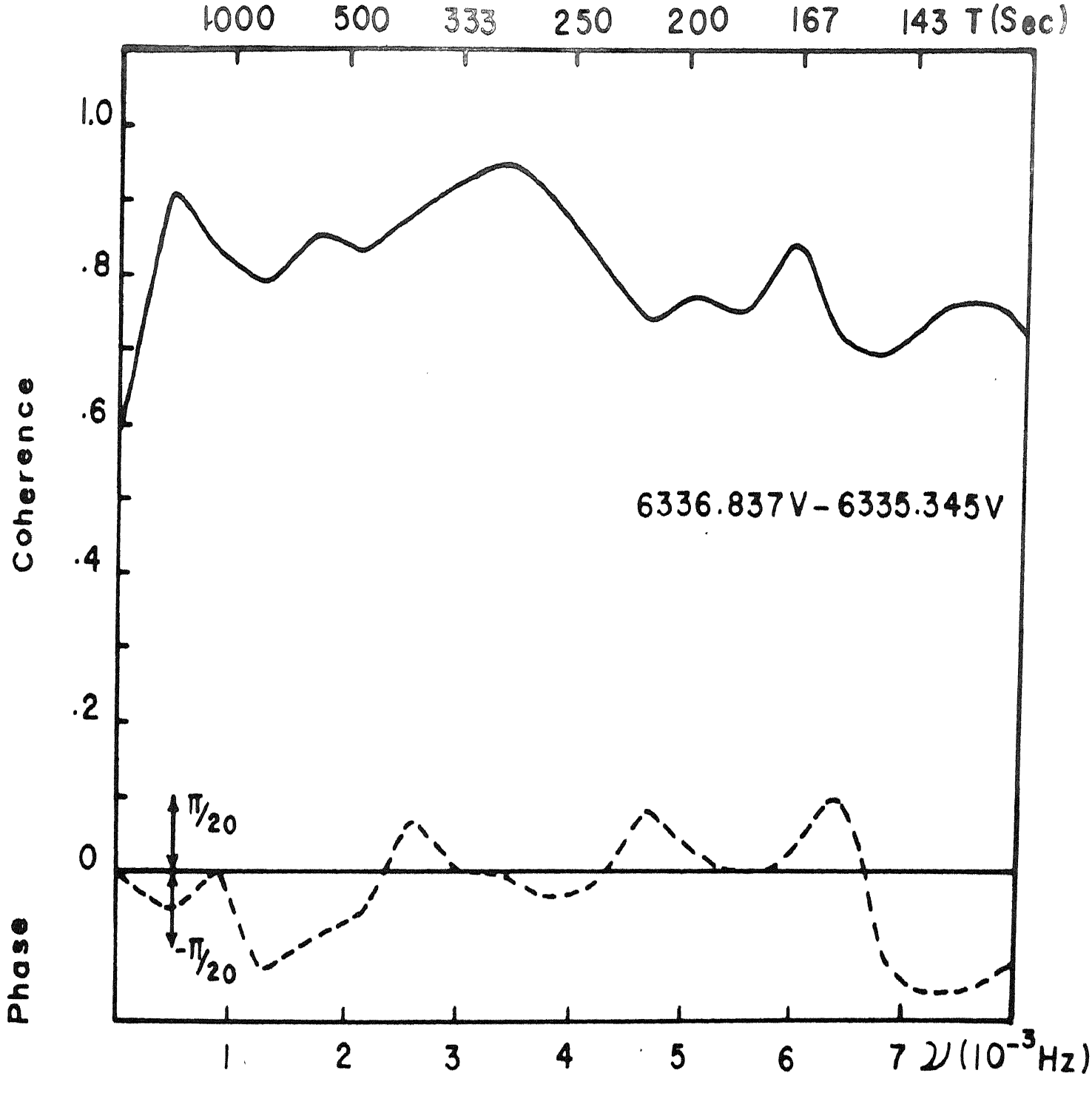
1000
500
333
250
200
167
143 T(Sec)
1.0
.8
.6
.4
.2
0
Coherence
6336.837V-6335.345V
π/20
-π/20
Phase
1
2
3
4
5
6
7 ν(10⁻³Hz)

Fig. IV-4

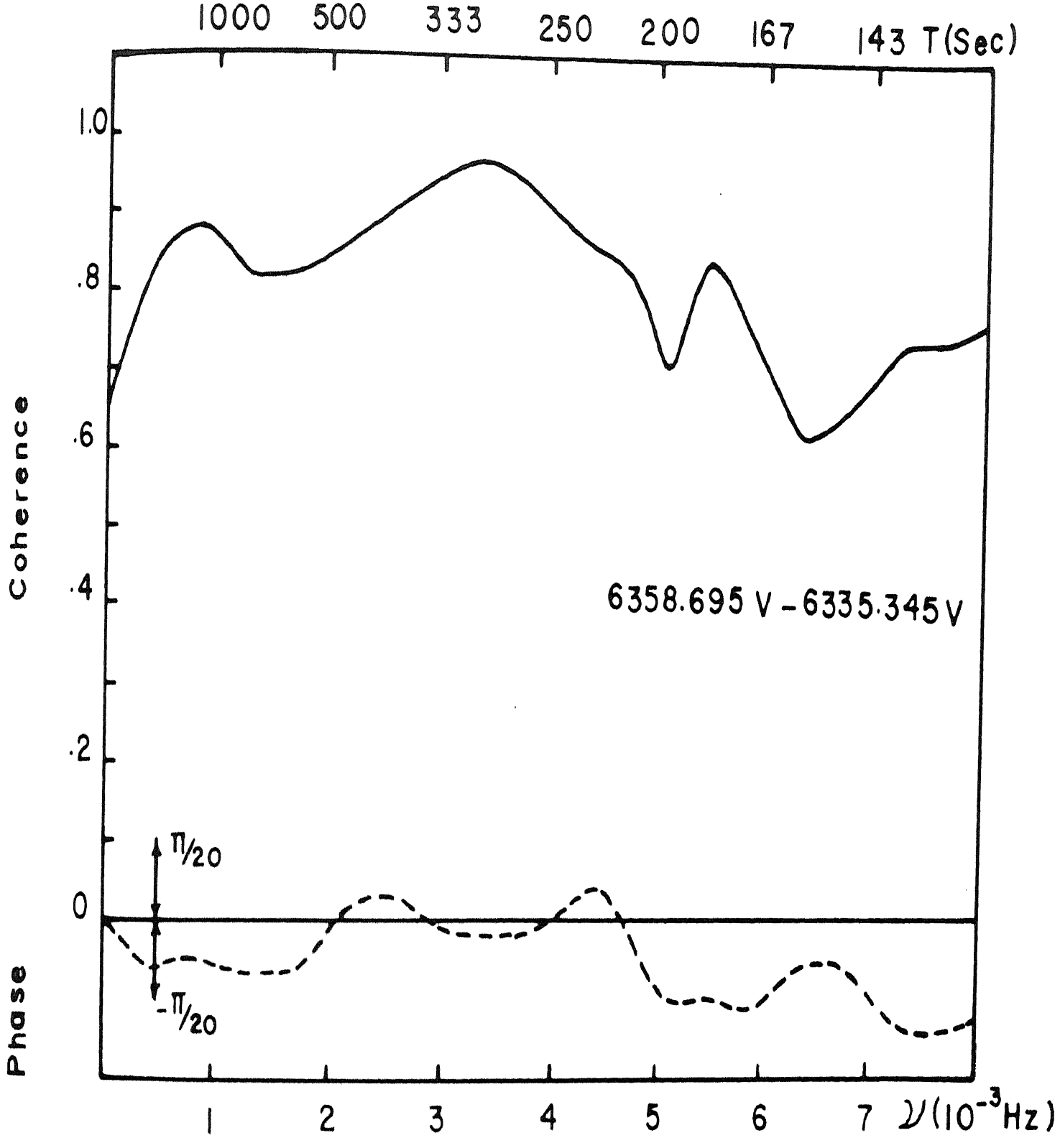
1000 500 333 250 200 167 143 T(Sec)
1.0
.8
.6
.4
.2
0
Coherence
Phase
6358.695 V - 6335.345 V
π/20
-π/20
1 2 3 4 5 6 7 ν(10⁻³Hz)

Fig . IV-5

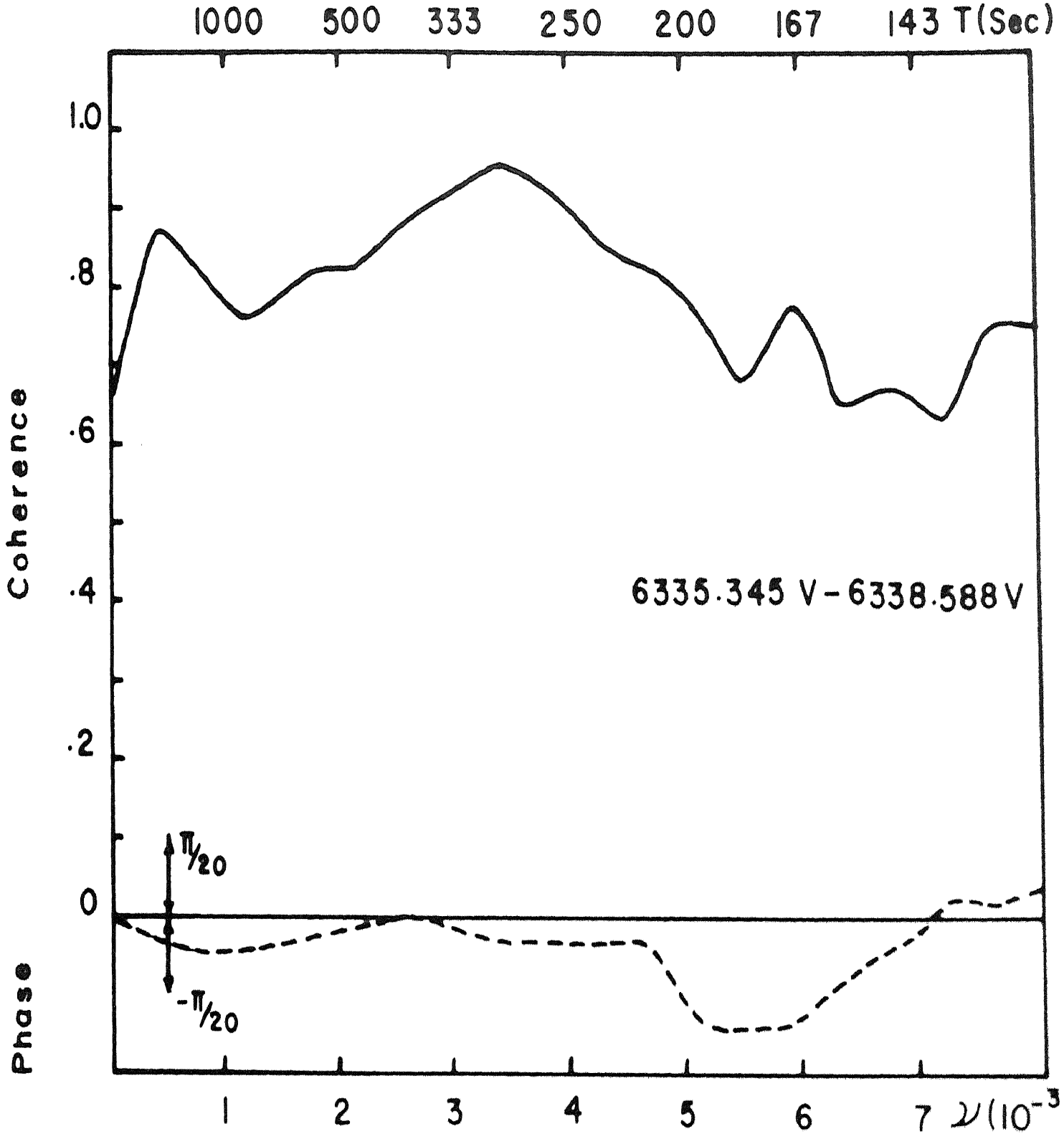
1000 500 333 250 200 167 143 T(Sec)
1.0
.8
.6
.4
.2
0
Coherence
Phase
6335.345 V - 6338.588 V
π/20
-π/20
1 2 3 4 5 6 7 ν(10⁻³

Fig . IV - 6

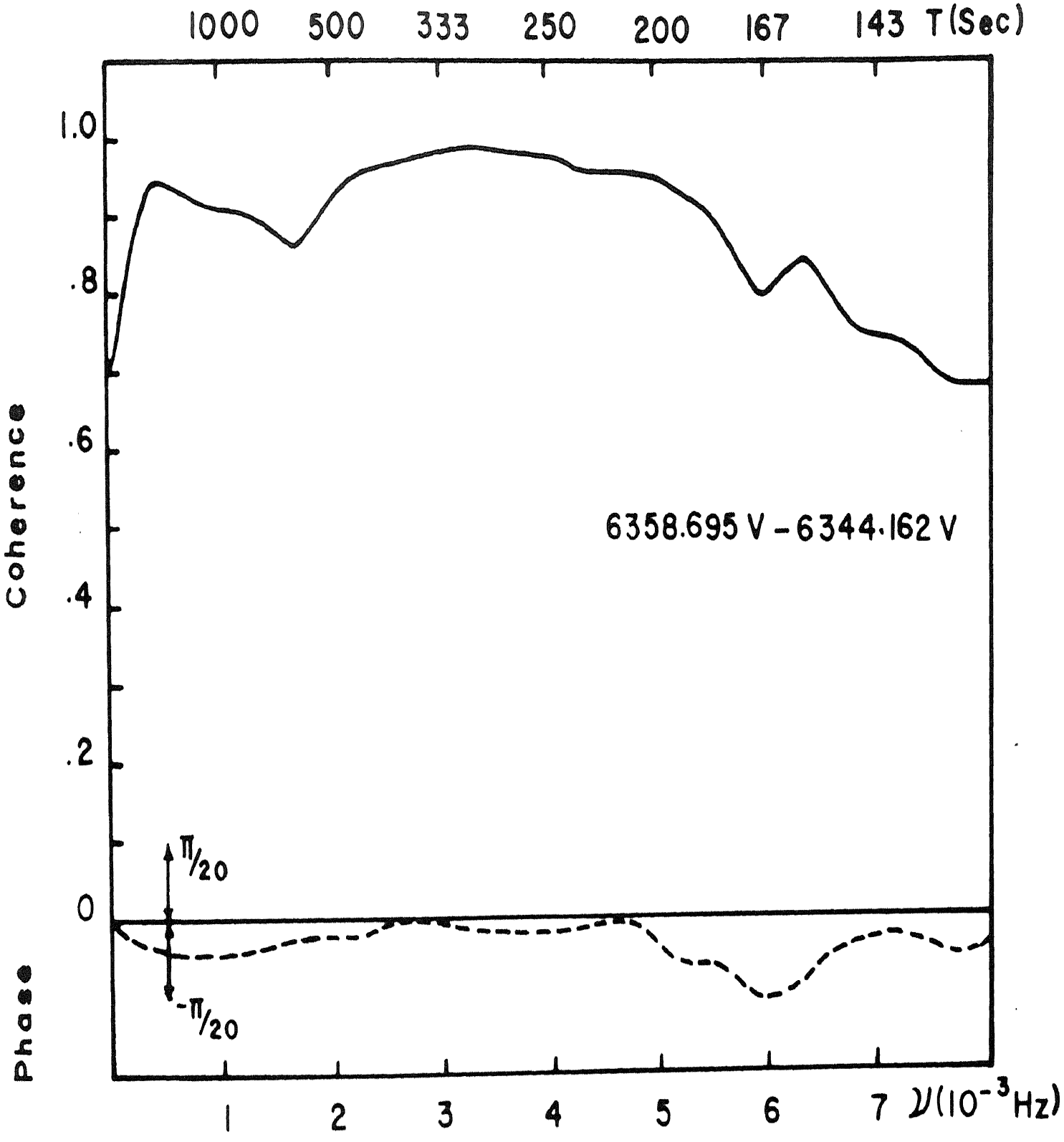
1000 500 333 250 200 167 143 T(Sec)
1.0
.8
.6
.4
.2
0
Coherence
Phase
6358.695 V - 6344.162 V
π/20
-π/20
1 2 3 4 5 6 7 ν(10⁻³Hz)

Fig . IV - 7

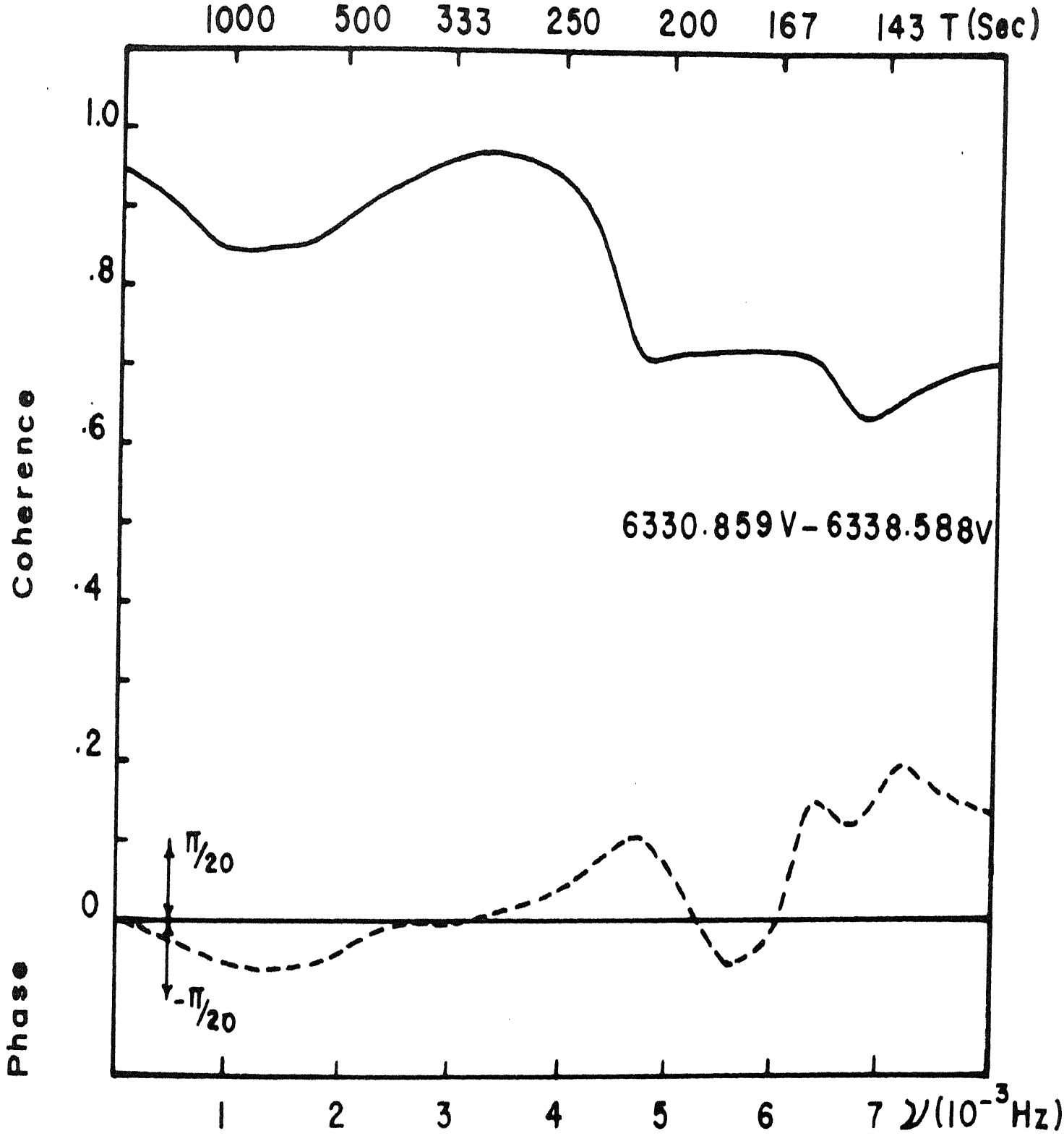
1000 500 333 250 200 167 143 T(Sec)
1.0
.8
.6
.4
.2
0
Coherence
Phase
6330.859V-6338.588V
π/20
-π/20
1 2 3 4 5 6 7 ν(10⁻³Hz)

Fig . IV-8

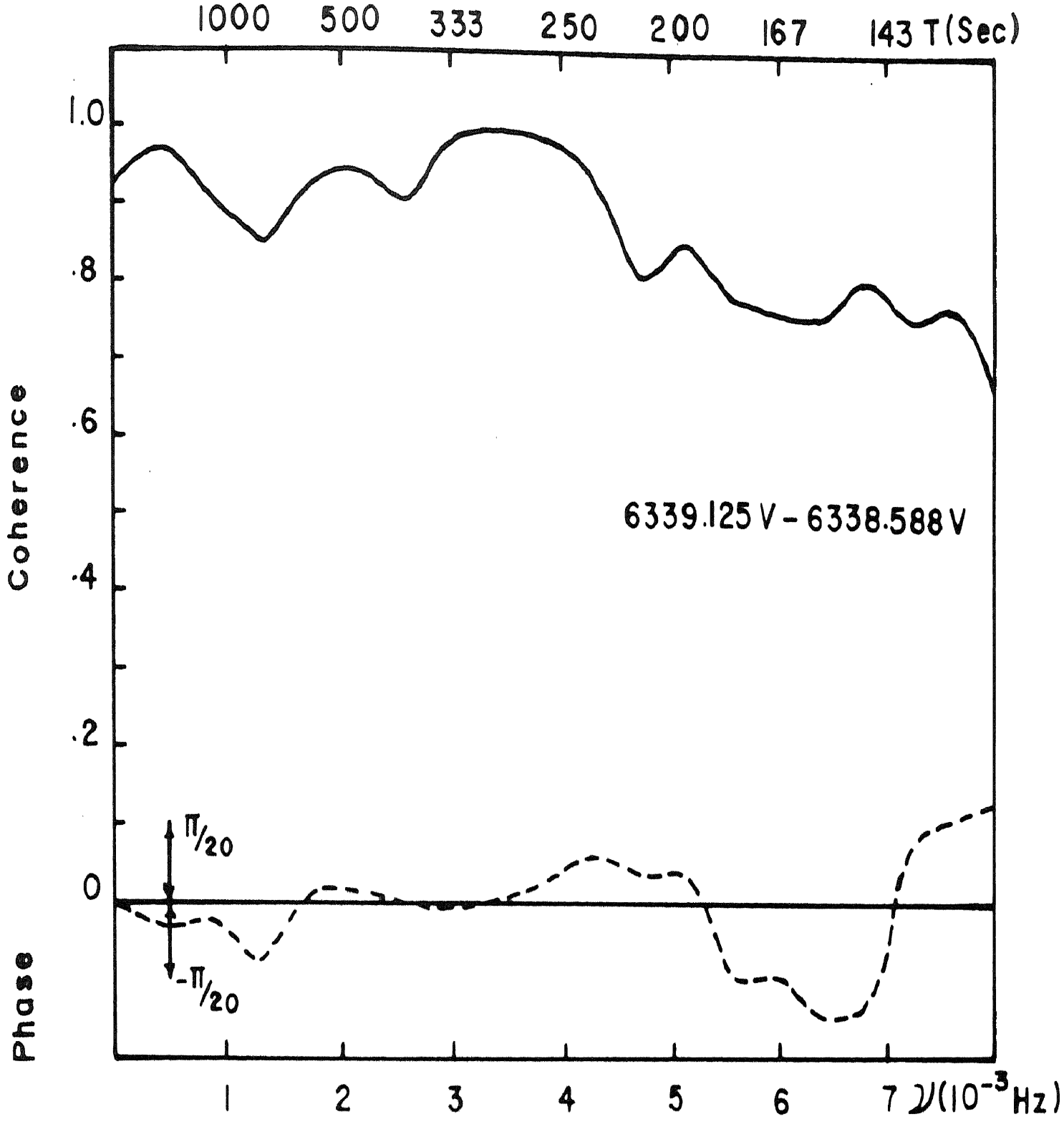
1000 500 333 250 200 167 143 T(Sec)
1.0
.8
.6
.4
.2
0
Coherence
Phase
6339.125 V - 6338.588 V
π/20
-π/20
1 2 3 4 5 6 7 ν(10⁻³Hz)

Fig . IV - 9

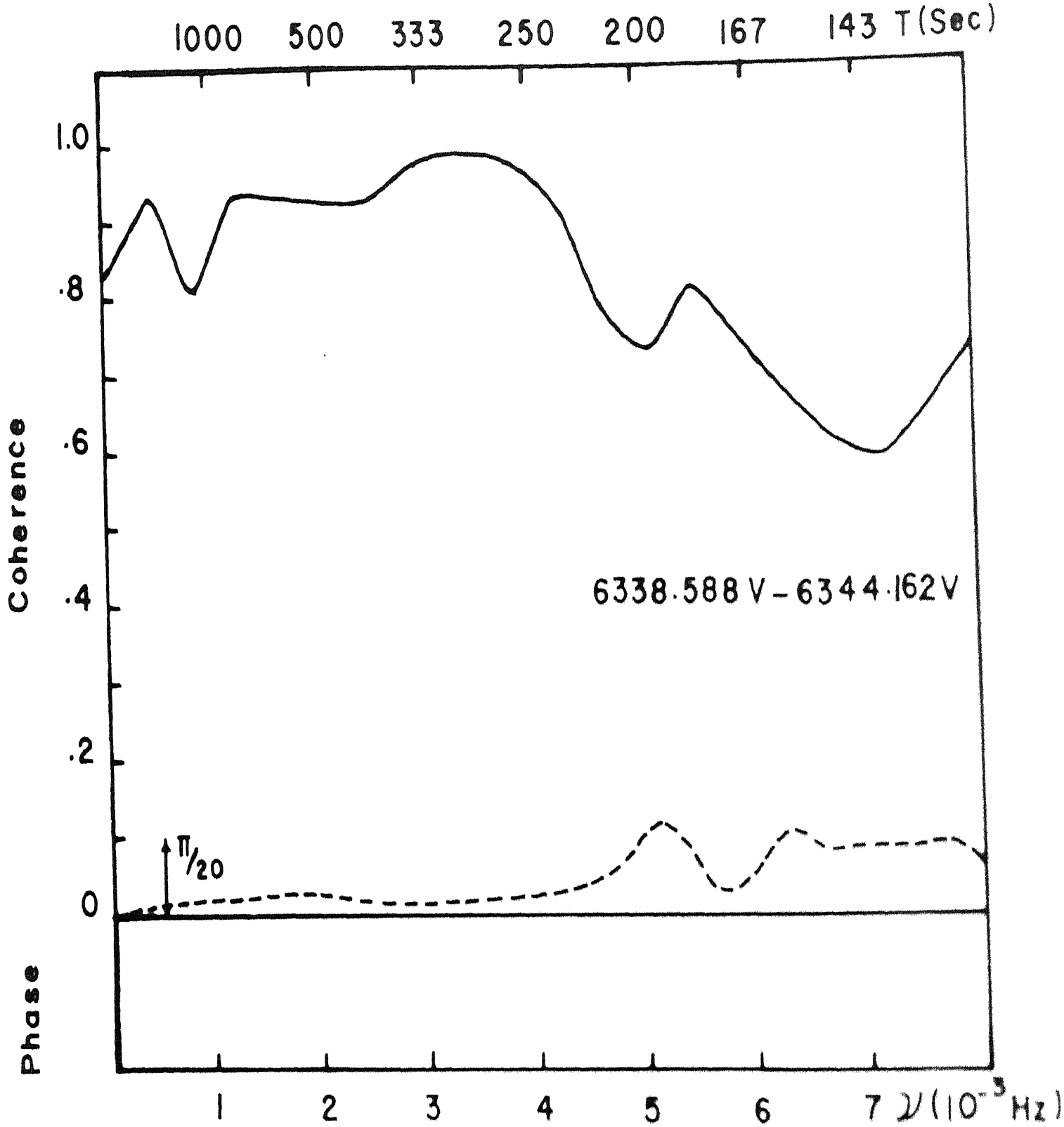
1000 500 333 250 200 167 143 T(Sec)
1.0
.8
.6
.4
.2
0
Coherence
6338.588 V - 6344.162 V
π/20
Phase
1 2 3 4 5 6 7 ν (10⁻³ Hz)

Fig . IV - 10

range is negligible. The values of the phase difference between pairs of lines are entered in Table IV-1 for the three frequency ranges.

Table IV-1

Phase difference between velocities in pairs of lines in the three ν ranges

Figure No.	Pairs of lines λ in Å	Phase in the frequency		
		Low (0 to 2.5×10^{-3} Hz)	Oscillatory (2.5 to 4.0×10^{-3} Hz)	High (5 to 7×10^{-3} Hz)
IV-4	Lead of 6336 over 6335	-5°	0 to -2°.5	Fluctuates too much.
IV-5	Lead of 6358 over 6335	-5°	-1°.6	-9°
IV-6	Lead of 6335 over 6338	-4°	-2°.5	-13°
IV-7	Lead of 6358 over 6344	-5°	-1°	-7°
IV-8	Lead of 6330 over 6338	-4°.5	0	+9°
IV-9	Lead of 6339 over 6338	-3°	0	-9°
IV-10	Lead of 6338 over 6344	1.0	1.0	+9°

The values of the lags from these sequence spectra also show that the phase velocity in the resonance range possesses a value many times the velocity of sound. In the high frequency region we find a time lag appropriate to the propagation of sound waves. This may mean either that in the resonance frequency range, there are standing acoustic waves which show insignificant phase difference between two levels or that these are internal gravity waves which do not have a vertical phase velocity. But at these levels the radiative relaxation time is too fast and hence gravity waves may not exist. It is, therefore, possible that the oscillations seen in the standing wave mode in the resonance range, are those excited by the non-propagating frequencies, suggested by Moore and Spiegel (1964). However, the existence of a finite time lag in this range would point to the evidence of some propagation of energy, although most of the oscillations are in the standing wave mode.

CHAPTER V

VELOCITY AND BRIGHTNESS OSCILLATIONS

5.1. Analysis of brightness oscillations

I have studied the intensity fluctuations in the continuum and in the line wings and core of FeI 6358.695 line of the sequence A1082. The continuum is exposed to a degree very favourable for studying the brightness fluctuations. Only 62 out of 120 frames were chosen for intensity measurements. Measurements were made from the microphotometer traces. During the measurements on the line wings, the microphotometer slits were located practically at the same $\pm \Delta\lambda$ value as in the velocity measurements. The width of the microphotometer slit was smaller than that of the comparator and was located central to it. Because of this, the depth averaging is less in the intensity measures. In the steep parts of the profile, the intensity fluctuation is the sum of the contributions from the intrinsic variation in intensity and from the Doppler shift. The effect of the Doppler shifts were eliminated by averaging the traces at $+\Delta\lambda$ and $-\Delta\lambda$.

From the microdensitometer traces, intensities were derived via the characteristic curve. The intensity data of the continuum, line wing and line core were read off at intervals of 1080 km on the sun. The fiducial line for stepping off this interval was again the shadow of the hair line on the spectrograph slit. This procedure ensured that the intensities read off and the earlier velocity measurements pertain to the same region on the sun. These intensity measurements are with reference to an arbitrary zero. As in the case of velocities, a mean line was fitted to each one of the I (x) curves which are the intensity run along the length of the spectral line. The mean line was provided by the average of the intensity measures of 62 frames. Then the quantity $I(x) - \bar{I}(x) = \Delta I(x)$ was read off at the 61 points. With these, the ratio $\Delta I(x) / \bar{I}(x)$ was computed for the 61 points, which gave the fluctuating component of the intensity. This procedure gave for all the three sets, values of

$$\frac{\Delta I_{cont}}{I_{cont}} , \quad \frac{\Delta I_{wing}}{I_{wing}} \quad \text{and} \quad \frac{\Delta I_{core}}{I_{core}} .$$

Each set consists of an array with 61 rows and 62 columns. These are shown as a two dimensional plot i.e. as functions of position on the sun and time in Figure V-1. The fluctuations in the

FIGURE V-1

Sample plot of intensity fluctuations vs time and position in the continuum and in the line wing and core of FeI 6358.695. The individual curves represent intensity at consecutive points separated by 1080 km on the sun.

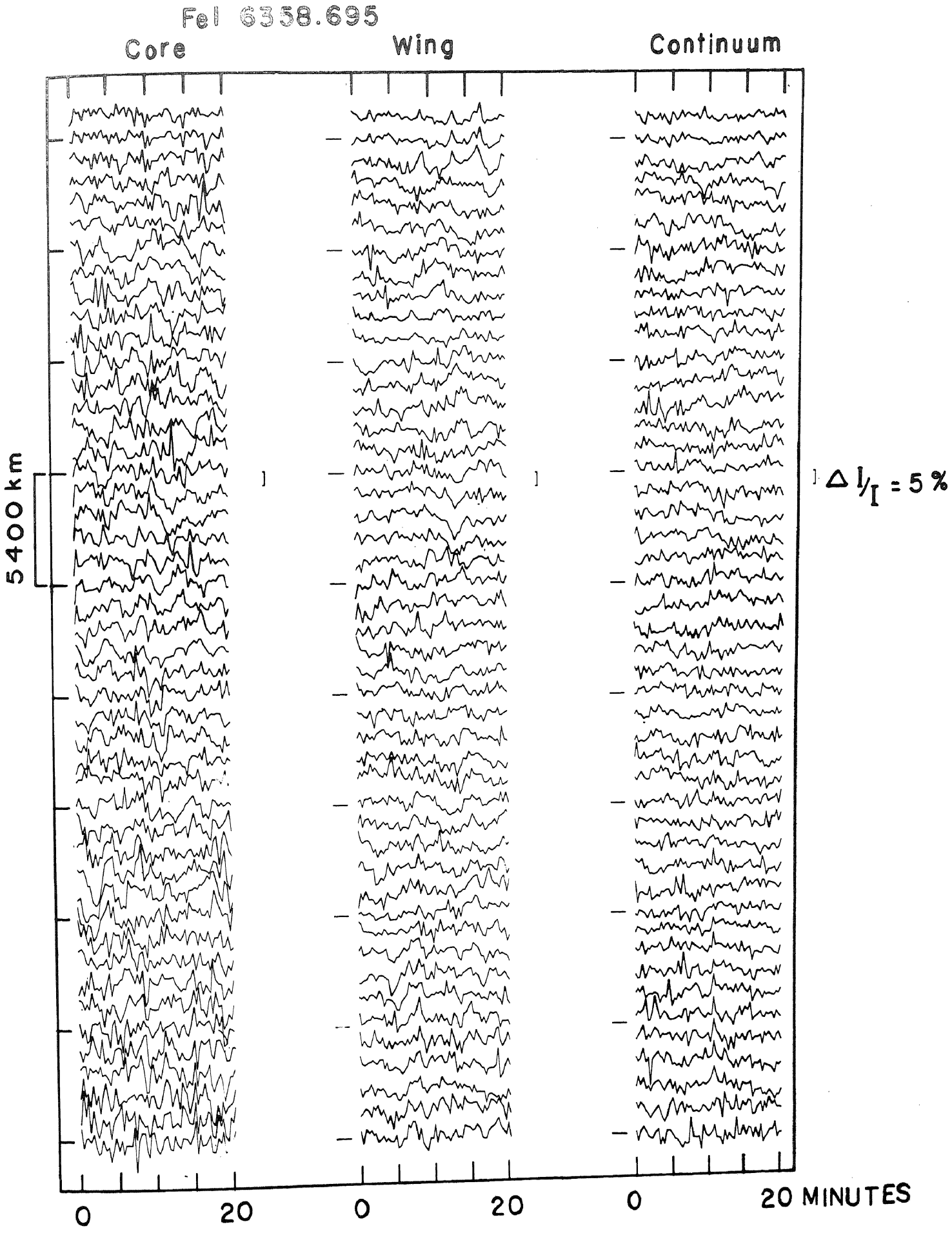
FeI 6358.695
Core
Wing
Continuum
5400 km
Δ I/I = 5 %
0
20
0
20
0
20 MINUTES

Fig. V-1

continuum are the weakest and appear to be random in nature. The fluctuations in the line wing have a close resemblence to those in the continuum. In the line core, the variations are striking and resemble the quasi-periodic oscillations of velocities. I then obtained the power spectra of the three groups of intensities by the methods described in Chapter III for velocity power spectra. The power spectra are shown in Figures V-2 to V-4.

The continuum intensity power spectrum starts with maximum power at zero frequency falling off rapidly at higher frequencies as is typical of convective motion. It shows a definite, but a very weak oscillatory component at $\nu = 3.5 \times 10^{-3}$. Edmonds and McCullough (1966) have studied this feature in their analysis of the granulation brightness fluctuations using several sets of data. They have arrived at the conclusion that in the granulation, a maximum of about 2 per cent of the total fluctuating power is contributed by the oscillatory mode.

The power spectrum of the line wing variations resembles that of the continuum, with maximum power at the zero frequency and with a weak oscillatory component at

FIGURE V-2

Power spectrum of the intensity fluctuations in the continuum . Most of the power is concentrated near the very low frequencies. The weak oscillatory component is seen at $\nu = 3.5 \times 10^{-3}$ Hz.

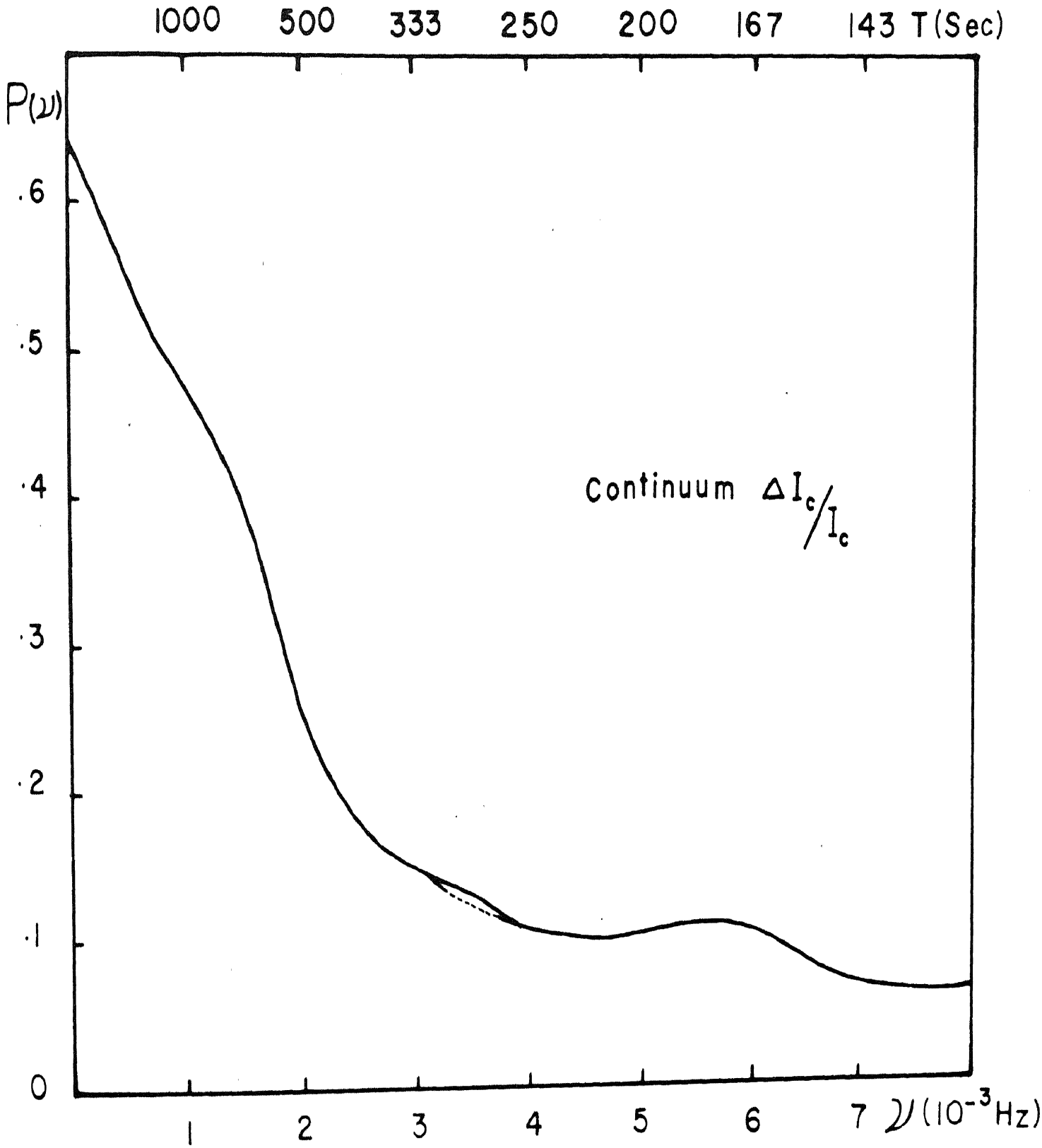
1000
500
333
250
200
167
143 T(Sec)
P(ν)
.6
.5
.4
.3
.2
.1
0
Continuum $\Delta I_c/I_c$
1
2
3
4
5
6
7 ν (10⁻³Hz)

Fig . V - 2

FIGURE V-3

Power spectrum of the intensity fluctuations in the wing of FeI 6358.695 line. The curve resembles the continuum curve with a weak oscillatory component at $\nu = 3.5 \times 10^{-3}$ Hz.

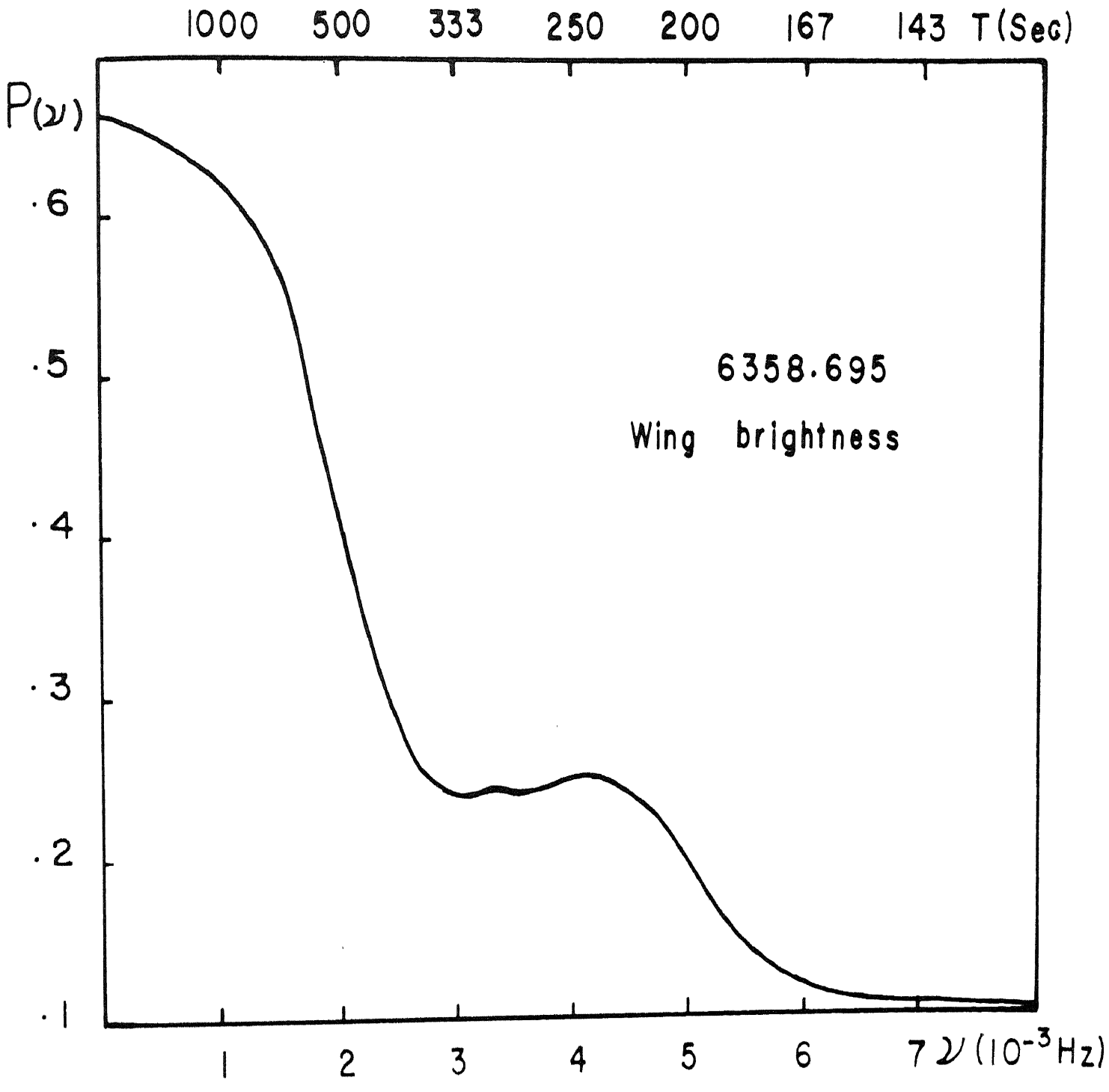
1000 500 333 250 200 167 143 T(Sec)
P(ν)
·6
·5
·4
·3
·2
·1
6358.695
Wing brightness
1 2 3 4 5 6 7 ν (10⁻³ Hz)

Fig . V - 3

FIGURE V-4

Power spectrum of the intensity fluctuations in the core of FeI 6358.695 line. The peak in the power at $\nu = 3.5 \times 10^{-3}$ Hz is very prominent, showing the predominance of the oscillatory component.

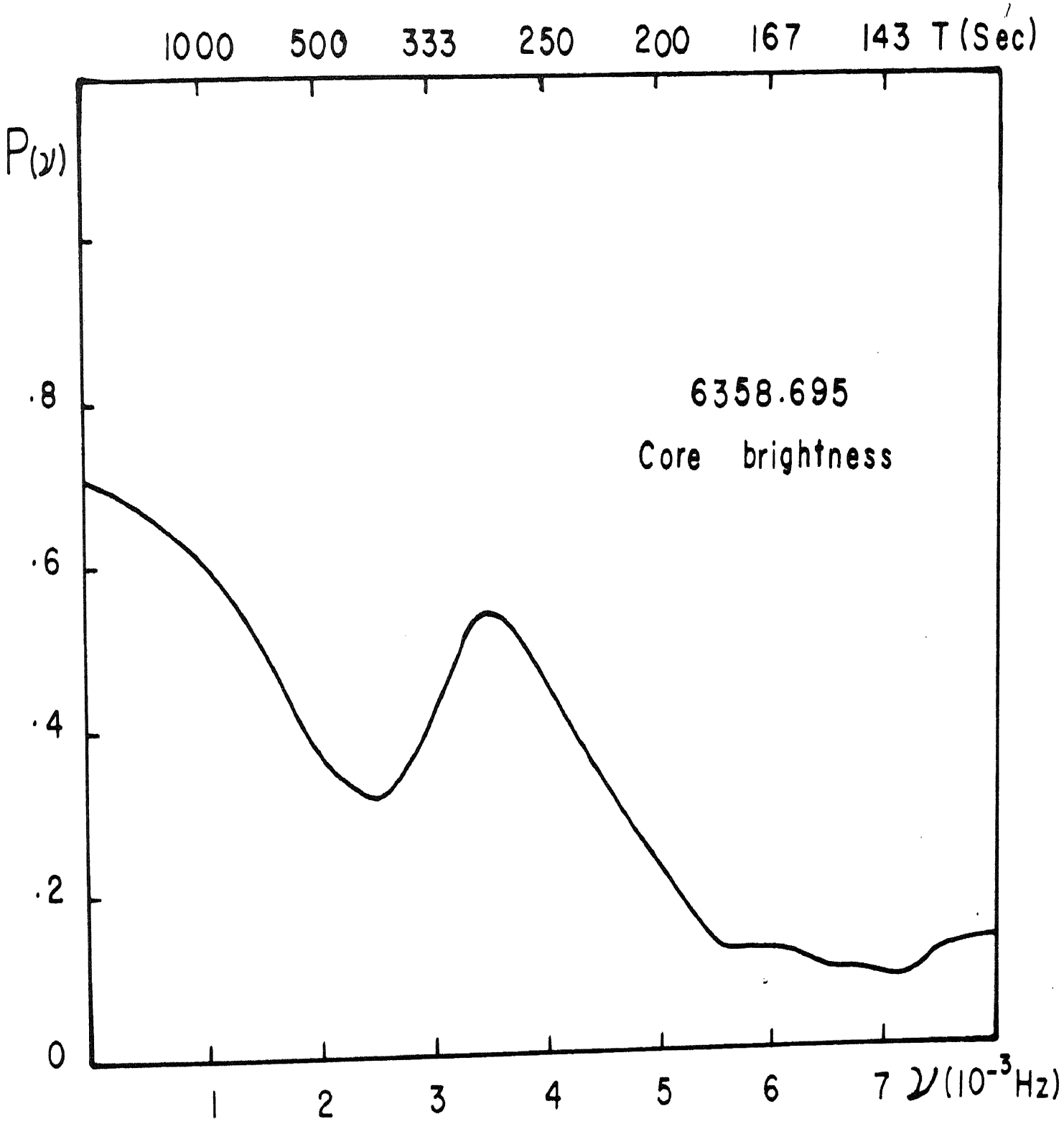
1000 500 333 250 200 167 143 T (Sec)
P(ν)
.8
.6
.4
.2
0
6358.695
Core brightness
1 2 3 4 5 6 7 ν (10⁻³ Hz)

Fig . V - 4

$\nu = 3.5 \times 10^{-3}$ Hz. The brightness fluctuations in the line core have a power spectrum characterised by two regions where the power is concentrated. One is near the zero frequency range and another at $\nu = 3.5 \times 10^{-3}$ Hz. which is the resonance range in the corresponding velocity field. These findings are in good agreement with the earlier observations on the continuum and cores of strong lines by Evans et-al (1963). The high power near the zero frequency is obviously due partly to the convective motions also noticed in the velocity field power spectra as well as due to the presence of "persistent features" as interpreted by Evans et-al (1963).

5.2. Cross-spectral analysis of Intensity fields

The brightness fluctuations in the wings of FeI 6358 and in the line core were cross-correlated with those in the continuum and their coherence and phase spectra were computed. These are shown in Figures V-5 and V-6. The ling wing and the continuum show a high coherence in general. In the low frequency range the coherence reaches a value as high as 0.95. In the range $\nu = 2.0$ to 4.0×10^{-3} the wing brightness lags behind the continuum by about 14° or 12 sec. The lag noticed by Edmonds et-al (1965) between the fluctuations in the central intensity

FIGURE V-5

Coherence and phase spectra of the wing brightness fluctuations in FeI 6358.695 against continuum. Around $\nu = 3.0 \times 10^{-3}$ Hz. the wing brightness lags behind the continuum by about 13°.

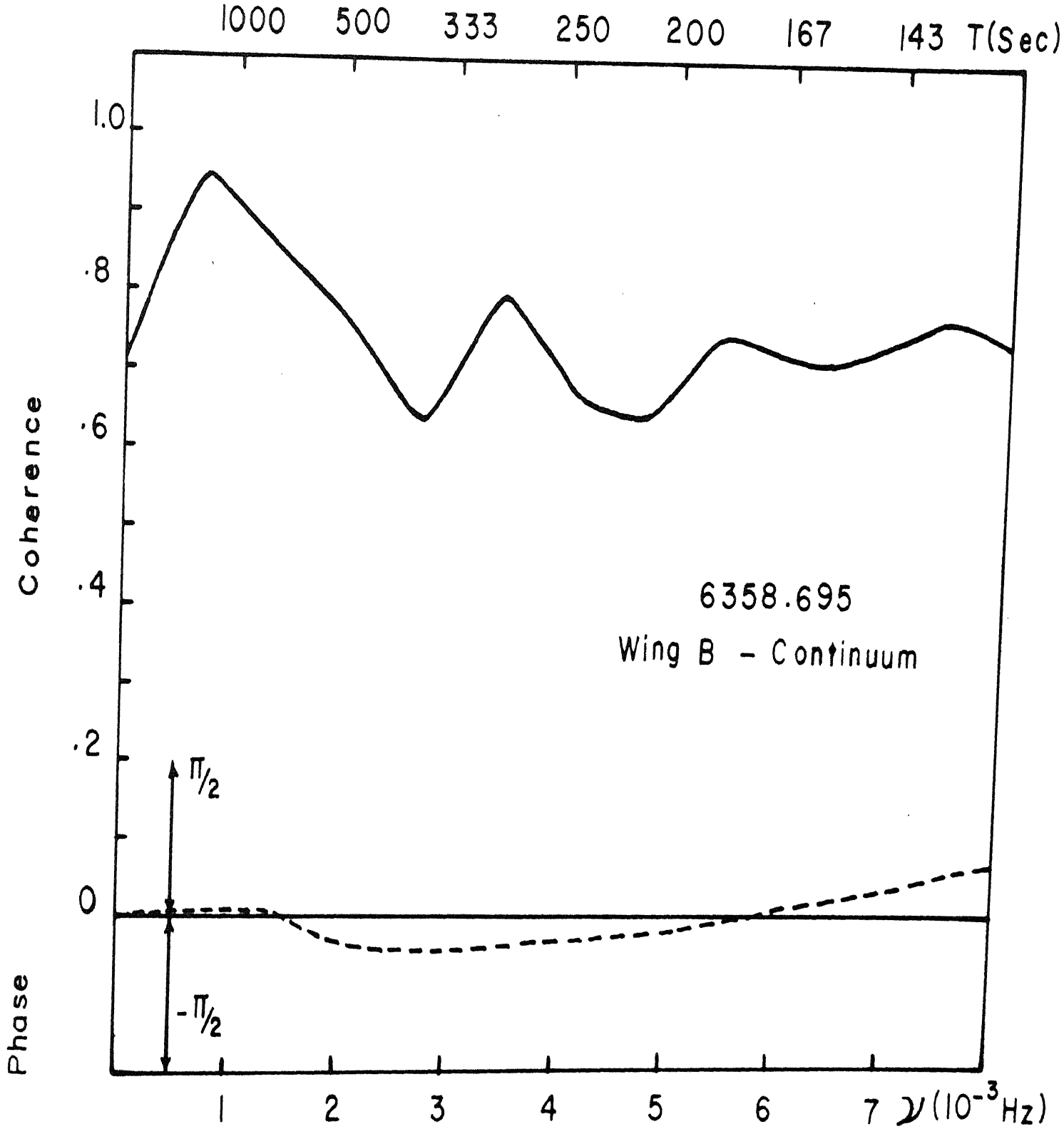
1000 500 333 250 200 167 143 T(Sec)
1.0
.8
.6
.4
.2
0
Coherence
Phase
6358.695
Wing B - Continuum
π/2
-π/2
1 2 3 4 5 6 7 ν (10⁻³ Hz)

Fig . V - 5

FIGURE V-6

Coherence and phase spectra of the core brightness fluctuations in FeI 6358.695 against continuum. The core brightness leads the continuum by 57° in the range ν = 2.0 to 5.0 x 10^{-3} Hz.

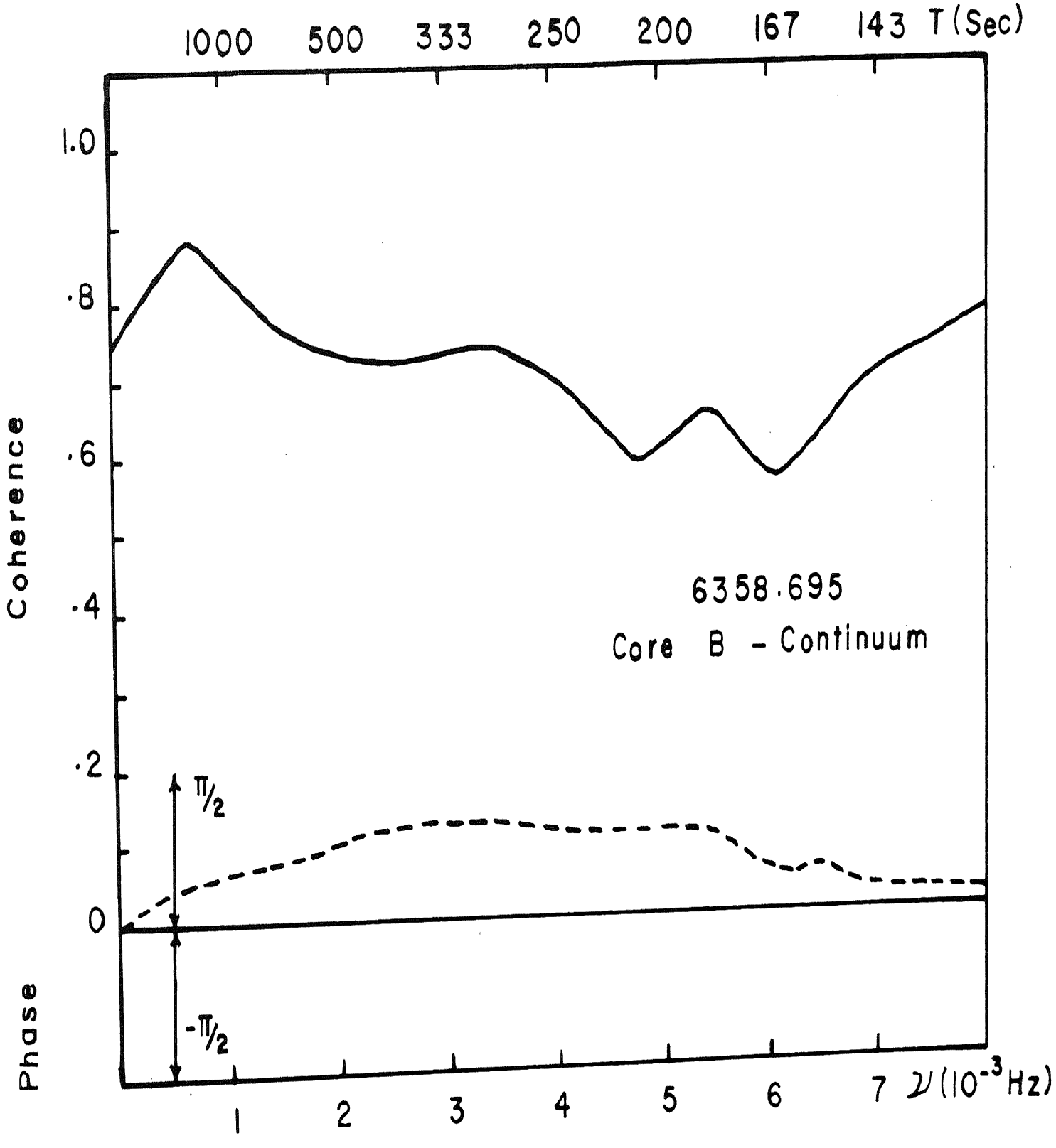
1000 500 333 250 200 167 143 T (Sec)
1.0
.8
.6
.4
.2
0
Coherence
Phase
6358.695
Core B - Continuum
π/2
-π/2
1 2 3 4 5 6 7 ν (10⁻³ Hz)

Fig. V-6

$\Delta\nu_0/\nu_0$ of CI 5052 and the continuum is about 12 seconds. It is reasonable to expect that wings of FeI 6358 and the core of CI 5052 are formed almost at the same levels and should show similar lags with reference to the continuum.

Between the core and continuum brightness, the coherence has a peak of 0.88 near the zero frequency. This high coherence gives more weightage to the presence of convective motions at these levels. The coherence elsewhere drops down to an average of 0.65. The core brightness is seen to lead the continuum over the entire frequency range and has a value of 57° at $\nu = 3.5 \times 10^{-3}$ Hz. This lead, suggests that the source of temperature fluctuations in the line wings (or in the cores of weak lines) and in the core of strong lines, is different. This behaviour of the brightness variations has been interpreted in terms of the radiative relaxation time by, Noyes and Leighton (1963). The thermal relaxation time for a thin atmosphere approximation is given by

$$\tau = \frac{3}{32} \frac{k}{m_H T^3 K(z)}$$

where k (z) is the Planck mean absorption coefficient per gram of hydrogen, T is the temperature, and $1/k$ is a characteristic length of the perturbation (Spiegel 1957).

This assumption is valid for regions of $\tau_c << 1$. The relaxation time at different altitudes have been calculated by Noyes and Leighton (1963) with this relation. The relaxation time is only of the order of a few seconds in the lower levels due to the relatively high concentration of H^- ion, which is the main source of opacity. At very high levels, the concentration of H^- ion falls off and the relaxation time rises to hundreds of seconds. Thus, the thermal properties of lines originating in the deeper layers of the photosphere i.e. weak lines and wings of strong lines are controlled by the ambient radiation field which is the intensity pattern of the granulation. Hence the brightness variations at these levels lag behind those in the continuum. The atmosphere at these levels does not respond to the compressional changes of pressure and density induced by the velocity oscillations. The radiative relaxation time is very small compared to the period of oscillation and hence any temperature perturbations so caused are smoothened out. This smoothing out of these perturbations renders the temperature field practically isothermal. Thus, we do not expect the power spectrum curves for the continuum, cores of weak lines or wings of strong lines to show any significant level of power in the 5-minute period range.

FIGURES V-7 to V-10

Coherence and phase spectra of the velocity fields in

FeI 6338.588

NiI 6339.125

FeI 6335.345

and FeI 6358.695

against brightness fluctuations in the continuum. In the range 1 to 4 x 10^{-3} Hz., the velocities in all the lines lag behind the continuum features.

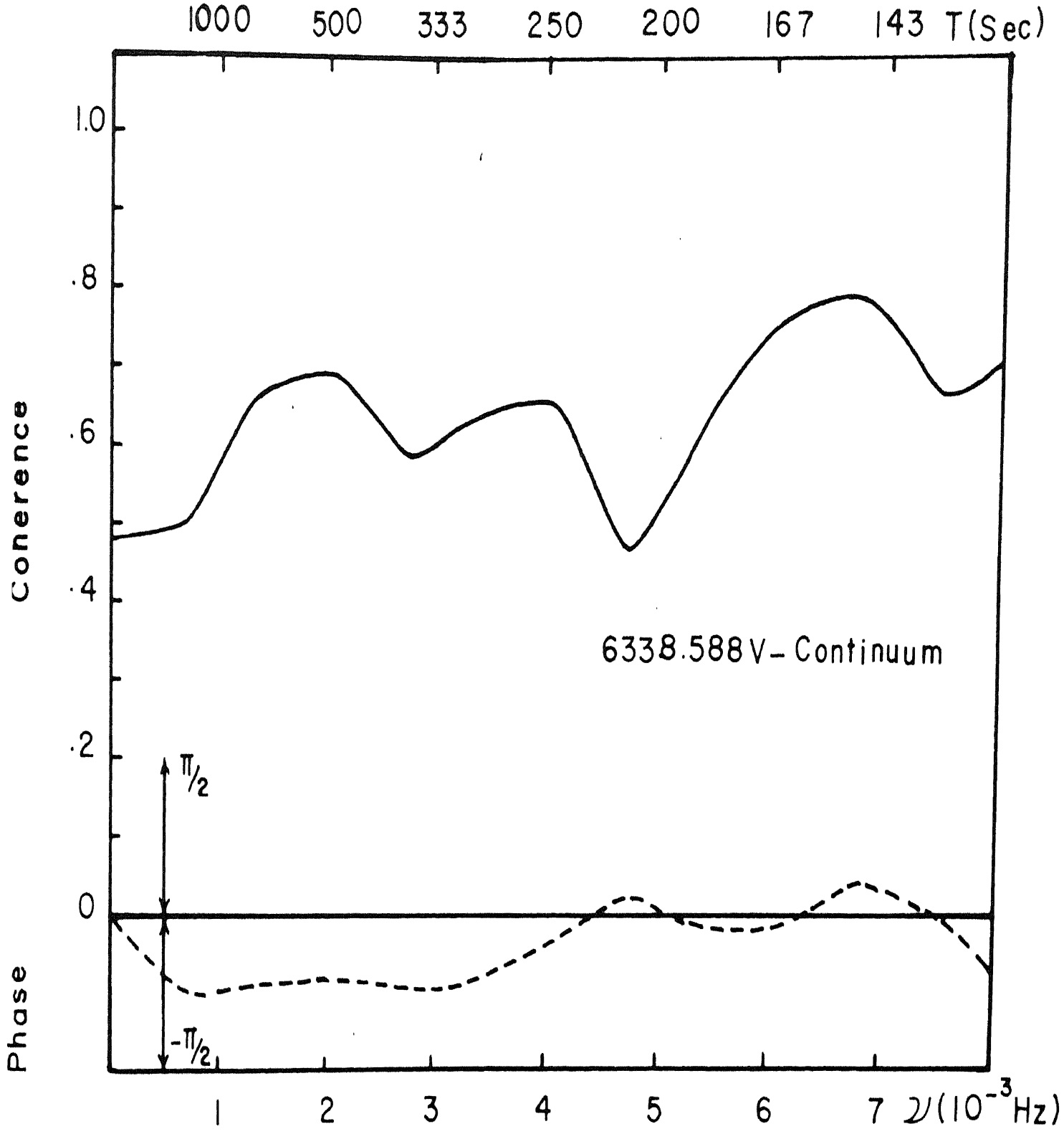
1000
500
333
250
200
167
143 T(Sec)
1.0
.8
.6
.4
.2
0
Conerence
Phase
6338.588 V - Continuum
π/2
-π/2
1
2
3
4
5
6
7 ν(10⁻³Hz)

Fig . V - 7

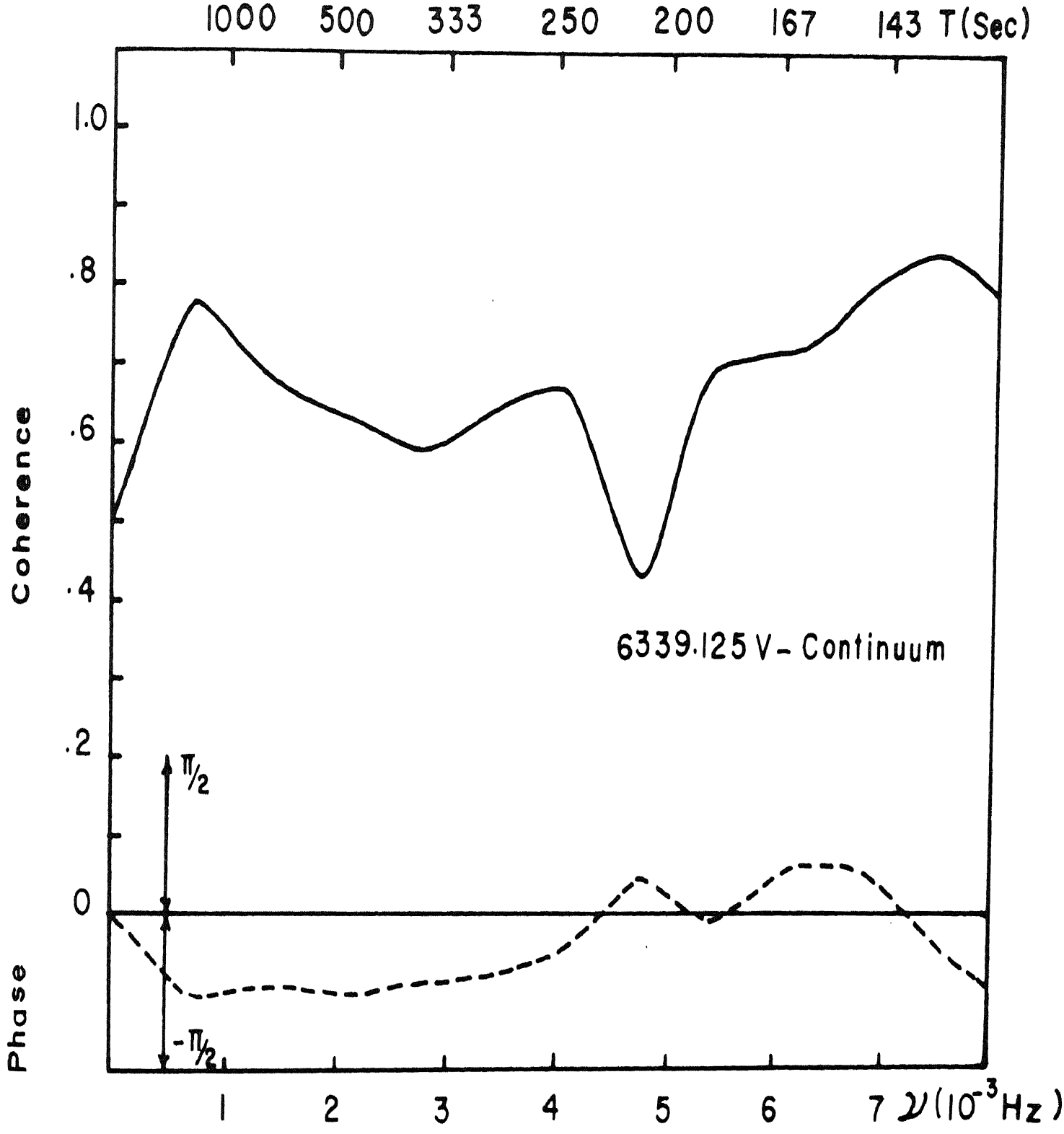
1000 500 333 250 200 167 143 T(Sec)
1.0
.8
.6
.4
.2
0
Coherence
Phase
6339.125 V - Continuum
π/2
-π/2
1 2 3 4 5 6 7 ν(10⁻³Hz)

Fig . V - 8

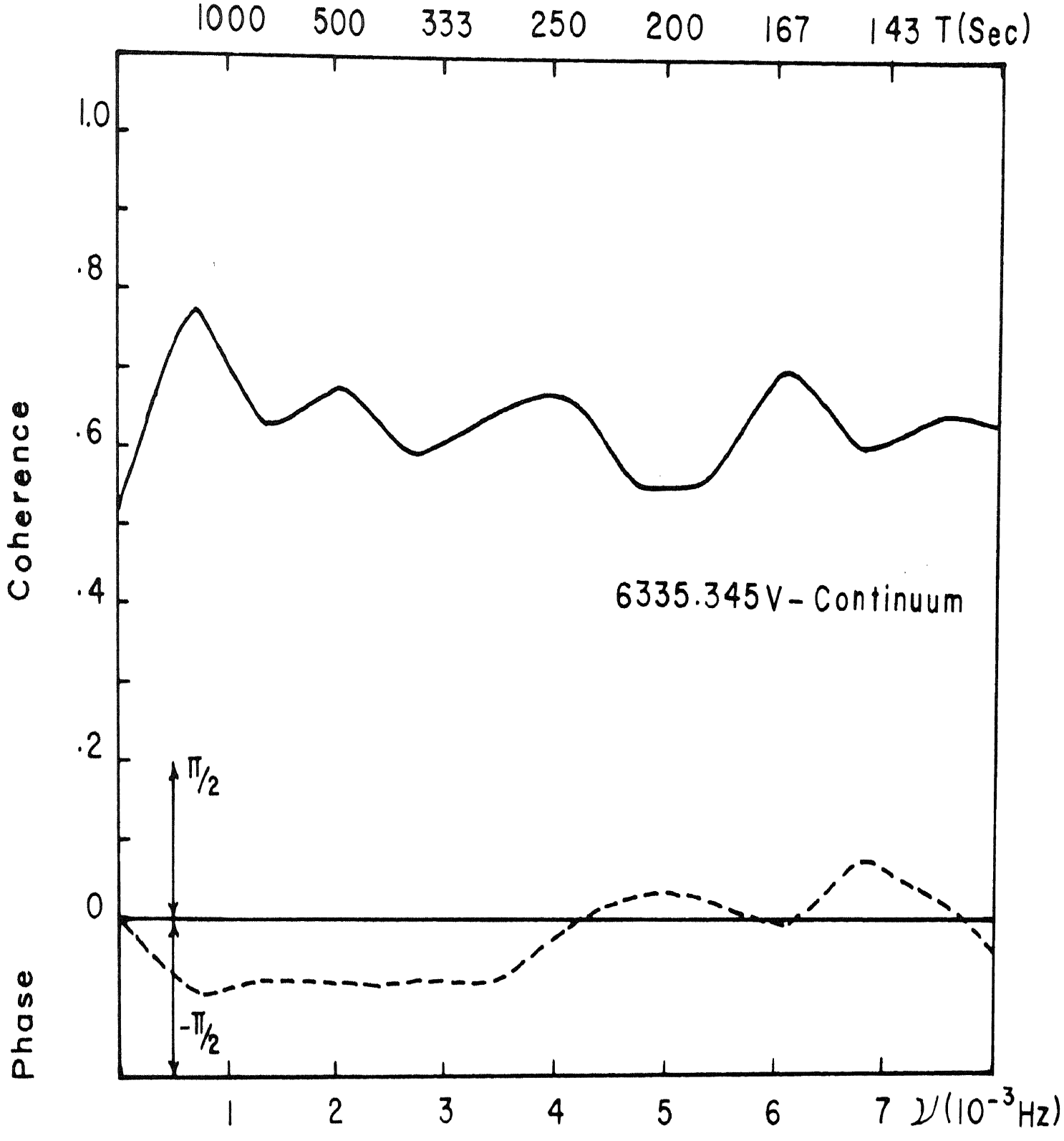
1000
500
333
250
200
167
143 T(Sec)
1.0
.8
.6
.4
.2
0
Coherence
Phase
6335.345V - Continuum
π/2
-π/2
1
2
3
4
5
6
7 ν(10⁻³Hz)

Fig . V - 9

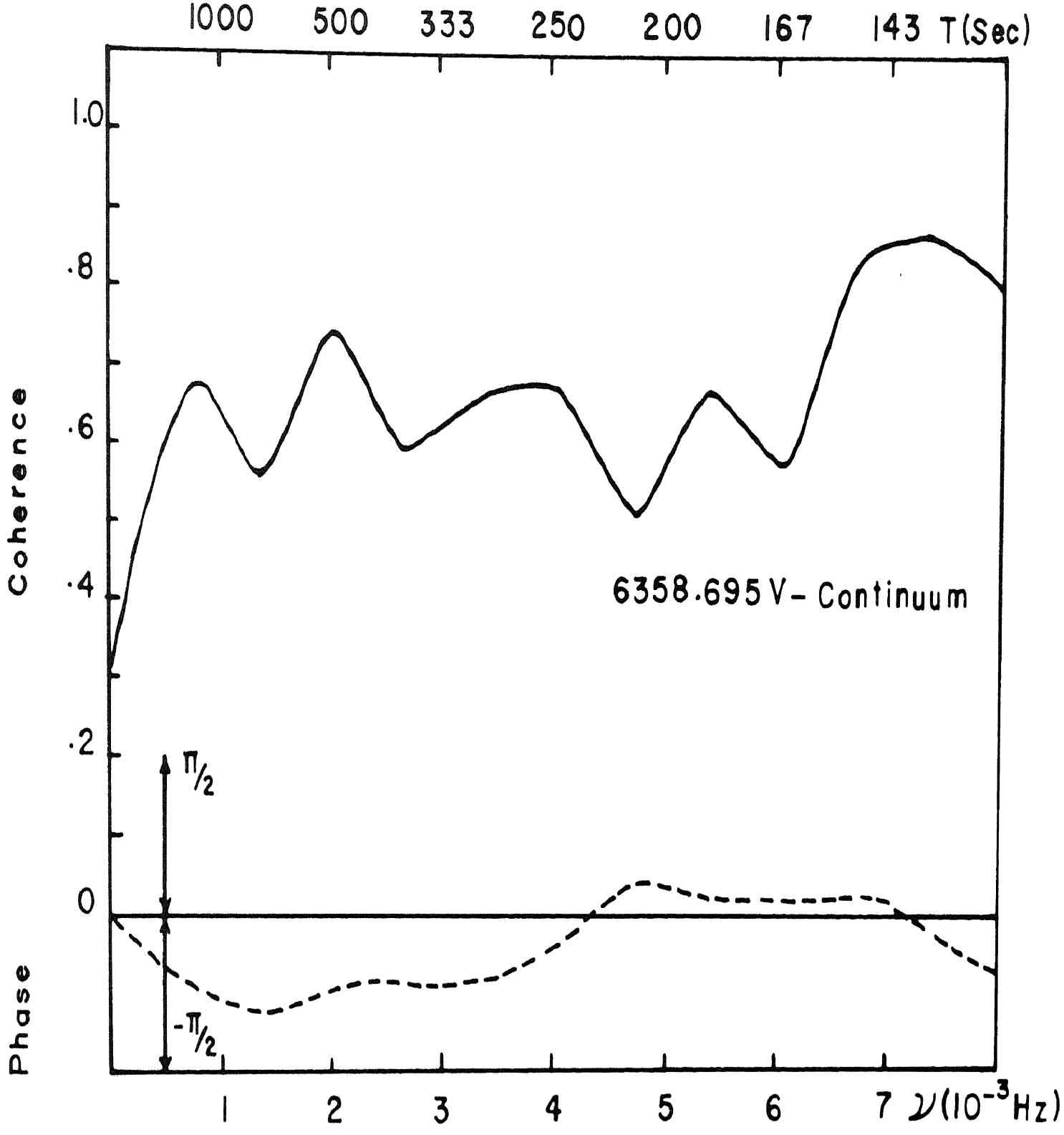
1000
500
333
250
200
167
143 T(Sec)
1.0
.8
.6
.4
.2
0
Coherence
Phase
6358.695 V- Continuum
π/2
-π/2
1
2
3
4
5
6
7 ν(10⁻³Hz)

Fig . V-10

fluctuates about a mean value of 0.6. This value of coherence is an evidence for the close association of upward velocities and brightenings in the continuum. In the frequency range ν = 0 to 4 x 10^{-3}, the upward velocities lag behind the brightenings in the continuum by about 34 to 38°. This agrees well with the lags obtained by Evans et-al (1963) for FeI 5171 line and by Edmonds et-al (1965) for CrI 5051.9. It is interesting to note that Evans and Michard (1962) from a qualitative study of the films estimated, "that the appearance of a strong bright feature in the continuum is followed by an oscillation in the lines (FeI 5171 and MgI 5172) initiated by a violet shift, and that the first velocity maximum occurs about 40 seconds after the maximum brightness in the continuum feature". The phase somewhat reverses its sign in the region of high frequencies. In the low frequency part, all the four lines show a very consistent phase lag between upward velocity and bright continuum features. This is very consistent with the phase relationship to be expected in convective motions too, which prevail in this frequency range. Edmonds et-al (1965) found the phase reversed, in this region.

Finally, I have cross-correlated the velocity measurements in the line FeI 6358.695 with (i) core brightness and (ii) wing brightness in the same line. The phase and coherence spectra of these are plotted in Figures V-11 and V-12. In the case of velocity Vs core brightness curve, the coherence has a mean value around 0.7 from ν = 2 to 5.5 x 10^{-3}. In the low frequency region, the coherence rises to 0.85 and beyond ν = 5.5 x 10^{-3} it drops to about 0.4 and rises again. The intensity oscillation in the core leads the velocity oscillation by about 93°.5. This agrees with the findings of Evans et-al (1963) on the FeI 5171 line and also those of Frazier (1968) and Tannenbaum et-al (1969). Ofcourse, it must be agreed that the two oscillations compared here pertain to two different levels; but the justification is from the earlier argument that the temperature oscillations in the core of strong lines are caused by the compressive motions induced by these velocity oscillations themselves. The atmosphere, at these levels, possessing a high value for the radiative relaxation time, behaves adiabatically and so the changes in temperature, pressure and density are all in phase. Now, for a standing wave the velocity oscillations lag the temperature and pressure

FIGURE V-11

Coherence and phase spectra of the velocity fields against the core brightness in FeI 6358.695. The velocity oscillations lag behind the brightness fluctuations by 93°.

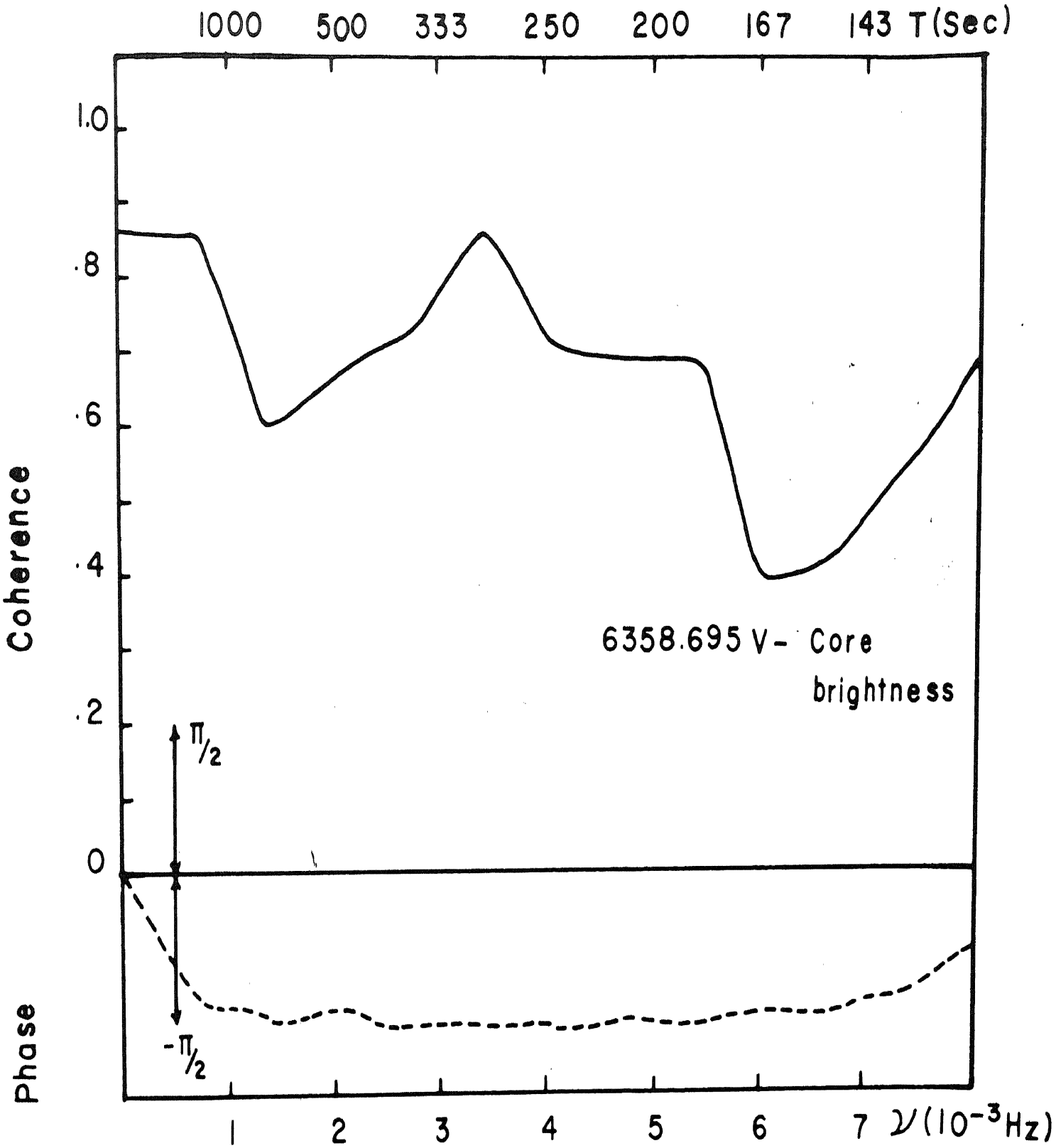
1000
500
333
250
200
167
143 T(Sec)
1.0
.8
.6
.4
.2
0
Coherence
6358.695 V- Core
brightness
π/2
-π/2
Phase
1
2
3
4
5
6
7 ν(10⁻³Hz)

Fig . V-11

FIGURE V-12

Coherence and phase spectra of the velocity fields against the wing brightness in FeI 6358.695. In the range $\nu = 0$ to 5×10^{-3} Hz., the velocity lags behind the wing brightness by about 21°.

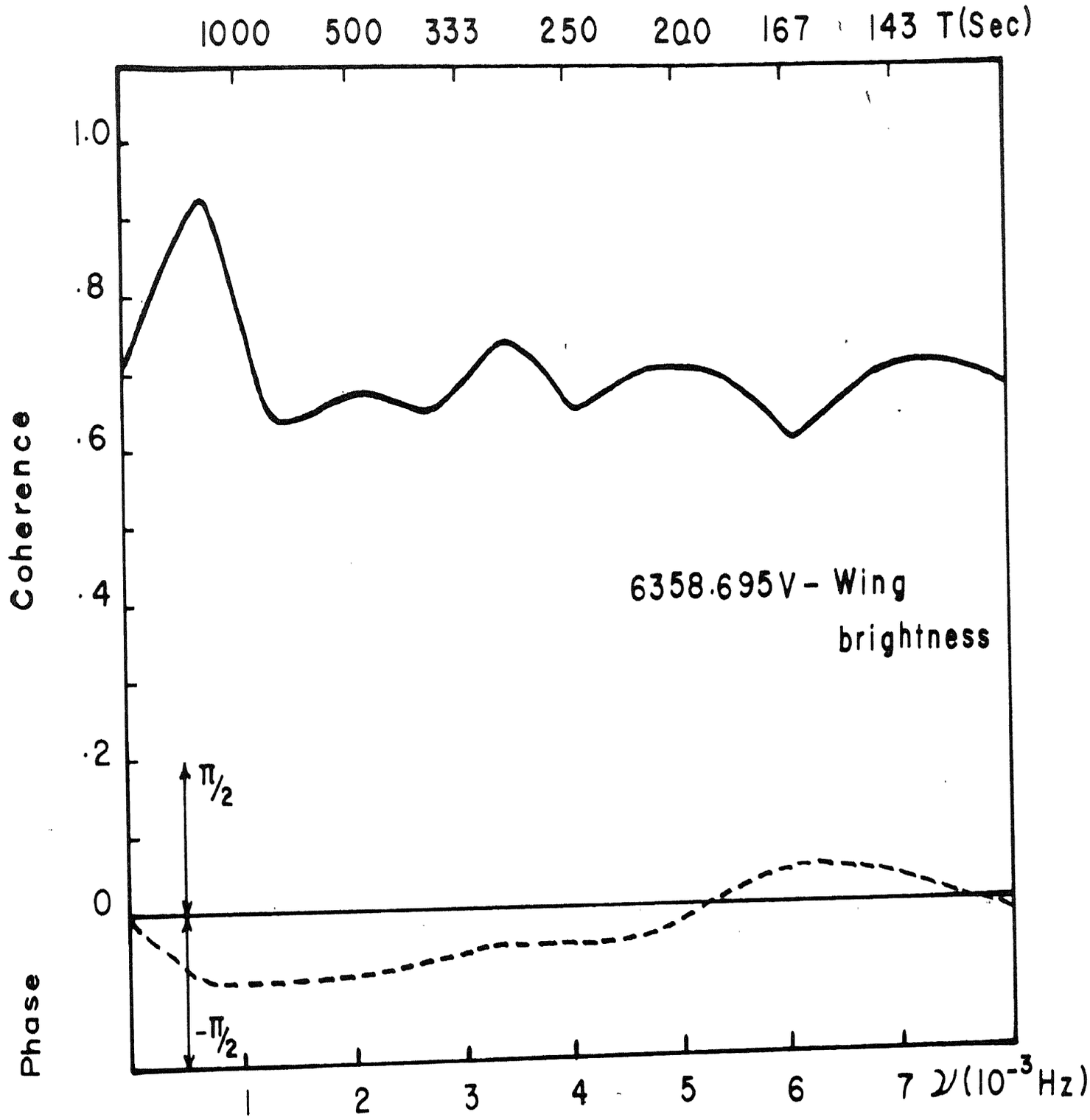
1000 500 333 250 200 167 143 T(Sec)
1.0
.8
.6
.4
.2
0
Coherence
Phase
6358.695V - Wing
brightness
π/2
-π/2
1 2 3 4 5 6 7 ν(10⁻³Hz)

Fig . V - 12

oscillations by 90° (Whitney 1958). Hence, the phase relations observed above confirm the existence of the standing wave motion. That standing waves exist in this range of frequencies were shown earlier in Chapter IV by the insignificant phase lag between the velocity fields of lines originating at different heights.

The velocity lags behind the wing brightness by about 21° near $\tau = 3.5 \times 10^{-3}$. With the continuum the phase lag of the velocity is 38°. This supports the argument that the changes in the line wing brightness reflect only those of the continuum, for the phase lag of 21° resembles the phase lag between the velocity and the continuum with allowance made for the radiation field to reach the level of the wings.

CHAPTER VI

A REVIEW OF THE RESULTS OF THE PRESENT STUDY

6.1. General

The present investigation has brought out the spatial properties in terms of depth and the temporal behaviour of the velocity and temperature fields in the solar atmosphere based on the study of fourteen spectral lines. The choice of a large number of lines originating in the entire photosphere and the low chromosphere at graded levels has enabled us to achieve a very good insight into the behaviour of the inhomogeneities sampled at close intervals in height in the solar atmosphere. There are a few spectral lines whose mean depth of formation overlap. This gives the advantage of confirming the properties of the oscillations derived from one spectral line by another having nearly the same depth of formation.

6.2. Review of the results

The main conclusions that emerge from this investigation are:

1) The velocity fields observed simultaneously at different levels show vertical oscillatory motion with an average period around 300 sec. The velocity time plots for the various lines, at successive points 1080 km apart on the solar surface show a high degree of coherence in the oscillations at different levels. This is also seen to be so from the results of the cross-spectral analysis between the velocities at two different levels. The "High resolution" analysis enabled the determination of the most probable period of oscillation for each line with an accuracy of 5 seconds. The CI 6587 line formed in the very deep photosphere (mean depth of formation log τ = 0.2 shows a period of 304 seconds. The weak lines having a mean depth of formation around log τ = -0.6 have a period ranging from 295 to 300 seconds. The remaining lines originating at mean levels from log τ = -0.8 to log τ = -1.2 have a period of 295 seconds. This shows that the period of oscillation decreases with height in the solar atmosphere.

2) In the low frequency range, the presence of the convective overshoots are seen well in all the lines, but the amount of power falls very rapidly with increasing height. This is confirmed by the high coherence of

velocity and intensity fluctuations near the zero frequency range. The low frequency power may not be due to gravity waves, as these waves cannot exist at these levels, due to the relatively small radiative relaxation time (Souffrin 1966). The existence of these waves at higher levels, is, however, not ruled out, as the radiative relaxation time increases fast with height at higher levels (Souffrin 1966) and according to Lighthill (1967) these waves can be generated even beyond the temperature minimum, by the penetrating 'tongues of turbulence' from levels below.

3) The coherence and phase spectra of velocities between pairs of lines show that the high level lines lag behind the low level lines. But the value of the phase lag in the resonance range is very small being of the order of 5 seconds for lines having their mean depth of formation 110 km apart. This suggests that in this range these are primarily standing waves. In the high frequency domain the phase lag increases and the propagation velocity agrees well with the velocity of acoustic waves in the medium. These presumably provide the non-thermal source for heating the corona.

4) The power spectra of the intensity fluctuations in the continuum, line wing and line core, show large power in the neighbourhood of the zero frequency. The high coherence in this frequency range between the three intensity fluctuations should be considered as an additional evidence of the penetration of the convective motions to these higher levels represented by the line wings and line core. Unlike the continuum and the line wing, the core brightness shows clearly the oscillations. In the FeI 6358 line, the intensity oscillation in the line core leads the velocity oscillation by 93°, in the resonance range. This again confirms the standing mode for the oscillations in the 300 sec. period range. The velocity in FeI 6358 lags behind the continuum fluctuations by 38° and lags behind the wing brightness by 21°. Also the wing brightness lags the continuum by 14° and the core brightness leads the continuum by 57°. These give support to the fact, that the line wing fluctuations are caused by the granulation field, while the line core fluctuations are independent of those of the granulation.

6.3. Some problems for future investigation

This field of study, namely, the dynamical characteristics of the macroscopic inhomogeneities have been

engaging the attention of the solar physicists during the past two decades and will continue to be a fertile field for investigations for many years to come.

Our information of the velocity and intensity fields at the high chromospheric levels, is very scanty. These can be obtained using the balmer lines. More observations of the phase relations between the velocity and intensity are necessary both in the photosphere and chromosphere, to help in determining the dynamic characteristics of the oscillations. Another point of great interest is the role of spicules in the heating of the corona. This will primarily rest on the identification of the spicules with disc features. It is known that, at the boundaries of the chromospheric network seen in the Ca^{+} K line spectroheliograms, there is an excess heating and also that this network boundary bears a good correlation with the boundary of the supergranulation cell. The magnetic fields piled up at the supergranular boundary are presumably responsible for this excess heating along the boundary. We do not know for certain whether these brighter regions along the boundaries of the chromospheric network are really bases of the spicule bushes. It would be of great significance to find out whether the chromospheric and coronal heating is localised in the regions

above these spicule bushes. Whether any relation exists between the small scale velocity oscillations and the supergranulation flow is a problem that can be examined by simultaneous observations of velocity fields in any photospheric or chromospheric line and intensity fields in the Ca^{+} K line. Also a detailed study of the behaviour of the oscillatory velocity fields in active regions would provide information on the extent of influence of magnetic fields on these oscillations.

The transformation of the waves propagated upwards into shock waves is only a hypothesis, put forward, to achieve a suitable energy dissipating agency. It may be interesting to detect these shock waves. The quasi-periodic movements detected in the solar chromosphere and corona by Durasova et-al (1971) by observations at 3.3 cm gives encouragement for further work in this direction. Similar observations carried out at mm wavelength will provide a link between the optical observations and those in the cm wavelengths.

Summing up, it is certain, that only the accumulation of such observations in large quantities on the inhomogeneities obtained through studies of their velocity and

intensity fields at all levels in the solar atmosphere, will offer a basis for the interpretation and understanding of the fundamental problem of the transport of mechanical energy and subsequent heating of the outer layers of the solar atmosphere.

REFERENCES

Bhattacharyya, J.C.	1972	Solar Phys. (In press)
Biermann, L.	1946	Naturwiss, 33, 118
Biermann, L.	1948	Zs. f. Ap. 25, 161
Blackman, R.B., Tukey, J.W.	1958	The measurement of power spectra, Dover Publications, N.Y.
Bray, R.J. and Loughead, R.E.	1967	The Solar granulation, Chapman and Hall Ltd., p. 32.
Class, W.J.	1951	Recherches Astronomiques De L' Observatoire D'Utrecht, XII, Part I, 3
Corliss and Warner	1964	Astrophys. J. Suppl.VIII, No.83, 395
Deubner, F.L.	1967	Solar Phys. 2, 133.
Durasova, M.S., Dobrin, M.M. and Yudin, G.I.	1971	Nature, 229, No.3, Physical Sciences p. 82
Edmonds Jr., F.N., Michard, R., and Servajean, R.	1965	Ann. Astrophys. 28, 534
Edmonds Jr., F.N., and Mc Cullough, J.R	1966	Astrophys. J. 144, 754
Elste, G.,	1955	Zs. f. Ap. 37, 201
Elste, G.,	1967	The structure of the quiet photosphere and the low chromosphere - Proc. of the 'Bilderberg' Conference, Ed. de-Jager, Springer-Verlag, Holland.
Evans, J.W. and Michard R.	1962	Astrophys. J. 135, 812

Evans, J.W., and Michard R.	1962	Astrophys. J. 136, 493
Evans, J.W., Michard R, and Servajean, R.	1963	Ann. Astrophys. 26, 368.
Evershed, J.,	1909	Month. Not. Roy. Astr. Soc. 69, 454.
Evershed, J.,	1922	Month. Not. Roy. Astr. Soc. 82, 392
Frazier, E.N.	1968	Astrophys. J. 152, 557
Goodman, N.R.	1957	Scientific Papers No.10, Engineering Statics. Lab., New York University.
Hart, A.B.	1956	Month. Not. Roy. Astr. Soc. 116, 38
Howard, R.	1962	Astrophys. J. 136, 211
Howard, R.	1967	Solar Phys. 2, 3.
Jager, C. de, and Kuperus, M.	1961	Bull. Astron. Inst. Neth. 16, 71.
Jensen, E. and Orrall, F.Q.	1963	Astrophys. J. 138, 252
Katterbach, K and Krause, H.	1949	Zs. f. Ap. 26, 137
Kuperus, M.	1965	Recherches Astronomiques de L' Observatoire D' Utrecht, XVII.
Leighton, R.B., Noyes R.W., and Simon, G.W.	1962	Astrophys. J. 135, 474
Lighthill, M.J.	1952	Proc. Roy. Soc. London, A. 211, 564
Lighthill, M.J.	1954	Proc. Roy. Soc. London, A. 222, 1.

Lighthill, M.J.	1967	Aerodynamic Phenomena in Stellar Atmospheres, I.A.U. Symposium No.28, p. 429
Moore, D.W., and Spiegel, E.A.	1964	Astrophys. J. 139, 48
Musman, S., and Rust, D.M.	1970	Solar Phys. 13, 261
Nirupama, S.	1965	Ph.D Thesis, University of Madras.
Noyes, R.W., and Leighton, R.B.	1963	Astrophys. J. 138, 631
Noyes, R.W.	1967	I.A.U. Symposium No.28 - Aerodynamic Phenomena in Stellar Atmospheres - Academic Press.
Osterbrock, D.E.	1961	Astrophys. J. 134, 347
Pecker, J-C.	1953	Ann. Astrophys. 16, 321
Pierce, A.K., and Waddell, J.H.	1963	Mem. Roy. Astr. Soc. 68, 89
Plaskett, H.H.	1954	Month. Not. Roy. Astr. Soc. 114, 251
Proudman, I.	1952	Proc. Roy. Soc. London, A. 214, 119
Richardson, R.S. and Schwarzchild, M.	1950	Astrophys. J. 111, 351
Schatzman, E.	1949	Ann. Astrophys. 12, 203
Schwarzchild, M.	1948	Astrophys. J. 107, 1
Souffrin, P.	1966	Ann. Astrophys. 29, 55
Spiegel, E.A.	1957	Astrophys. J., 126, 202
Stuart, F.E. and Rush, J.H.	1954	Astrophys. J., 120, 245

Tanenbaum, A.S., Wilcox, J.M., Frazier, E.N., and Howard, R. 1969 Solar Phys. 9, 328

Whitaker, W.A. 1963 Astrophys. J., 137, 914

Whitney, C. 1958 Smithsonian Contrib. Astrophys. 2, 365